Investigation of the Removal of Arsenite ion from Ground Water Using $FeCl_3 \cdot 6H_2O$ Modified Sugarcane Bagasse Biochar

Maykle Mulugeta Tegegne

A Thesis Submitted to

The Department of Chemical Engineering

School of Mechanical, Chemical, and Material Engineering

Presented in Partial Fulfillment of the Requirement for the Degree of Master's in Chemical

Engineering (Specialization in Process Engineering)

Office of Graduate Studies

Adama Science and Technology University

September, 2023

Adama, Ethiopia

Investigation of the Removal of Arsenite ion from Ground Water Using $FeCl_3 \cdot 6H_2O$ Modified Sugarcane Bagasse Biochar

Maykle Mulugeta Tegegne

Major Advisor

Dr. Alemu Gizaw

Co-Advisors:

Dr. Mulugeta Yilma

A Thesis Submitted to

The Department of Chemical Engineering

School of Mechanical, Chemical and Materials Engineering

Presented in Partial Fulfillment of the Requirement for the Degree of Master's in Chemical

Engineering (Specialization in Process Engineering)

Office of Graduate Studies

Adama Science and Technology University

September, 2023

Adama, Ethiopia

DECLARATION

I hereby declare that this Master Thesis entitled "**Investigation of the Removal of Arsenite ion from Ground Water Using $FeCl_3 \cdot 6H_2O$ Modified Sugarcane Bagasse Biochar**" is my original work. That is, it has not been submitted for the award of any academic degree, diploma, or certificate in any other university. All sources of materials that are used for this thesis have been duly acknowledged through citation.

Maykle Mulugeta Tegegne	_____	_____
Name of the Student	Signature	Date

RECOMMENDATION

We, the advisors of this thesis, hereby certify that we have read the revised version of the thesis entitled "**Investigation of the Removal of Arsenite ion from Ground Water Using $FeCl_3 \cdot 6H_2O$ Modified Sugarcane Bagasse Biochar"** prepared under our guidance by Maykle Mulugeta Tegegne submitted in partial fulfillment of the requirements for the degree of Mater's of Science in Chemical Engineering. Therefore, we recommend the submission of the revised version of the thesis to the department following the applicable procedures.

Alemu Gizaw (PhD)		07-11-2023
Major Advisor	Signature	Date
Mulugeta Yilma (PhD)		07-11-2023
Co-advisor	Signature	Date

APPROVAL PAGE

We, the advisors of the thesis entitled "**Investigation of the Removal of Arsenite ion from Ground Water Using $FeCl_3 \cdot 6H_2O$ Modified Sugarcane Bagasse Biochar**'' and developed by Maykle Mulugeta Tegegne, hereby certify that the recommendation and suggestions made by the board of examiners are appropriately incorporated into the final version of the thesis.

Alemu Gizaw (PhD)	_____	07-11-2023
Major Advisor	Signature	Date
Mulugeta Yilma (PhD)	_____	07-11-2023
Co-advisor	Signature	Date

We, the undersigned, members of the Board of Examiners of the thesis by Maykle Mulugeta Tegegne have read and evaluated the thesis entitled "Investigation of the Removal of Arsenite ion from Ground Water Using $FeCl_3 \cdot 6H_2O$ Modified Sugarcane Bagasse Biochar'' and examined the candidate during the open defense. This is, therefore, to certify that the thesis is accepted for partial fulfillment of the requirement of the degree of Master of Science in Chemical Engineering.

_____	_____	_____
Chairperson	Signature	Date
_____	_____	_____
Internal Examiner	Signature	Date
_____	_____	_____
External Examiner	Signature	Date

Finally, approval and acceptance of the thesis is contingent upon submission of its final Copy to the Office of Postgraduate Studies (OPGS) through the Department Graduate Council (DGC) and School Graduate Committee (SGC).

_____	_____	_____
Department Head	Signature	Date
_____	_____	_____
School Dean	Signature	Date
_____	_____	_____
Office of Postgraduate Studies, Dean	Signature	Date

ACKNOWLEDGEMENT

I would like to acknowledge, give my warmest gratitude and praise for the almighty GOD who was there for me through all these years and for my respected advisors Alemu Gizaw (PhD) and Mulugeta Yilma (PhD), words cannot express my gratitude, without your invaluable advice and support this research would not reach this stage. I am also grateful for my colleague's classmates for their help in editing, late night responses and moral support.

Most importantly, my heartfelt, sincere thanks should go to my beloved sister Marta Mulugeta, raising me to the heights that I am in at present with her love, courage, and support. My special gratitude and deep love go to the number one mother ever, whose name is Tsigiework Ergete, and to my beloved love Melakie Masrie for their mysterious love and kindness, my stories, I feel your smiles at heaven. I dedicate this thesis to them.

Finally, all in all, anybody who put a dot on this research, I would love to thank you from the bottom of my heart.

TABLE OF CONTENTS

Contents

LIST OF TABLES

LIST OF FIGURES

LIST OF ABBREVIATIONS AND ACRONYM

AAS	Atomic Absorption Spectroscopy
BC	Biochar
BET	Brunauer–Emmett–Teller
DTG	Derivative Thermogravimetric
EDS	Electrostatic adsorption
ED	Electro dialysis
FT-IR	Fourier Transform Infrared Spectroscopy
FWHM	Full Width at Half Maximum
IBSCB	Iron Modified Sugarcane Bagasse
IX	Ion Exchange
IBSCB	Iron(III) chloride hexahydrate modified Sugarcane Bagasse
MF	Microfiltration
NF	Nano filtration
PZC	point zero charge
RO	Reverse Osmosis
SCB	Sugarcane Bagasse
SEM	Scanning Electron Microscopy
TGA	Thermo gravimetric Analysis
UF	Ultrafiltration
UV	Ultraviolet–visible
XRD	X-Ray Diffractometry

ABSTRACT

The presence of an excess arsenite ion (As III) in the human body leads to serious humans and other organism's health problems. The increased As (III) level may be a result of natural and anthropologic activities. Therefore, it is essential to develop widely available, sustainable, effective, and low-cost adsorbent for As (III) removal to combat the problem. This work aimed to synthesize and characterize $FeCl_3.6H_2O$ loaded SCB bagasse based biochar for As (III) removal from water. SCB bagasse biochar was prepared at 450 ^oC pyrolysis temperatures with 1hour residence time. The $FeCl_3.6H_2O$ loaded SCB biochar was produced by mixing SCB biochar with 0.5M of $FeCl_3.6H_2O$ solution for 24 hours at room temperature. FT-IR, XRD, BET, and TGA were used to characterize the specific functional groups, crystalline structure, specific surface area, and thermal stability, respectively. A successful surface loading of hydroxyl functional groups, and structure of the $FeCl_3.6H_2O$ loaded SCB biochar were both confirmed. The sugarcane bagasse (SCB) biochar and the $FeCl_3.6H_2O$ loaded SCB biochar have been shown to have BET specific surface areas of 14.88 and 97.38 m^2/g, respectively. Furthermore, investigations on the effects of adsorption parameters namely contact time, adsorbent dose, pH, and initial arsenite concentration have been conducted. The result confirmed that 89.89% of arsenite ion was removed from synthetic water at optimum condition of 180 min, 1.5 g adsorbent dose, the pH level of 4, and 10 mg/L of initial arsenite concentration. Furthermore, the adsorption parameters such as equilibrium isotherm, kinetics, and thermodynamic properties were conducted. The Langmuir model provided the best fit for the adsorption isotherm data, with a maximum adsorption capacity of 27.70 mg/g., The kinetic model's result demonstrated that pseudo-second-order, best fit to the kinetic experimental data with a maximum R^2 of 0.9737. The result of the thermodynamic parameters demonstrated that the adsorption process is spontaneous and endothermic. Phosphate and carbonate observed highly compete for active sites on the adsorbent during arsenite removal. The removal efficiency of 69.16% of As (III) was obtained after 4 cycles of desorption-adsorption experiment, which indicated excellent reusability of the adsorbent. All these outcomes were shown that $FeCl_3.6H_2O$ loaded SCB biochar was a wonderful, attractive adsorbent for the removal of As (III) from water.

Keywords: *Adsorption; Arsenite; $FeCl_3.6H_2O$ loaded SCB biochar; Isotherm; Kinetics*

CHAPTER ONE

INTRODUCTION

1.1. Background

Heavy metals have been considered to be an issue for both human and environmental health due to their toxic and non-biodegradable nature (Tchounwou et al., 2012). Both atmospheric and anthropogenic activities, such as mining and smelting operations, wastewater irrigation, the use of fertilizers and pesticides, and traffic emissions, could cause these components to accumulate on to soils and streams (X. Yang et al., 2016). Arsenic (As), a metalloid that causes cancer, poses an extreme risk to the health of people and animals and is primarily found in the environment in the form of oxyanion (N. A. Shaheen et al., 2018). Depending on the redox conditions of the environment, it may exist in aqueous solution in either of the two oxidation states of arsenate As(V) or arsenite As(III). Arsenic may be released into surface and groundwater as a result of the dissolution of arsenide minerals and human activities such as the use of pesticides, chemical industries and the burning of fossil fuels (Smedley & Kinniburgh, 2002).

In natural ecosystems, arsenic is a hazardous element that is frequently present. Geochemical reactions, industrial waste discharges, or agricultural use of arsenical pesticides are some of the sources of its occurrence in natural streams. In many regions of the world, arsenic element is found as oxides in the soil, sediments, and water and is the result of both anthropogenic and natural processes. Arsenic exists in Nature in four different chemical oxidation states: -3, +3, 0, and +5 (Bissen & Frimmel, 2003). The most frequently arsenic forms naturally found are arsenite (H_3AsO^{3-} As(III)) and arsenate ($HAsO_4^{2-}$ As(V)). While As(III) exists as arsenious acid (H_3AsO_3, H_2AsO^{3-}, $HAsO_3^{2-}$) under slightly reducing conditions, As(V) is the major species present under oxidizing conditions and exists as oxyanions of arsenic acid (H_3AsO_4, $H_2AsO_4^-$, $HAsO_4^{2-}$ and AsO_4^{3-}) (Sankar et al., 2014).

The International Agency for Research on Cancer (IARC) has classified substances containing arsenic as group 1 carcinogens (Bissen & Frimmel, 2003). As(III) is approximately 60 times more toxic than As(V) (Chwirka et al., 2000) and As(III) has more mobility than As(V) because neutral As(III) is less likely to bind to mineral surfaces than As(V). The US-EPA and WHO both adhere to the 10 ppb (0.01 mg/L) threshold for the presence of As in drinking water, although many other

nations throughout the world including China, Bangladesh, Mexico, and Nepal retain the former WHO recommendation of 0.05 mg/L(Mohan & Pittman, 2007).

The majority of conventional As removal techniques are very effective when the original As concentration in the water is larger (> 100 mg/L), yet the water quality criterion for many counties is residual As content less than 0.05 mg/L. As a result, a straightforward treatment approach is needed to effectively eliminate As at a low operating and capital expense. An efficient method for removing as should also produce the least amount of sludge and have a straightforward design with minimal negative effects on the environment. Due to its adsorptive qualities, which include a highly porous structure, a wide surface area, a high surface alkalinity, and the presence of diverse surface functional groups, bio-char is increasingly being used as a water amendment(Niazi et al., 2018). Due to its capacity to store carbon, the carbonaceous material known as bio-char has generated a great deal of attention(Lehmann, 2007).

Additionally, numerous research have demonstrated how biochar may be used to lessen the mobility and bioavailability of harmful heavy metals (Bakhshi et al., 2014). However, because most bio-char surfaces have a net negative charge, the sorption of negatively charged arsenate and arsenite onto such surfaces is constrained (Beesley & Marmiroli, 2011). Various modifications of bio-char surfaces have been reported to enhance As sorption (Beesley & Marmiroli, 2011). (I. C. Chen et al., 2011) found that As sorption was significantly improved by pyrolysis of biomass and Fe oxide bio-char composites. A byproduct of the sugar and alcohol industries, sugarcane bagasse is produced in enormous quantities (Nie et al., 2018). It has been claimed that sugarcane bagasse bio-char materials are capable of being used to filter aqueous solutions of arsenic, lead, tetracycline, chromium, zinc, copper, and phosphorus (Khairul et al., 2017).

Cellulose, hemicellulose, and lignin are the three primary ingredients in sugarcane bagasse. As a result, it is a suitable raw material for the production of adsorbents based on biochar (Mpatani et al., 2021). Various modification strategies have been proposed in an effort to improve the adsorptive capacity of BC (Mamtimin & Wang, 2022). Magnetic BC can be produced by soaking BC in magnetic particles, such as Fe salts, Fe oxides, and nano zero-valent iron (nZVI)(S. M. Shaheen et al., 2022).

1.2. Statement of the Problem

Arsenite contamination in groundwater poses a significant threat to human health and well-being, particularly in regions where groundwater is a primary source of drinking water. Arsenite (As(III)) is one of the most toxic forms of arsenic, known for its carcinogenic properties and adverse health effects. Arsenite doesn't not break down into inert by-products like organic contaminants, the majority of which are subject to biological destruction. Arsenite contamination of water can result in serious health problems for humans and other organisms, including problems with the skin, nervous system, respiratory system, cardiovascular system, liver, kidney, bladder, and prostate, immune system, and endocrine system.

As a result, numerous organizations have set allowable contamination level for the arsenite content material in drinking water. For example, the United States of America Environmental protection agency (USEPA) has installed a maximum contaminant level (MCL) of 10 micrograms per liter (µg/L). In the other case, the world Health Organization (WHO) and European Economic Network (EEC) have set up 10 micrograms per liter (µg/L) limit (Rezvani et al., 2019).

Different physiochemical techniques have been employed to remove arsenite from water, including precipitation, coagulation, ion exchange, and reverse osmosis. Many of these procedures costs lots of money and demand lots of energy. They might also produce massive sludge that needs to be treated. Additionally, certain methods did not allow for the recovery of the mineral and metals.

Finding the right technique, such as adsorption, is therefore crucial. Adsorption has the advantages of being inexpensive, readily available, sustainable, and ecologically beneficial (Alagha et al., 2020). Many different adsorbents, including siderite, hematite, zeolite, and tea waste, are employed in adsorption procedures to remove arsenite ions from water and wastewater (Dai et al., 2019). In order to remediate arsenite-contaminated groundwater in underdeveloped nations, it is necessary to find affordable, accessible, and non-toxic adsorbents. The goal of this study was to develop a arsenite adsorbent that is easily available, sustainable, effective, inexpensive, and ecologically friendly. To the best of my knowledge, no previous research has been conducted on the $FeCl_3.6H_2O$ loaded SCB biochar as an adsorbent for arsenite removal from groundwater.

1.3. Objective

1.3.1. General objective

The general objectives of this work is Preparation and characterization of $FeCl_3 \cdot 6H_2O$ loaded sugarcane bagasse biochar as an Adsorbent for Arsenic(III) removal from ground water.

1.3.2. Specific objectives

- Preparation and characterization (before and after adsorption) of $FeCl_3 \cdot 6H_2O$ modified biochar from sugarcane bagasse.
- Investigate the removal efficiency of Arsenic(III) by varying pH, initial concentration of Arsenite and amount of adsorbent using prepared adsorbents.
- To determine adsorption kinetics, adsorption isotherms and thermodynamics of As(III) by the prepared adsorbents using batch experiments.
- To study adsorbent regeneration, and investigate influence of competing ions on the adsorption of arsenic(III) ions.
- Investigate the performance of the adsorbent using real ground water.

1.4. Scope of the study

By preparing synthetic water with a known concentration based on the groundwater arsenite ion concentration in different countries, this study investigates the adsorption capability of locally accessible adsorbents for the removal of arsenite. Suitable locally available materials sugarcane bagasse was collected from the nearest sugar factory and were used as adsorbents for the removal of arsenite. Several physical and chemical characteristics of the adsorbents were investigated using techniques such as BET surface area analysis, Fourier Transform Infrared Spectroscopy (FT-IR) analysis to identify the functional groups, and Scanning Electron Microscopy to identify the surface characteristics of the adsorbents. Then, using the one factor at a time method through a batch experiment, the adsorption efficiency based on the various experimental parameters was examined, and the optimal adsorption conditions were selected. The parameters include adsorbent dose from 0.5 g/L to 3 g/L, pH from 2 to 12, contact time from 30 min to 210 min, agitation speed of 250 rpm and initial analyte concentration from 5 to 30 mg/L was utilized. Additionally, the effects of co-existing ions including phosphate, sulphate, and carbonate was investigated. To determine the viability of the adsorption process and to determine the maximum adsorption capacity of the adsorbents, three isotherm models Langmuir, Freundlich, and Temkin were studied. Similarly,

pseudo-second order reaction mode and pseudo-first order reaction models were used to study the adsorption kinetics process. The performance of $FeCl_3 \cdot 6H_2O$ loaded sugarcane bagasse biochar for real ground water was also evaluated in this experiment.

1.5. Significant of the study

Arsenic contamination in water sources is a significant environmental and public health concern. This study focuses on developing $FeCl_3 \cdot 6H_2O$ modified SCB biochar adsorbent for the removal of Arsenic(III) from water, which can contribute to mitigating the health risks associated with arsenic exposure and safeguarding water quality. The loading of $FeCl_3 \cdot 6H_2O$ into the sugarcane bagasse biochar can potentially enhance its adsorption capacity and selectivity for Arsenic(III) ions. Investigating the preparation and characterization of this adsorbents provides insights into its efficiency and performance, which can contribute to the development of more effective water treatment technologies for arsenic removal. Developing an affordable adsorbent for arsenic removal is crucial, particularly for economically disadvantaged regions that are most affected by arsenic contamination. By utilizing sugarcane bagasse, which is a low-cost and widely available material, this study explores a potentially cost-effective adsorbent for water treatment, making it more accessible for communities facing arsenic contamination issues.

CHAPTER TWO

LITERATURE REVIEW

2.1. Introduction to Arsenic

Arsenic is a universal element that is present in the atmosphere, living things, rocks, soil, and bodies of water (Alka et al., 2021). Arsenic is commonly known as a hazardous heavy metal but actually it is a semi-metal (Alka et al., 2021). All living things have very small amounts of arsenic, which is found everywhere in the solid form of minerals. There are around 150 types of minerals which contain arsenic, some of which are referred to as arsenic ore (Dhakal, 2018). Arsenic naturally occurs in the environment together with other elements such oxygen, chlorine, carbon, mercury, lead, Sulphur, hydrogen, and gold. Natural processes including volcanic eruption, weathering reactions, and some biological and anthropogenic activities are responsible for the present level of arsenic accumulation. However, due to human activities such as the use of arsenical pesticides to enhance cultivation, the use of fertilizers to improve the quality of the soil, and the addition of arsenic to livestock feed, arsenic is now accumulating in soil (Dhakal, 2018).

The main reason of arsenic moving from its ground state to the air and water resources is the smelting of non-ferrous metals in conjunction with the generation of fossil fuels. The main contributors to arsenic accumulation in the environment are the combustion of coal in boilers and electrical power producing plants. The mobilization of arsenic can also be done by mining operations then arsenic may have leaked into the water from the soil and sediments. Some of the facts about arsenic are: Arsenic is the 33^{rd} element in the periodic table and the 20^{th} most common element in the crust of the earth (Dhakal, 2018), The atomic weight of arsenic is 75 g/mole, and its density is 5.7 g/cm^3 (Rathi & Kumar, 2021), Arsenic has a melting point of 814°C and a boiling point of 615°C, respectively (Rathi & Kumar, 2021), Arsenic can exist in a variety of oxidation states, including -3, 0, +3, and +5, whereas the two that are most frequently seen in natural water are the trivalent and pentavalent oxidation states (Dhakal, 2018), The concentration of arsenic in natural waterways can vary widely, starting at 0.5 g/L and going up to more than 5000 g/L (Dhakal, 2018), One application for arsenic compounds is the production of specific types of glass, wood preservation (sodium and zinc arsenates), and the generation of laser light from electric current in

some semiconductors (Alka et al., 2021), According to the WHO, 10 g/L of arsenic is the maximum amount that can be present in drinking water without having any negative effects (WHO & World Health Organization, 2019).

2.2. Forms of Arsenic

Arsenic's oxidation state is influenced by environmental factors such as temperature, pH, related ionic species, and oxidation reduction conditions. As these environmental factors vary, so does the oxidation state of arsenic. It's possible that if these factors change, arsenic shifts from a less dangerous state to a more toxic form (Dhakal, 2018). Arsenic's capacity for relative movement under a variety of redox situations makes it more problematic than other oxyanion forms of other elements (Dhakal, 2018). Inorganic arsenic, which has two oxidation states arsenate As(V) and arsenite As(III) is the major form in groundwater (Rathi & Kumar, 2021). As(III) is considerably more mobile and hazardous than As(V). Since arsenite loves reducing conditions and is therefore present in anaerobic ground fluids, arsenate is a form of arsenic that is thermodynamically stable. Arsenite is more poisonous than arsenate in biological systems, and these inorganic forms of arsenic are more toxic than the organic forms (Rathi & Kumar, 2021). It is also claimed that the efficiency of removing arsenate from arsenic using traditional treatment methods is higher than that of removing arsenite (Dhakal, 2018).

pH and redox potential conditions are the two most significant factors that affect the nature of arsenic species. The As(V) species persist in the pH range and under oxidizing conditions as oxyanions ($H_2AsO_4^-$ and $HAsO_4^{2-}$). $H_2AsO_4^-$ is present at a lower pH than $HAsO_4^{2-}$, which is present at a higher pH. Other forms, including H_3AsO_4 and AsO_4^{3-}, can be found in extremely acidic and extremely basic environments, respectively. Similar to As(V) , As(III) species occur in protonated form as H_3AsO_3 in reducing environments and at pH values lower than 9.2 (Alka et al., 2021). At higher pH, negatively charged arsenite species ($H_2AsO_3^-$ and $HAsO_3^{2-}$) becomes dominant (Alka et al., 2021).

2.3. Methods of Arsenite Removal

Physical-chemical techniques such as: adsorption, membrane separation, coagulation/flocculation, oxidation, and ion exchange, and biological techniques are commonly used in water treatment

systems (i.e., activated sludge and membrane bioreactors). Systems of treatment that aim to remove heavy metals include oxidation, membrane systems, ion exchange, and adsorption (Amen et al., 2020). The majority of these techniques achieve 80–100% clearance, effectively removing arsenite. 90% of the Arsenite loading is efficiently removed by coagulation-flocculation when alum and titanium (IV) sulfate are used as the coagulant. The effectiveness of using this approach on a wide scale is however limited by the creation of a secondary composition of As-rich sludge. Oxidation is only done to change arsenite from its miscible state to arsenate, which lessens its toxicity. Reverse osmosis and nano-filtration membrane systems in membrane technology have shown high (up to 85%) removal rates for arsenate, although arsenite must first be oxidized for effective removal before treatment. Adsorption is the basis for ion exchange, which uses resins to adsorb As ions and achieve removal rates of up to 85% (Siddiq et al., 2022). Comparatively, the adsorption method is superior to other As removal methods. Adsorption offers low cost, minimal creation of secondary hazardous waste products, easy operational controls, and high removal rates. Additionally, some adsorbents can be regenerated (Amen et al., 2020).

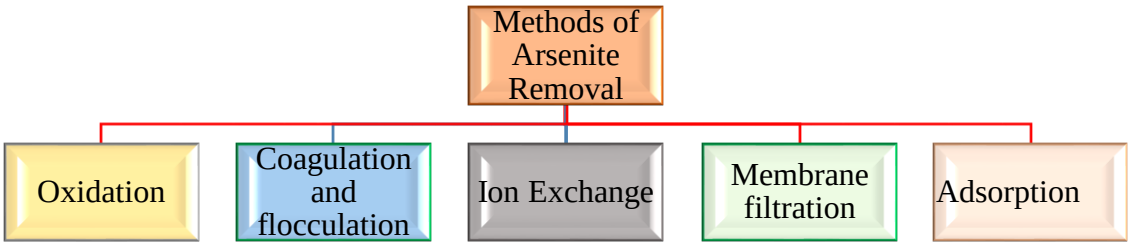

Figure 2.1: Arsenite removal technology from groundwater

2.3.1. Oxidation

Arsenic is primarily present as As(III), which are uncharged molecules, in groundwater due to its pH being close to neutral and minor reducing circumstances. But there are other methods that effectively remove the negatively charged As(V). To convert As(III) to As(V) before treatments like filtration, coagulation, and adsorption, oxidation has thus been used as a pre-treatment technique (Baig et al., 2013). Aeration is the easiest method for oxidizing arsenic, however because of the slow reaction rate, it may take several weeks to completely oxidize the substance (Amen et al., 2020). As a result, other powerful oxidants are also utilized to accelerate the oxidation process, including hydrogen peroxide, ozone, and manganese oxide (Bordoloi et al., 2013). Under varied pH conditions and water compositions, the oxidation of As(III) using four common oxidants is investigated. These oxidants are chlorine dioxide, sodium hypochlorite, potassium permanganate,

and mono chloramine. The findings demonstrate that mono chloramines have a low rate of oxidation while potassium permanganate has the highest rate of oxidation (Sorlini & Gialdini, 2010). In the presence of oxygen, the oxidation rate is largely increase by UV irradiation (Mondal et al., 2013). Although oxidation is a straightforward process that can be used to cleanse huge volumes of water, it can also result in undesirable harmful byproducts that require additional treatment.

2.3.2. Coagulation and Flocculation

Arsenic that is soluble in water can be converted into floc, which is easier to separate from water by sedimentation or filtering, through the coagulation reaction between arsenic and coagulants. As a result of positively charged coagulants reducing the negative charge of arsenic colloids, floc or big aggregates occur (Amen et al., 2020). Therefore, three mechanisms can be used to clarify how arsenic is removed from water by coagulation and flocculation: 1) direct precipitation reactions between arsenic and coagulants; 2) co-precipitation of arsenic during the growth of insoluble flocs; and 3) electrostatic adsorption of arsenic species onto the surface of the formed solid aggregates. In order to remove the flocs, coagulation is typically followed by filtering, which is a common and efficient method for removing arsenic. Uncharged As(III) must be converted to As(V) in order for coagulation to remove it more effectively. The most widely used coagulants are those based on iron and aluminum, such as alum ($Al_2(SO_4)_3.18H_2O$), ferric chloride ($FeCl_3$), and ferric sulfate ($Fe_2(SO_4)_3.7H_2O$) (Amen et al., 2020). In addition, aggregates that are better suited to being separated from water are promoted by the use of flocculants.

Arsenic that has been adsorbed onto aluminum hydroxide or precipitate $Al(AsO_4)$ may be present in the Al-As combination. Similar to how arsenic and iron species are known to form such complexes, sedimentation or filtration can remove ions (Mondal et al., 2013). Arsenic can be adsorbed at rates of up to 46 mg As(V)/g ferric chloride and 23 mg As(V)/g alum, respectively, due to the creation of hydrous ferric oxide and hydrous aluminum oxide. Compared to aluminum-based coagulants, iron-based coagulants are more efficient. Additionally, the iron-based coagulants are stable throughout a larger pH range (Mondal et al., 2013). The main influencing factors for arsenic coagulation are pH, dosage of coagulants and coexisting anions. The adsorption of arsenic to the oxide surface is favored at a low pH which is below the zero charge points of the oxides.

2.3.3. Ion exchange

Arsenic removal from water has frequently used the ion exchange approach. Arsenic interacts with ions on the solid phases, which are often synthetic resins, in a physio-chemical process that is used. Charged functional groups, such as strongly and weakly acidic groups or strongly and weakly basic groups, can be used to change the surface of synthetic resins by Covalent bonding (Singh et al., 2020). The resin is typically treated with chloride ions to remove arsenic. As a result, until the resin's ability to exchange ions is exhausted, which occurs when the majority of the exchange sites are loaded with arsenic, water containing arsenic passes through the resin columns with lower arsenic levels but greater chloride levels (Amen et al., 2020). The ion exchange resins can be re-generated by exchanging the loaded arsenic using NaCl solutions.

The exchange capacities for arsenic using strong base anionic exchange resins are from 1 to 1.4 mEq/mL. Besides, ion exchange is also affected by other coexisting anions such as phosphate, sulfate and nitrate by competing for exchange sites with arsenic. Generally, these anions have higher affinity to the resins than arsenic does. The ion exchange is less sensitive to the pH conditions. However, it requires the uncharged As(III) to be oxidized to As(V) before passing through the resin column and the oxidant should be removed in case the chemicals cause damage to the resins (Amen et al., 2020).

2.3.4. Membrane Filtration

Arsenic species can be separated from water by passing through a semi permeable membrane under the pressure as driving force. Membrane has been regarded as one of the most promising technologies for deep treatment of water. There are four types of membrane filtration processes that are most widely studied for arsenic removal. They are microfiltration (MF), ultrafiltration (UF), Nano filtration (NF), and reverse osmosis (RO), of which MF is the low-pressure membrane process while the other three need high pressure to provide driving force (Mondal et al., 2013). The property that decides if arsenic can be separated from water is the pore size of the membranes. Among the four membranes, RO and NF are able to separate arsenic by capillary flow or solution diffusion due to the pore sizes smaller than 2 nm in diameter. Pore sizes of MF and UF are not small enough to remove soluble arsenic. But they can be used to removal particulate arsenic after coagulation and flocculation (Bakshi et al., 2018).

Research has shown that the combination of coagulation and microfiltration is more efficient than that of coagulation and sedimentation (Bakshi et al., 2018). The advantage of membrane filtration processes for arsenic removal is independence of pH. In addition, there is no toxic by-product generated from the process. But the processes can be affected by the presence of specific colloids which foul the back wash. So, pretreatment is need for water containing high level of colloids. Another disadvantage for membrane method is the high cost and high energy consumption, which may not be acceptable for people in rural areas in developing countries (Mondal et al., 2013).

2.3.5. Adsorption

The adsorption process is one of the numerous methods now available for removing arsenic from water, and is considered to be one of the most promising methods due to its low cost, high efficiency, and simplicity of operation (Hao et al., 2018). Contaminants adhere to the surface of a adsorbent (solid) during the decontamination of water through adsorption, which removes them from suspension. The qualities of the initial solution mixture and the adsorbent surface strongly influence adsorption. Effective decontamination depends on the porous structure of the adsorbent, where van der Waals forces and/or electrostatic attraction allow immobilization and capture of the pollutants (Siddiq et al., 2022). The more surface area a medium has, the more material it can hold because adsorption is a surface phenomenon. Each adsorbent media has unique associated qualities, capabilities, and expenses (Bakshi et al., 2018).

The process of collecting arsenic species onto the solid surface by physical as well as chemical forces is known as adsorption for the removal of arsenic. Adsorbent dosage, adsorbent particle size, pH, initial adsorbate concentration, temperature, and contact time are some of the variables that have an effect on the adsorption process (H. T. Nguyen, 2022). Mohan and Pittman critically analyzed the performances of several adsorbents, including the standard activated carbon, natural components, industrial by-products, metal oxides, and composite materials, to better understand how concepts for the design of arsenic adsorbents developed (Bakshi et al., 2018). Due to its large specific surface area, activated carbon is the most well-known adsorbent. The pH of the water affects how well activated carbon adsorbs arsenite ion. One of the main determinants of As adsorption has been identified as the pH of the solution. At pH levels below the point of zero charge (PZC), a high rate of adsorption for As (V) has been observed. While As(III) has been reported to exist as nonionic (H_3AsO_3) form at pH less than five and therefore electrostatic attractions do not

play a role until pH 9 of the solution, the presence of positive charges on the adsorbent surface at lower pH range favors electrostatic interactions between negatively charged As(V) ions (Leng et al. 2019). The surface of carbon-based nanomaterials like graphene and carbon nanotubes is functionalized by hydroxyl (-OH) or carboxyl to remove arsenic (-COOH) (Kuila et al., 2012).

Arsenic species from ground water are successfully removed from the environment using iron-based adsorbents, which have undergone substantial development (Chowdhury, 2017). Some adsorbents, including zero-valent iron and granular ferric hydroxide (GFH), have also been manufactured on an industrial scale for use as commercial adsorbents (Hao et al., 2018). Despite their demonstrated high efficacy in removing arsenic, the majority of described adsorbents rarely find practical field applications because of the interfering ions in the water. Due to the unique chemical reaction between arsenic and iron, typical anions like Cl^-, NO_3^-, SO_4^-, and CO_3^- are not expected to have a major impact on the adsorption of arsenic on iron-based adsorbents (Pintor et al., 2018). Arsenic and phosphate can strongly fight for the same adsorption sites, which lowers the arsenic adsorption capacity (Tofik et al., 2016).

Adsorption can be categorized into physical adsorption (physisorption) and chemical adsorption (chemisorption) in nature. Physical adsorption has relatively weak intermolecular forces. It does not allow the sharing or transfer of electrons. Hence always maintains as individuality of interacting species. Even though the process is slow due to the occurrence of diffusion of molecules, the interactions are fully reversible which enables desorption to occur at a similar temperature. Not only the adsorbed molecules are free to move and cover the entire surface, but also have low heat in the case of physical adsorption (Hao et al., 2018)..

The main characteristic of chemical adsorption is the large interaction potential, which leads to a high heat of adsorption close to the value of the chemical bond. This fact, combined with other spectroscopy, electron spin resonance, and susceptibility measurements, confirms that chemical adsorption involves the transfer of electrons and the formation of true chemical bonds between the adsorbate and the solid surface. Because chemisorption involves chemical bonding, it often occurs at high temperatures and is generally, related to the activation energy. Furthermore, the adsorbed molecules are located in specific locations and therefore cannot freely migrate to the surface. Table 2.1 Comparison of physical and chemical adsorption. Generally, adsorption can occur at any interface. That is either gas-solid interface or liquid-solid interface (Abdalla et al., 2020).

Table 2. 1: Difference between chemical and Physical Adsorption

Parameters	Chemical Adsorption	Physical Adsorption
Force of Attraction	Strong attraction forces or chemical bond such as ionic bonds	Weak inter particle bond as vanderwaal forces
Temperature	Higher heat of adsorption	Low heat of adsorption
Electron transfer	electron transfer leading to bond formation between adsorbate and surface	Not involve electron transfer, although polarization of adsorbate may occur.
Adsorption layer	Monolayer only	Monolayer or multilayer
Kinetics Adsorption	Activated, may be slow and irreversible	Rapid, non- activated and fully reversible
Adsorption sites	Site specific	Not site specific,

The most literature studies showed that adsorption process could considered an efficient treatment method for the removal of emerging compounds from water. It allows reaching good removal percentage. In addition, a process does not imply by-products formation, which could be more toxic than parent compounds. It is obvious that adsorption process encompassed in an integrated treatment system, which involves many factors, such as available space for the construction of treatment facilities, waste disposal constraints, desired finished water quality, and capital and operating costs. All these factors imply the achievement of the optimal operating conditions for low-cost high efficiencies (Hao et al., 2018).

2.4. Mechanism of Adsorption

The two primary techniques for heavy metal adsorption on biochar and modified biochar are chemical and physical adsorption. Van der Waals force or particular surface area play a major role in physical adsorption. Due to their minimal effects, they can, however, be ignored (Hao et al.,

2018). The electrostatic attraction/repulsion, columbic interaction, ion-dipole/charge-dipole interaction, intra-particle diffusion, surface complexes (bidentate/binuclear inner-sphere), and hydrogen bonding mechanisms (carboxyl/carbonyl groups of adsorbent and surrounding water environment) can all be used to understand how arsenic binds to oxygen-containing functionalized mesoporous biochar materials (Bostick & Fendorf, 2018).

Anionic bonding is favored at low pH levels by protonation of the oxygen-containing electron-transferring functional groups (-C=O, -OH, -C-O-C, and -C=C/C=O-). By means of an electrostatic attraction and columbic forces mechanism, as species (Agrafioti et al., 2014). The surface of the adsorbent becomes less positively charged at higher pH levels, which inhibits the adsorption of arsenate (through electrostatic repulsive forces). A powerful permanent dipole can still interact with anions in a positive way through charge-dipole/ion-dipole interaction, respectively (Goswami et al., 2020). The specific adsorption mechanisms of biochar and modified biochar for heavy metals are shown below.

2.4.1. Surface Adsorption

Heavy metal ions can form specific metal complexes with a variety of acidic groups, such as carboxyl and phenolic hydroxyl, in water and soil to provide active adsorption sites that enable the surface adsorption of heavy metals. The primary deciding elements are the chemical bond on the biochar's surface, the diffusion action of heavy metal ions, and other variables (Tan et al., 2015). A large amount of oxygen-containing functional groups and minerals were present on the surface of the biochar gel generated from rice straw, which could be employed as an adsorption site for AS(III) and Cd(II). When (Qian et al., 2016) developed bio-char colloids using rice straw, they found that the main adsorption mechanism was that the biochar gel's surface was made of rice straw.

2.4.2. Electrostatic Adsorption

Electrostatic adsorption, which is necessary for establishing ionic bonding, can be affected by zeta potential and pH (Qian et al., 2016). Chen Zhuang et al. found that iron nitrate-modified reed biochar (FeBC) could remove As(V) at a rate of up to 94.52%. The main adsorption mechanism was the electrostatic adsorption of positive charges with As(V) and Cd(II) on the surface of the modified FeBC. (Qian et al., 2016).

2.4.3. Ion exchange

Ion exchange is essentially the exchange process between charged cations and protons on the surface of biochar and dis-solved heavy metal ions under suitable pH conditions (C. S. Zhu et al., 2019). Ion exchange is influenced by the type of functional groups on the biochar's surface, the size of the pollutants, and the nature of the charge. Because high concentrations of metal ions will compete with heavy metal ions, lowering the effect of ion exchange and preventing the adsorption of heavy metals, the effect of ion exchange is correlated with the concentration of metal ions on the surface of biochar (Alothman et al., 2015).

2.4.4. Chemical precipitation

OH^-, SO_4^{2-}, SO_3^{2-}, and CO_2^{2-}, anions present in carbon dioxide minerals, serve as many of the heavy metals' adsorption sites and mix with them to form water-insoluble precipitates (Alothman et al., 2015). High P, S, Si, and Al concentration in biochar's elemental composition may indicate that there are more mineral acid ions on its surface, which may help biochar be more effective at removing heavy metals.

Table 2.2: Adsorption mechanism of arsenite ion by biochar and modified biochar

Mechanism	Principle	Main Influencing Factors	References
Surface adsorption	✓ The biochar surface contains various acidic groups capable of forming specific metal complexes with heavy metal ions due to their presence in water.	✓ Surface chemical bond group ✓ Diffusion effect of heavy metal ions ✓ Temperature	✓ (Tan et al., 2015) ✓ (Qian et al., 2016)

Electro-static Ad-herence	✓ Ionic bonds, formed between anions and cati-ons	✓ Zeta potential ✓ pH value. ✓ Degree of dispersion	✓ (Qiaetal.,2016)
IonEx-change	✓ The charged cations and pro-tons on the sur-face of the bio-char exchange with the dis-solved heavy metal ions in an exchange reac-tion.	✓ Nature of the surface func-tional groups ✓ Size of the pollu-tants ✓ Live nature ✓ pH value	✓ (Alothman etal.,2015), (C. S. Zhu etal., 2019)
Chemical Precipitation	✓ Heavy metal ions and anions combine to gen-erate a precipi-tate that is insol-uble in water.	✓ pH value. ✓ Electrolyte con-centration ✓ Complexing ef-fect	✓ (Alothman etal.,2015)

Additionally, diffusion of the adsorbate into the sorbent and surface complexation with the phenolic hydroxyl groups on the paralyzed biomass surface are also regarded as significant mechanisms of the removal process (Niazi et al., 2018).

$biochar\ COO^- + H^+ \rightarrow biocharCOOH^+$ …… $(equ\ 2.1)$

$biochar\ COOH^+ + H_3A_SO_4 \rightarrow$ biochar $COO^- + H_2A_SO_4^- + H_2O$ …… $(equ\ 2.2)$

$H_2A_SO_4^{2-} \leftrightarrow HA_SO_4^{2-} + H^+\ pk_1 = 6.9$ …… $(equ\ 2.3)$

$biocharCOOH^+ + H_2A_SO_4^- \rightarrow biocharCOOH\ A_SO_4^- + H_2O$ …… $(equ\ 2.4)$

$biocharCOOH^+ + HA_SO_4^- \rightarrow biochar\ COO\ A_SO_4^-$ …… $(equ\ 2.5)$

The formation of condensed aromatic carbon as a result of structural orientation or distortion of the backbone ligno cellulosic structure is driven by negative surface charges with acidic functional groups like -COOH, -COH, and -OH, as shown by spectroscopic characterization of functionalized char materials (Amen et al., 2020). For the electrostatic interactions and covalent linkage involving arsenate and electron-donor chemicals, these functional groups are regarded as key reaction sites. Depending on the chain length of the microcrystalline cellulose agents, carbonization of the surface of biomass/agricultural waste materials at various pyrolysis temperatures results in an array of parallel hexagonal channels that supply 1.45-3.20 mmol g of charged electron exchange groups, such as laconic/Quinone group (Ngyuyen et al., 2019). The equivalent EDS spectra for char produced from rice straw with As immobilized showed mass changes of the minor elements, providing proof that As was adsorbed onto the char particles. Images clearly showed that anionic arsenic species were successfully immobilized on carbon-rich material, and that Mn, Ti, Mg, and Fe co-occurred on its smooth surfaces made up of intra- and intergroup cross-linking (Niazi et al., 2018).

2.5. Sugarcane Bagasse

The residue that remains from sugarcane after cane juice is extracted is known as sugarcane bagasse. Bagasse is a carbon-rich biomass, abundant and suitable for the manufacture of biofuel or biochar, like the majority of agricultural wastes. Numerous experiments have been conducted to investigate the possibilities of pyrolysing bagasse to produce biofuel (Inyang et al., 2020). Bagasse contains 25% hemicellulose, 25% lignin, and around 50% cellulose. Bagasse's chemical composition is approximately 50% cellulose, 30% pentosanes, and 2.4% ash. Due to its composition, SCB is a perfect material to use as reinforcement fibre in composite materials in order to produce new materials with unique physical and chemical properties (Inyang et al., 2019).

The numerous and diverse functional groups in lignocellulose matter act as a significant attractive force for the binding of polluting ions. The macromolecules that constitute bio adsorbents derived from sugarcane bagasse include lignin, cellulose, hemicelluloses, proteins, as well as humic and fulvic substances. These functional groups, which include OH^-, $COOH^-$, NH_2^- and OCH_3^- groups, act as adsorptive sites. Through ion exchange, adsorption, or the donation of electron pairs (complexation), these sites allow the bio adsorbents to draw in and bind polluting ions. Sugar-cane bagasse and its derivatives are particularly effective at removing pollutants because of the exist-

ence of such special binding sites and its high quantities of silica (10.3%). Additionally, its biological polymers, such cellulose and lignin, can give the newly developed adsorbent materials additional characteristics (Sarker et al., 2017).

According to (Sarker et al., 2017), sugarcane bagasse's ability to remove pollutants depends not only on the sorbent material's chemical composition but also on how it is morphologically organized. Bagasse fy ash and activated carbon derived from sugarcane bagasse are also efficient adsorbents which can remove a variety of contaminants from water, including metals, dyes, phenolic compounds, herbicides, and pesticides.

Sugarcane bagasse (SCB) is an inexpensive source of lignocellulosic biomass and a plentiful agro-industrial waste. Around the Wonji-Shoa, Metahara, and Finchaa sugar plants in Ethiopia, sugarcane is cultivated on around 33,777 ha of the country's land (Tena Gashaw et al., 2018). Currently, these companies produce 893,270 tons of Ethiopian sugarcane bagasse (ESCB) annually on average. Though some portion of it is burnt to provide energy and some, used as livestock feed, on an average, nearly 123,011 tons of surplus is to spare without any considerable application (Jabasingh & Ki, 2016). To remove any undesirable components, pretreatment of any lignocellulosic material is essential. The proper pretreatment method selection is influenced by the cellulose's inhibitory degradation (the slowing down of the degradation caused by the presence of lignin, extractives, and furan derivatives), operational costs, technical setup, and energy input (Jabasingh & Ki, 2016).

2.6. Methods of Biochar Production

Porous, carbon-rich biochar is produced when organic biomass is burned in the absence of oxygen at temperatures between 300 and 800 °C using feedstock from plants or animals (such as pinewood, oak wood, perilla leaf, and others) (Nhuchhen & Afzal, 2018). A non-living biomass removes arsenite from water during the adsorption process by physicochemical processes. Hydroxyl (-OH), carboxyl (-COOH), phenolic, amino ($-NH_2$), sulfhydryl (-SH), alcoholic, and ester groups are the primary functional groups present in bio char (Ali et al., 2020). On the surface of the biosorbent, several functional groups have a significant ability to remove As through processes such adsorption, complexation, ion exchange, diffusion, or co-precipitation. Traditional techniques like ion exchange, precipitation, membrane filtration, reverse osmosis, and electrodialysis are recognised as being harmful to the e nvironment(Ali et al., 2020). More biomass is being converted to biochar as a result of growing interest in using it for various applications. Pyrolysis, hydrothermal

carbonization, gasification, and torrefaction are examples of thermochemical conversion processes (Yaashikaa et al., 2020). The method of production must be appropriate for the type of biomass used, and the process conditions such as heating rate, temperature, residence time, etc. must be optimal for a maximum yield of biochar. Since the process involves the weight loss of the biomass, the form of biochar made from plant biomass varies depending on the conditions. Water loss around 100 ^{o}C initially caused weight loss, which was followed by cellulose, hemicellulose, and lignin degradation over 220 ^{o}C. The methods of thermochemical conversion and the circumstances surrounding the m are discussed.

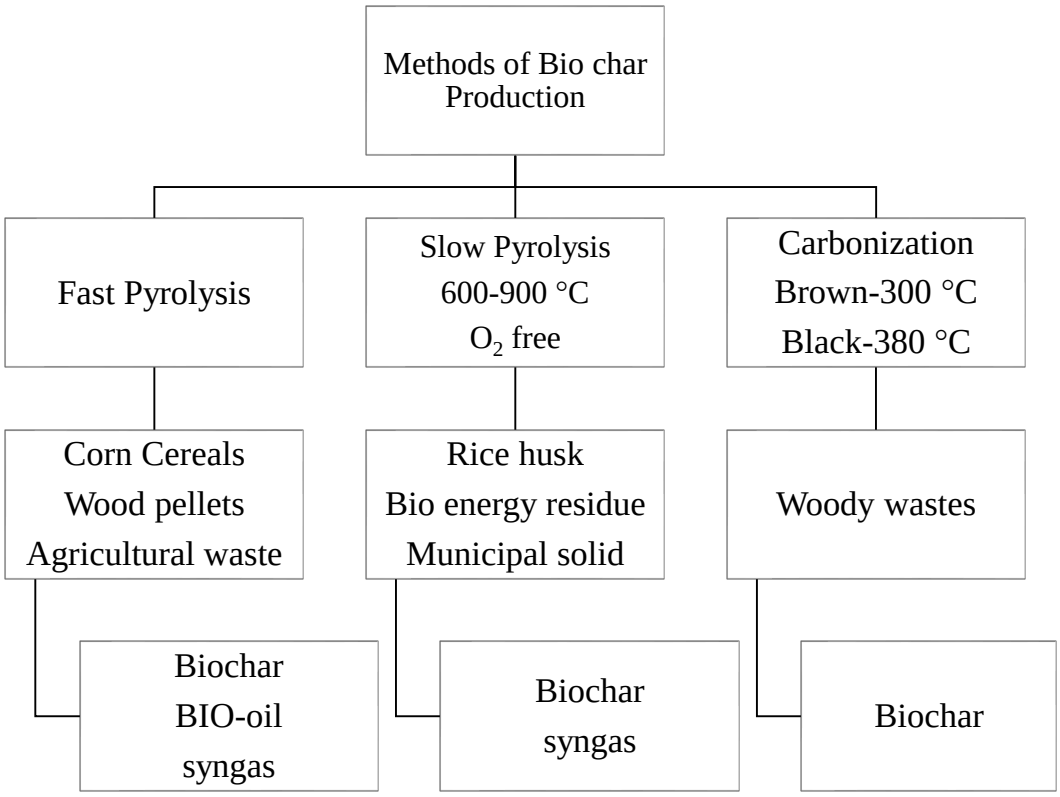

Figure 2.2: Methods of biochar production

2.6.1. Pyrolysis

Pyrolysis is the term for the thermal breakdown of organic compounds at temperatures between 250 and 900 ^{o}C in an oxygen-free environment (Yaashikaa et al., 2020). This method is an alternative method for converting waste biomass into products with added value like biochar, syngas, and bio-oil. The lignocellulosic ingredients, such as cellulose, hemicellulose, and lignin, go through reaction processes like depolymerization, fragmentation, and cross-linking at particular temperatures during the process, producing a variety of products in the form of solid, liquid, and

gas. Char and bio-oil are the products that are solid and liquid, whilst carbon dioxide, carbon monoxide, hydrogen, and syngas (C_1-C_2 hydrocarbons) are the products that are gaseous. For the production of biochar, a variety of reactors are employed, including agitated sand rotating kilns, bubbling fluidized beds, waggon reactors, muffle furnaces, and paddle kilns (Yaashikaa et al., 2020). Biochar is more widely accessible than other carbon compounds due to its large range of raw materials and straightforward preparation methods. Furthermore, biochar and its modified derivatives work effectively in a variety of water treatment fields, including adsorption, catalysis and membrane filtration (Jabasingh & Ki, 2016).

In general, as the temperature is raised during the pyrolysis process, the output of biochar drops and the production of syngas rises. Depending on the heating rate, temperature, residence time, and pressure, pyrolysis can be divided into fast and slow pyrolysis processes. Fast pyrolysis: Fast pyrolysis is considered to be a direct thermochemical process that has a strong potential for use in the production of liquid bio-oil from solid biomass. Fast warming rates of biomass particles (>100 C/min), short combining times of biomass particles and pyrolysis fumes (0.5-2 s) at high temperatures, and moderate pyrolysis treatment temperatures (400-600 ^{0}C) are all characteristics of fast pyrolysis settings. Slow pyrolysis: In slow pyrolysis, the heating rate is relatively low (about 5-7 C/min) and has a very slow reaction time (Yaashikaa et al., 2020). The majority of biomass is composed of cellulose, hemicellulose and lignin. These components are converted into biochar using different reaction conditions and mechanisms.

2.6.1.1. Cellulose decomposition

By decreasing the degree of polymerization caused by two processes, the mechanism of cellulose degradation has been identified: 1) Through slow pyrolysis, which involves cellulose degradation at a slower heating rate and a longer residence time 2) By fast volatilization, which results in the production of levoglucosan through fast pyrolysis, which takes place at a high heating rate. In addition to the solid result biochar, levoglucosan also goes through the dehydration process to generate hydroxymethyl furfural, which can break down to produce either liquid or gaseous products, such as bio-oil or syngas, depending on its state after decomposition (Shen & Gu, 2019).

2.6.1.2. Hemicellulose decomposition

Hemicellulose degradation processes are comparable to those of cellulose. Depolymerization of the hemicellulose results in the formation of oligosaccharides. Decarboxylation, intramolecular

rearrangement, depolymerization, and aromatization are some of the possible processes that could result in the production of biochar or the decomposition of the chemical into syngas and bio-oil (Al Arni, 2018).

2.6.1.3. Lignin decomposition

Contrary to the cellulose and hemicellulose decomposition mechanisms, the lignin decomposition mechanism is complex (J. Huang et al., 2012). Free radicals are produced when the -O-4 lignin bond breaks. By absorbing protons from different species, these free radicals form degraded compounds. Moving to different molecules, the free radicals start a chain reaction (J. Huang et al., 2012).

2.6.2. Hydrothermal Carbonization

Due to the ability to produce biochar at a low temperature of 180–250 ^{0}C, hydrothermal carbonization is regarded as a cost-effective approach (J. Huang et al., 2012). To distinguish the product produced from dry methods like pyrolysis and gasification, the product employing the hydrothermal process is referred to as "hydrochar (Fang et al., 2018). The biomass is mixed with water and put in a closed reactor during the process. For stability, the temperature is gradually raised. The following items are produced at various temperatures: Biochar below 250 ^{0}C is known as hydrothermal carbonization, biooil between 250 and 400 ^{0}C is known as hydrothermal liquefaction, and gaseous products are all produced at these temperatures. Hydrothermal gasification is the process of producing syngas at temperatures exceeding 400 ^{0}C, including CO, CO_2, H_2, and CH_4 (Q. Zhang et al., 2017).

The intermediate product, 5-hydroxymethylfurfural, and its derivatives are produced through a sequence of processes involving the hydrolyzed product, including dehydration, fragmentation, and isomerization. Additionally, the reaction produces the hydrochar through intramolecular dehydration, condensation, and polymerization (Q. Zhang et al., 2017). The mechanism is complicated by lignin's high molecular weight and complex structure. Starting with a dealkylation and hydrolysis reaction, lignin degradation results in phenolic compounds such phenols, catechols, syringols, etc. Repolymerization and crosslinking of intermediates form the char in the final stage. Similar to the pyrolysis reaction, the lignin components that are not dissolved in the liquid phase are converted to hydrochar (Bakraoui et al., 2020).

2.6.3. Torrefaction and flash carbonization

A recently developed method for producing biochar is torching. It uses a slow rate of heating, hence the term "mild." Utilising inert ambient air in the absence of oxygen at a temperature of 300 ^{0}C and a variety of decomposition processes, the oxygen, moisture, and carbon dioxide present in the biomass were eliminated (Yu et al., 2017). Biomass parameters like particle size, moisture content, surface area, heating rate, energy density, etc. are altered during the torrefaction process. Torrefaction can be carried out in one of two ways: (a) steam torrefaction, which uses steam to treat biomass at a temperature of no higher than 260 °C for a 10-minute period. (b) Wet torrefaction, also known as hydrothermal carbonization, occurs when biomass is in contact with water at a temperature of 180–260 °C for a period of 5–240 minutes. (c) Oxidative torrefaction: This method involves treating biomass with oxidising agents, such as gases used in combustion to produce heat energy. To create the necessary temperature, this heat energy is employed. An incomplete pyrolysis process serves as the torrefaction process' mechanism (Yu et al., 2017).

2.7. Factors Affecting Biochar Properties

Biochar is primarily produced as a result of the pyrolysis process' reaction conditions. The key determinants of biochar's attributes include feedstocks, temperature, particle size, heating rate, etc. Rather than affecting the quality of the biochar, these factors have an immediate impact on its output. Determining the application of biochar requires in-depth understanding of analysing biochar characteristics. Biochar has been produced using a variety of biomass from various sources, including plant matter, agricultural byproducts, biomass from wood, solid wastes, etc. (Yu et al., 2017).

2.7.1. Feedstocks

A complex solid material, biomass is made up of biological, organic, or inorganic components that were derived from living or non-living organisms. The two types of biomass are (i) woody biomass and (ii) non-woody biomass. Woody biomass primarily consists of forestry and tree leftovers (Tripathi et al., 2016). Low moisture, low debris, minimal voidage, high density, and calorific value are characteristics of wood biomass. Solid industrial, agricultural, and animal wastes are included in non-woody biomass. High debris, high wetness, high voidage, low density, and low calorific value are characteristics of non-woody biomass (Tripathi et al., 2016). The moisture content of a biomass feedstock has a significant impact on biomass development. Water vapour,

liquid water, and moisture adsorbed inside the biomass's pores are only a few of the different ways that moisture can be found in biomass. Higher moisture levels in the biomass significantly reduce char formation and increase the amount of energy required to reach the pyrolysis temperature (Jafri et al., 2018).

2.7.2. Carbonization temperature

The most well-known method for converting biomass into biochar through a thermochemical degradation process in an oxygen-free atmosphere at a high temperature is pyrolysis. Pyrolysis cycles can be divided into three basic categories depending on the circumstances: (i) Slow pyrolysis (temperatures below 300 0C), (ii) Moderate Pyrolysis (temperatures between 300 and 500 ^{0}C), and (iii) Quick Pyrolysis (temperatures above 500 ^{0}C). Biochar's physical-chemical characteristics and structure, such as its elemental composition, pore structure, surface area, and functional groups, are affected by the pyrolysis temperature (Jafri et al., 2018). Due to the influx of volatiles at high temperatures, pyrolysis temperature has an effect on these properties (Jafri et al., 2018).

2.7.3. Residence time

The production of biochar gradually decreased as the residence time at low pyrolysis temperature (300 ^{0}C) was extended, while pH and the number of biochars with iodine adsorption stayed reformist. However, increasing the residence time at high pyrolysis temperature (600 ^{0}C) had little effect on biochar yield or pH, while it decreased the number of biochars that were able to bind iodine (Dhyani & Bhaskar, 2018).

2.8. Methods of Modification of Biochar to Enhance Adsorption

Additionally, the adsorption of biochar can be considerably improved during or even after the initial production. As stated by (Rajapaksha et al., 2016), post-pyrolysis Ni/Mn modification can provide a larger adsorption capacity (6.52 g/kg) than pre-pyrolysis modification (0.549 g/kg). Depending on the target pollutant, a variety of approaches are employed to enhance SCB biochar adsorption, including chemical, physical, steam activation, gas purging, and impregnation of metals or their oxides (Rajapaksha et al., 2016). Chemicals such as acids, bases, and/or strong antioxidants like $KMnO_4$ and H_2O_2 are used to modify the functional groups on the surface of SCB biochar (Baltrnait 2018). Metal impregnation is another approach of chemical modification to get removal of inorganics and anions (Rajapaksha et al., 2016).

According to (P. et al., 2017), For eliminating significant inorganic loadings, chitosan and a number of metals (Mg, Mn, Fe, and Al) are extremely efficient modifications. The majority of investigations have focused on the impregnation of iron-based composites due to As's unique reactivity with iron. Despite the fact that some bio chars have extremely small surfaces, it has been found that treating iron considerably raises As removal rates (P. et al., 2017). The same biochar with $ZnCl_2$ has the highest removal rates, followed by NaOH, $FeCl_3$, $AlCl_3$, and KOH, in a comparison of different biochar modifications for the removal of arsenite (P. et al., 2017). When activating SCB biochar surfaces, physical alteration can also be accomplished by adding steam or air to generate a more porous structure (Braghiroli et al., 2018). In order to improve the sorption of anionic pollutants and to facilitate the recovery of contaminant-saturated biochar from treatment, the magnetic modification of SCB biochar is a more often used method (Braghiroli et al., 2018). A number of heavy metals and other extremely persistent substances, such as PFAs, can be efficiently adsorb by iron-enriched modifications because of their magnetic characteristics (P. et al., 2017). There are several approaches to modify the biochar some of them are listed bellow.

2.8.1. Chemical modifications

Chemical approaches for biochar alteration can entail a one-step modification or a two-step modification process. Both carbonization and activation are accomplished in a single phase when the activating chemical agent is present. Contrarily, in a two-step method, the biomass feedstock is first carbonised and then activated using the appropriate chemical agent or pre-treated before the carbonization process. Chemically modifying biochar can be done in a number of ways, some of which include:

2.8.1.1. Acid/base treatment and chemical oxidation of biochar

The physico-chemical characteristics of biochar can be significantly changed by acidic or alkaline modification. Increased O/C and H/C molar ratios after sulfuric acid treatment are examples of how the biochar modification results in more acidic functional groups on its surface. Increases in O/C and H/C ratios indicated that hydrophobicity had decreased (B. Li et al., 2017). The expansion of micropores into meso- or macropores caused by nitric acid treatment results in the formation of additional acidic functional groups in the resulting acidic modified biochar, including carboxylic, ketonic, hydroxyl, and other oxygen-containing moieties (Hadjittofi et al., 2014). As a result of the increased polarity, wastewater contaminants may be chemisorbed using biochar that has been

treated with acid. Biochar that has undergone alkaline treatment has a greater surface area and a higher surface aromacity ratio. Chemically modified biochar (H/C), which has a lower O/C value compared to acid-modified biochar, has a greater N/C ratio (Godwin et al., 2019). Low O/C ratio indicates that basic modified biochar's hydrophilic properties decreased as aromaticity increased. The surface of modified biochar and the modifying agents crosslink as a result of an increase in oxygen and nitrogen and a decrease in carbon (Godwin et al., 2019). The increased N/C ratio indicates that more nitrogen-containing groups, which are responsible for biochar's fundamental features, are present on the surface of modified biochar. This facilitates the sorption of organic contaminants and negatively charged ions from wastewater (Godwin et al., 2019).

2.8.1.2. Modification of functional groups (carboxylation and amination)

Chemical modifications can be performed on biochar's surface functional groups and hydrophilicity to meet specific needs, such as the adsorption of contaminants from contaminated groundwater and wastewater (Godwin et al., 2019). According to some reports, biochar generated at low temperatures between 250°C and 400°C has more C=C and C-H functional groups. Furthermore, chemical oxidation using H_2O_2, $KMnO_4$, HNO_3, H_3PO_4, or a mixture of HNO_3/H_2SO_4 has been used to introduce acidic functional groups, such as carbonyl, carboxylic, phenolic, and lactonic groups, onto the biochar surface at relatively low temperatures (Fu et al., 2019). It was discovered that the capacity of modified biochar for lead removal in packed columns was about 20 times more than the capacity of unmodified biochar. The column containing modified biochar was still very effective at removing lead and other heavy metal ions (such as Ni^{2+}, Cu^{2+}, and Cd^{2+}) from water flow in a multi-metal solution. The heavy metal ion adsorption sequence by the modified biochar was $Pb^{2+} > Cu^{2+} > Cd^{2+} > Ni^{2+}$, according to model results for the multi-metal system. Tetracycline adsorption was enhanced by the KOH modification because it increased the O-containing functional groups (O—H, C—H, C==O, and COOH) on the surface of biochar. O-containing functional groups on the surface of alkali-modified biochar made it easier for tetracycline molecules to create H_2 bonds with one another at neutral pH (Rajapaksha et al., 2016). It was determined that biochar may successfully remove tetracycline from wastewater. Additionally, alkali modification of BC can increase the biochar's capacity for adsorption. The main causes of the adsorption are hydrogen bonds and interactions (Rajapaksha et al., 2016).

2.8.1.3. Treatment with organic solvents

Another practical approach for increasing the amount of carboxylic functional groups on the surface of biochar is to modify it using acidified methanol. After esterification, the carbonyl groups in the biochar react directly with the methanol, modifying the biochar (Godwin et al., 2019). (Godwin et al., 2019) examined how well methanol-modified biochar attracted tetracycline (TC) from aqueous solutions. They added methanol to rice husk biochar to improve its TC adsorption capabilities and lower its natural amount of organic compounds. According to their findings, methanol-modified biochar outperformed virgin biochar in terms of adsorption capacity in 12 hours and equilibrium time by 17.2% and 45.6%, respectively. Additionally, they discovered that methanol-modified biochar had more hydroxyl and ester functional groups (O-containing groups) than pure biochar, which has an impact on the electron-donor-acceptor interactions between the biochar surface and the TC.

2.8.2. Magnetization of Biochar

To improve the adsorption capacity of biochar, numerous studies has been conducted. However, because of the small particle sizes and lower density, the separation and reuse of biochar after the removal of water pollutants remains one of the significant problems that has to be solved (Yi et al., 2020). To produce magnetic materials, the three processes of calcination, co-precipitation, and pyrolysis are generally used (Feng et al., 2021).

2.8.2.1. Impregnation pyrolysis

By impregnating biomass with a solution containing transition metal salts, removing the solvent, and then paralyzing the dried residue in a muffle furnace with a limited amount of oxygen or an inert atmosphere, magnetic biochar can be produced (Yi et al., 2020). As a result, pyrolysis and magnetization are completed in a single process, allowing the operating parameters (such as pyrolysis temperature, inert gas, and pyrolysis duration) to be used to precisely manage the physico-chemical properties and adsorption capacity of the magnetic bio-char (H. Yang et al., 2019). According to, the As(V) adsorption potential of magnetic biochar produced at various temperatures (400-800°C) ranged from 182.32 to 223.21 mg/g and was proportional to the pyrolysis temperature (Liu et al., 2019). Moreover, the species of iron oxides in formed in magnetic biochar are affected by the pyrolysis temperature. According to (Wang et al., 2020) studies, magnetic biochar's iron

oxide composition changed as the pyrolysis increased. In that order of temperature of formation, these oxides are zero-valent iron, hematite, magnetite, wustite, and others.

2.8.2.2. Co-precipitation

Biochar must first be dispersed into a solution containing transition metals in order to create magnetic biochar by co-precipitation. Following that, a certain amount of sodium hydroxide or ammonium hydroxide solution must be added, and the mixture must then be agitated for a period of time at pH 9 (Feng et al., 2021). By draining the supernatant, washing the residual material, and drying it, magnetic biochar is produced. This procedure, which is more complex than the impregnation-pyrolysis method but more regulated, enables the magnetic medium to be strongly bound to the biochar matrix (Yi et al., 2020). (L. Zhou et al., 2015) showed that the adsorption capacity for arsenic of magnetic biochar produced by co-precipitation was around seven times lower than that of magnetic biochar produced via impregnation-pyrolysis. However, it has been noted that magnetic biochar made through impregnation-pyrolysis removes fluoride more effectively than magnetic biochar made through co-precipitation. Prior to the synthesis of magnetic biochar for pollutant removal, target pollutant characteristics should be taken into account in order to enable the selection of the appropriate synthetic procedure.

2.8.2.3. Reductive co-deposition

While the reductive co-deposition process is similar to co-precipitation, it varies in that when transition metals are mixed with biochar, reducing agents such sodium borohydride or potassium borohydride are used to reduce the transition metals. After the reaction, the supernatant is taken out, and the remaining material is cleaned and dried under a vacuum to produce magnetic biochar. Impressively, this material contains largely zero-valent metals and nanoparticles, which makes the magnetic biochar strongly reducing and enhances its ability to remove pollutants (Yi et al., 2020). For example, (Zhou et al., 2021) observed that the majority of the Cr(V) had been converted to As(III) and that reductively co-precipitated magnetic biochar had an AS(V) adsorption capacity of 58.82 mg/g. This approach may have some safety concerns, especially if used at scale, since dangerous reductants are needed and hydrogen is generated during the reduction process. This technique enables the production of magnetic biochar with improved pollutant-removal efficacy (Yi et al., 2020).

2.9. Point of zero charge (PZC) of magnetic biochar

The physicochemical properties of magnetic biochar are also significantly influenced by pH, which affects both the type of impurities present and the surface charge of the materials (Yi et al., 2020). There are two primary methods for measuring the PZC of magnetic biochar: 1) measure the zeta potential of the magnetic biochar at different pH values, and then linearly fit these measurements to determine the pH at which the zeta potential is 0, which is denoted PZC (Yi et al., 2020). 2) immerse samples of the magnetic biochar in a range of NaCl solutions with varying PH, allow these mixes to react at a steady temperature for a period of time, and then measure the pH difference between the starting pH and the end solution pH (Y. Huang et al., 2020).

It has been confirmed that most biochars are negatively charged, and that the magnetization of biochars often changes their surface charge or even PZC. For example, (Oladipo et al., 2017) observed that a specific biochar's PZC was 7.30 while its magnetic derivative's PZC was 8.30. The PZC of magnetic biochar will also change with further alteration; for example, (Sun et al., 2019) observed a PZC change of 6.78 to 8.51 after a magnetic biochar was treated with potassium. A wide range of PZC values (2.4 to 9.81) (Sun et al., 2019) have been reported for magnetic biochar by different researchers. The main reasons for this wide range can be attributed to: the different methods for synthesis of magnetic biochar, the different raw materials used for magnetic biochar, the different physicochemical properties of magnetic biochar.

2.10. Biochar characterization techniques

Recent studies have shown the importance of detailed biochar characterizations in determining its economic and environmental uses and distinguishing it from other organic matter that performs related tasks, such as soil enhancement or environmental applications (Jeffery et al., 2011). Biochar has a wide range of uses depending on its characteristics, including its specific surface area, surface functional groups, stability, and structure, as well as, to a lesser extent, its elemental complexion (Y. Zhou et al., 2021). Choosing the appropriate characterization techniques for biochar is both very intriguing and difficult as a result of these qualities. Prior to any intended applications, a biochar's careful and thorough characterization requires an understanding of the connection between the circumstances of its production and its physiochemical properties (Patel et al., 2021). Four broad categories can be used to group SCB biochar's characteristics: 1) chemical properties (chemical composition, functional groups, pH, and ion exchange capacity,

physical properties (porosity, pore size distribution, specific surface area, structural properties, including surface and morphology) and thermal stability properties.

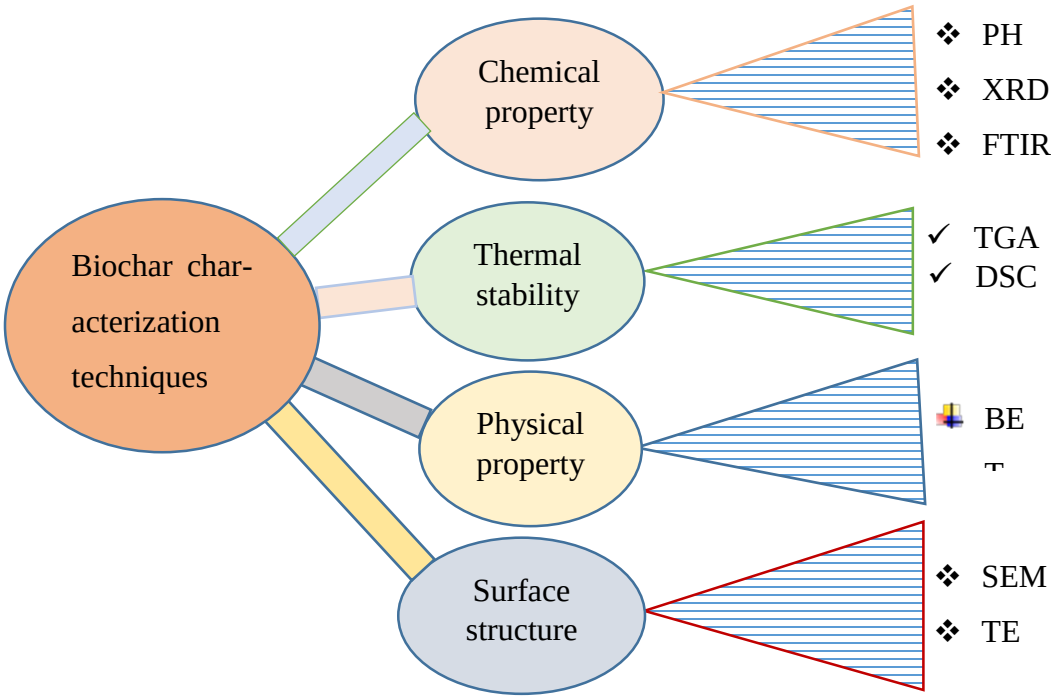

Figure 2.3: Classification of characterization techniques versus biochar properties

2.11. Adsorption Equilibrium Isotherms

Isotherm refers to the relationship between the equilibrium adsorbate concentrations in the liquid-phase and the equilibrium adsorption amount on the solid-phase at a certain temperature. Sorption equilibria deliver fundamental physicochemical data for assessing the relevance of sorption processes as a unit operation. Sorption equilibrium is normally described by an isotherm equation whose parameters express the surface properties and affinity of the sorbent, at a constant temperature and pH. Therefore an accurate mathematical description of the equilibrium isotherm, preferably based on a correct sorption mechanism, is essential to the effective design of sorption systems (Ho et al., 2002). We can model the equilibrium adsorption data by the isotherms, and investigate the adsorption information, such as the adsorption mechanisms, the maximum adsorption capacity, as well as the properties of adsorbents by the isotherms (J. Wang & Guo, 2020). According to the paper, studied by (Berkessa et al., 2019) adsorption isotherm can be described as a curve that explains the phenomenon governing the retention (release) or mobility of a substance to a solid at constant temperature and pH in an aqueous porous medium or aquatic environment.

Adsorption isotherm gives an idea about relation between the adsorbate and the extent of adsorbate adsorbed on the surface of adsorbent at fixed temperature (Mor et al., 2016). The adsorption equilibrium has continuously been clarified by the isotherm equations such that their parameters demonstrate the surface characteristics and affinity of the adsorbent toward the adsorbate (Ghadiri et al., 2017). The two popular isotherms are Langmuir and Freundlich isotherms which have been used to explain the equilibrium of an adsorption system (Nsami & Mbadcam, 2013).

2.11.1. Langmuir Isotherm

Langmuir isotherm decides the adsorption of ions on the surface of the adsorbent on the monolayer and comparable destinations on the surface (Mor et al., 2016). According to Langmuir isotherm, assumptions can be taken based on adsorption that occurs at specific homogeneous sites within the adsorbent (Nsami & Mbadcam, 2013).

2.11.2. The Freundlich Adsorption Isotherm

The Freundlich isotherm is an empirical equation employed to describe the heterogeneous system. This empirical model can be applied to non-uniform surface adsorption heat and non-uniform distribution of affinity and multi-layer adsorption. Historically, this was developed for the adsorption of animal charcoal, and indicates that the proportion of adsorbed water in the adsorbent in a given mass of solute is not constant at other solution concentrations. From these perspectives, the amount adsorbed is the sum of the adsorptions of all sites with their respective binding energies until the adsorption energy decreases exponentially when the adsorption process is complete, and the stronger binding sites are occupied first (Foo & Hameed, 2010).

At present, Freundlich isotherm is universally applied in varied systems especially for organic syntheses or considerably interactive species on triggered carbon and molecular sieves. The slope ranges between 0 and 1 is a measure of adsorption intensity or surface viciousness, turning better heterogeneous as its value gets closer to zero. Whereas, a value below unity implies a chemisorption process where 1/ n above one is indicative of collaborative adsorption (Ho et al., 2002).

2.12. Adsorption Kinetics Studies

Adsorption kinetics reflects the evolution of the adsorption process as a function of time. This is an important parameter to consider when choosing an adsorbent. Fast adsorption is recommended for treatment methods that use adsorption as a purification process. Several models have been

developed that describe the diffusion of solutes on the surface of particles and within pores (such as film distribution models, intra-particle diffusion models, out-of-particle diffusion models, and pore diffusion models). In the case of nitrates removal, simplified models such as pseudo-first-order kinetics and pseudo-secondary kinetics were common (Battas et al., 2019).

The adsorption dynamic is one of the foremost imperative issues for understanding both the mechanisms of adsorption and the evaluation of persuasive factors on the reaction rate. Kinetics explains solute take-up rates additionally characterize the residence time of the adsorbate at the solid-liquid interface. Kinetic modeling was used to investigate the adsorption mechanism and potential velocity control processes (Ghadiri et al., 2017)**.**

2.13. Adsorption Thermodynamics

Another important factor characterizing adsorption is the enthalpy of adsorption. During adsorption, the residual forces on the surface always decrease. In other words, the surface energy, which appears as heat, is reduced. Therefore, adsorption is always an exothermic process. That is, the enthalpy of adsorption (ΔH) is always negative. When a gas or liquid is adsorbed, the freedom of movement of its molecules is limited. This corresponds to a reduce in entropy of the adsorbed molecule after adsorption. For the process to be spontaneous, the thermodynamic requirement is that ΔG, must be added at a constant temperature and pressure, i.e. the Gibbs energy decreases. According to the equation, $\Delta G = \Delta H - T\Delta S$, if ΔH has a sufficiently high negative value - ΔG can be negative because TΔS is positive. Therefore, the spontaneous adsorption process is a combination of these two factors is added ΔG. As adsorption proceeds, ΔH becomes increasingly negative, eventually ΔH becomes equal to TΔS, and ΔG becomes zero (Ibrahim & Bsharat, 2018).

Generally, these parameters indicate whether the adsorption process is spontaneous as well as it also indicates whether it is exothermic or endothermic. The standard enthalpy changes (ΔH^o) in the adsorption process are: (i) Positive values indicate that the process is endothermic in nature. (ii) Negative values indicate that the process is heat generating in nature and that the amount of heat given when the metal ions on the adsorbent surface bind are released. This can be obtained with an adsorption rate (Cads) vs. temperature (T) plot. The adsorption rate increases as the temperature rises. This shows the endothermic process and the reverse phenomenon of fits. When the value of (ΔS^o) becomes positive, it shows an increment of the degree of freedom (or disorder) of the adsorbed species (Al-anber, 2011).

2.14. Factors Affecting the Arsenic Removal Efficacy

2.14.1. Effect of biochar dose

The amount of adsorbent used will change the equilibrium between the adsorbent and heavy metals, which will change how effectively the heavy metals are removed (Wu et al., 2018). For the most effective removal of As from water, bio-char must be used at the right dosage. Increasing the dose of biochar over the ideal level can decrease the effectiveness of its sorption (X. Chen et al., 2017). For the modified Cassia fistula (golden shower), a higher dose of biochar is used. 1 to 8 g/L of bio-char to remove As in batch experiments, from water (Alam et al., 2018). According to their research, the modified C. fistula bio-char's As removal effectiveness increased with doses up to 4 g/L (79.6%) for As(V) and 6 g/L (74.5%) for As(III) (Alam et al., 2018). The effect of Fe-modified corn straw (CS-Fe) biochar dosage on the ad-sorption of As(III) in aqueous solutions was investigated by Fan et al. in 2019. According to their findings, increasing the amount of CS-Fe biochar from 0.4 to 5 g/L increased the As(III) removal percentage (2.2 to 96%); however, continuing to raise the amount of biochar had no discernible impact on the removal percentage of As(III). The removal effectiveness of As by various biochars is dependent on the dose of biochar and can increase with the dose of biochar up to an optimal limit, after which there is no influence on As sorption. This might be partially caused by the saturation of biochar surface pores or binding sites with fine biochar particles in a closed batch system, reducing the surface area and limiting biochar's capacity to bind As and other PTEs (Amen et al., 2020).

2.14.2. Influence of solution pH

The solution pH has a significant impact on the protonation and deprotonation of functional groups on the surface of biochar, as well as the speciation and aqueous chemistry of arsenic in an aqueous medium (Hashimi et al., 2022). The pH is correlated with the H^+ concentration in the water. The concentration of H^+ in the solution has a major role in determining the adsorption mechanisms, particularly ion exchange and electrostatic contact (Xiao et al., 2022). A solution with a low pH has a larger concentration of H^+, which increases the likelihood that H^+ may interact with positively charged metal ions. Additionally, a high concentration of H^+ will encourage the protonation of the biochar adsorbent's surface (NH_2, OH), which will raise the positive charges on the adsorbent. Electrostatic repulsion will occur as the adsorbent's surface is protonated, allowing the negatively charged metal ions ($HCrO_4$) to be adsorbed at the surface of the biochar adsorbent (L. Li et al.,

2020). Niazi et al. investigated the effect of pH on the removal percentage of As(III) and As(V) from perilla leaf biochar that was pyrolyzed at 300°C and 700°C. They found that increasing the pH from 3.2 to 9.1 increased the removal percentage of As(III) (55-90%) on BC700. Between pH 7.2 and 9.1, the maximum As(III) removal percentage (88–90%) by BC700 is seen (Amen et al., 2020). However, BC300 in the acidic pH range (pH 3.0 to 6.2) only detects a relatively low clearance of As(III) (77%). At pH 7.2 in solutions, when(III) removal is at its maximum rate (79%), however when pH rises from pH 8 to pH 10, As(III) removal significantly declines (from 73% to 60%) (Amen et al., 2020).

2.14.3. Initial concentration of Arsenic

Another crucial element influencing the elimination of contaminants is the initial concentration. The adsorption capacity of arsenic increases from 0.67 mg/g to 8.70 mg/g when the initial of arsenic concentration is raised from 3 mg/L to 60 mg/L, whereas the removal efficiency of arsenic decreases from 88.92% to 58.00%. These factors could be reasons for this: 1) A decrease in arsenic adsorption can indicate that there isn't sufficient space to accommodate the high initial concentrations of arsenic. 2) The initial concentration increase enhanced the concentration gradient's mass transfer driving power, encouraging additional arsenic to migrate to the biochar surface (Tomczyk et al., 2020).

2.14.4. Contact Time

More complete adsorption results from longer residence times. As a result, it's important to understand how long it took to finalize the settlement to gain insight into the settlement process. Additionally, it offers details on the minimal amount of time needed for significant adsorption to happen and potential adsorbent diffusion control mechanisms (Al-anber, 2011). Adsorption is expected to be significantly influenced by contact time. According to the literature review, longer contact periods result in increased removal efficiency. This is because the solid and liquid are in contact for a longer period of time, allowing the medium and adsorbate to interact more effectively (Nabhan, 2019). To estimate the equilibrium time at 150 revolutions per minute, 100 ml of the test solution containing 5.14 mg/L As(III) in a dose of 20 g SWR is adsorbed by increasing the contact time from 0 minutes to 120 minutes while agitating the mixture in a 250 ml plastic bottle. The findings demonstrated that the arsenic removal rate increased over time, peaked at 60 minutes (0.071 As(III) mg/g), and subsequently stabilized (Berkessa et al., 2019).

2.14.5. Effect of competitive ions

Numerous anions interact with arsenic species in natural groundwater. By competing with arsenic for adsorption sites, these anions can hinder the removal of arsenic through adsorption. Among them are the anions phosphate, sulphate, and silicate, which are frequently found in most types of drinking water and ground water in vast excess to arsenic (Amen et al., 2020). The media capacity for As(V) purified volume reduces to 3700 BV and 1800 BV, respectively, as the SiO_2 content in the challenge water rises to higher values of 40 ppm and 80 ppm. When treated water lacks SiO_2, the hydrous zirconium oxide capacity on As(V) significantly rises (up to 25,000 BV) (Amen et al., 2020). Silica may have such a substantial adverse influence on arsenic adsorption due to two reasons that frequently act together. First off, challenge water has a silica content that is hundreds of times more than that of As(V), and given that silicate has a strong affinity for it, its adsorption is of a similar order of magnitude to that of arsenic. Silicate can thus compete for and occupy the majority of active adsorption sites. The second factor is silica's surface blockage. The existence of soluble silica in the form of meta- (SiO_3^{2-}) or ortho-silicates (SiO_4^{4-}) and their strong propensity to polymerize over a wide pH and concentration range are well known facts (Hao et al., 2018).

As an adsorbate, phosphorus and arsenic are close competitors. The comparable chemistry of the two compounds, namely the pKa-values of arsenic acid and phosphorous acid, is assumed to be the cause of the similarly high competition between phosphoric and arsenic anions. Additionally, hydrogen carbonate (HCO^{3-}) and fluoride, which have also been looked into, are cited as potential adsorption competitors (Shankar et al., 2014). When contrasted to the large concentrations frequently seen in natural water, hydrogen carbonate demonstrates that the material can be a formidable competitor for adsorption sites even if it does not at all have an adsorption capacity comparable to that of arsenite or arsenate. Since the ions in fluoride are tiny anions that are isoelectric with the hydroxide anion, it is anticipated that they will form potent inner-sphere surface complexes that will affect the adsorption of arsenate (Shankar et al., 2014).

2.15. Regeneration of biochar-based adsorbents

Regeneration of biochar adsorbent is an inverse adsorption process. Adsorbent regeneration is necessary for the adsorption cycle to function more effectively. As a frequent adsorption and desorption process, a good adsorbent would have a high capacity for reuse and recycling for industrial applications and may significantly lower the cost of biochar adsorbents (S. ye Wang et al., 2015).

The fact that the adsorption regeneration procedure can be repeated several times suggests that the adsorption effectiveness may marginally decline during the regeneration phase. The amount of cycles the biochar goes through frequently lowers adsorption effectiveness (S. ye Wang et al., 2015). After four sorption/desorption cycles for the elimination of As(III), using NaOH solution as an eluent, the reusable nature of goethite-modified biochar is evaluated (Shankar et al., 2018). After the first cycle, As(III) removal percentage was 98%; however, it slowly fell to 86% in the fourth cycle. This modest decline in As sorption may be caused by goethite particles being dissolved from the surface of the biochar by washing with NaOH (Shankar et al., 2017). Adsorbate desorption and adsorbate decomposition are the two types of regeneration. Thermal regeneration, solvent regeneration, microwave radiation regeneration, and supercritical fluid regeneration are a few strategies for regeneration (Shang et al., 2015). Elutants must be chosen correctly for effective desorption, which heavily depends on the type of bio sorbent and the method of bio sorption. Elutants must not harm biochar, be reasonably priced, and be environmentally sustainable (Das, 2010). For the desorption of contaminants from magnetic bio-sorbents, low concentrations of acids or bases (0.1–0.2 M) are recommended. According to published investigations, HCl, HNO_3, H_2SO_4, EDTA, $Ca(NO_3)_2$, NaOH, and $NaNO_3$ were tried as reagents for the regeneration. It was discovered that As could be removed from magnetic sorbents using 0.5 M NaOH, with HCl, HNO_3, and H_2SO_4 acting as better eluents (Baig et al., 2014).

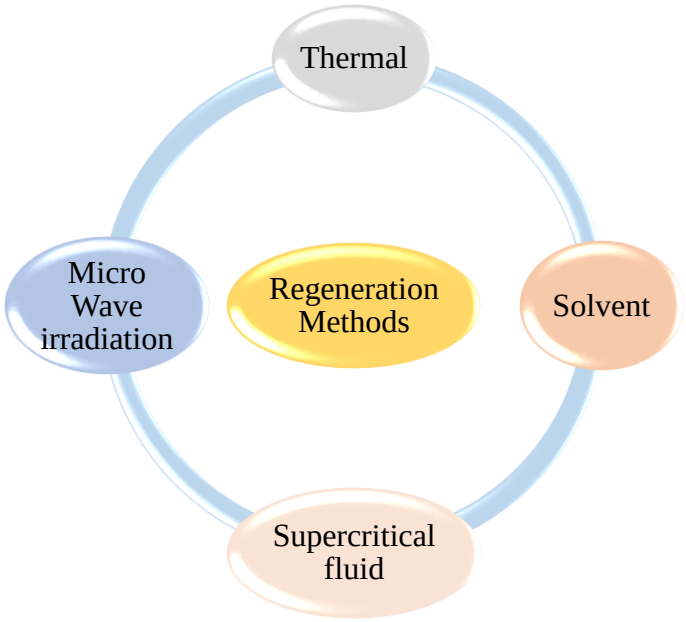

Figure 2.4: Methods of adsorbent regeneration

2.15.1. Thermal regeneration

One of the most efficient ways to produce desorption is thermal regeneration. Adsorbate is eventually reduced to a size smaller than the pore size of biochar after being carbonized and degraded at high temperatures (Dai et al., 2019). With the increase of pyrolysis temperature, the regeneration efficiency increased. The Entero-morpha prolifera biochar regenerated at 80 ^{0}C, 150 ^{0}C and 200 ^{0}C retained 35.00%, 45.00% and 48.00% of the initial pyrene uptake, while the regeneration rates of benzoapyrene were 31.00%, 41.00% and 40.00% respectively (Dai et al., 2019). The study demonstrated that thermal treatment might be used to eliminate dissolved organic carbon (Dai et al., 2019).

2.15.2. Solvent regeneration

Solvent regeneration breaks the adsorption equilibrium by altering the temperature and pH of the solvent in order to desorb the adsorbate from activated carbon. It does this by using the equilibrium relationship between biochar, solvent and adsorbate. Solvent regeneration is an excellent technique to take into consideration for organic matter adsorbents with high concentration and low boiling points (Dai et al., 2019).

2.15.2.1. Regeneration by inorganic chemicals

It refers to the process of removing adsorbate, also known as the acid-base regeneration method, using inorganic acids (such as hydrochloric acid and sulfuric acid) or alkalis, such as sodium hydroxide, and other chemicals. For instance, phenol adsorbed at high concentrations on charcoal is desorbed and recovered as sodium phonolite after being rinsed with sodium hydroxide solution (Kulikov & Novikov, 2017). Regeneration conditions are mild, inorganic chemicals are inexpensive, but treatment times are long and regeneration effectiveness is typically less than 80% (Dai et al., 2019).

2.15.2.2. Regeneration by organic solvent

The adsorbents obtained from organic solvents such benzene, acetone, and methanol were adsorbed on activated carbon. Adsorption is based on the similarity and integration principles (Kulikov & Novikov, 2017). With the aid of carbon adsorbate, 60.00% acetone has a desorption efficiency of 52.00% for yellow dye in water and 40.00% isopropanol has a desorption efficiency of 54.00% for red dye (Lu et al., 2017).

2.15.3. Microwave irradiation regeneration

By exposing biochar to microwave radiation, polar material molecules are encouraged to create polarized dipoles. The electromagnetic field can also be converted into heat energy concurrently. Heat is applied to cause the organic material trapped in the pore to volatilize. Biochar may be heated uniformly inside and out using microwave technology. Because the deposited adsorbates inside the carbon matrix did not exhibit much breakdown under microwave heating compared to conventional heating methods, the porous structure was better retained. Heating can breakdown and desorb the organic material in the pores of biochar. This heating technique demonstrated a more effective heating procedure for the ease of heat control (Dai et al., 2019).

2.15.4. Supercritical fluid regeneration

By altering the operating pressure, the supercritical fluid is employed as an extracting to achieve the separation. CO_2 is the most popular supercritical fluid. The advantages of supercritical fluid regeneration include a brief working cycle, a low operating temperature, and little biochar loss. Adsorbate can be recovered without having its chemical or physical characteristics altered. However, it has a high equipment cost and pressure resistance. It is only at the experimental stage right now (Dai et al., 2019).

CHAPTER THREE

MATERIALS AND METHODS

3.1. Chapter Overview

This chapter aims to present the materials used, sample preparation methods, and proper characterization techniques followed for various experiments that were performed in this research work. For simplicity, the utilized materials, experimental protocols, and characterization techniques were categorized into three sections. The first section describes the preparation of sugarcane bagasse biochar and modification of sugarcane bagasse biochar by iron chloride hexahydrate; The second section describes the characterization of sugarcane bagasse biochar and $FeCl_3.6H_2O$ modified sugarcane bagasse biochar; The third section describes studding of adsorption parameters through batch experiment. The fourth section describes studding of adsorption isotherm and kinetics of arsenite on $FeCl_3.6H_2O$ loaded sugarcane bagasse biochar adsorbent.

3.1. Materials, Chemicals and Reagent

The materials and reagents which were utilized in this research are listed as follows:

Table 3.1: List of Materials chemicals and reagents

Procedure	Chemicals	Equipment's
Preparation and modification of sugarcane bagasse biochar	$FeCl_3.6H_2O$, distilled water	Muffle furnace, vacuum filter, filter pa per, magnetic stirrer, beaker, Measuring cylinder, crucible, petri dish, electrical grinder, sieve, PH meter, conical flask and oven.
PZC determination of $FeCl_3.6H_2O$ loaded SCB biochar	Sodium Nitrate, distilled water, NaOH and HCl	Water bath, balance, PH meter, beaker, vacuum filter, conical flask and glove
Batch adsorption experiment	Arsenic trioxide, NaOH and HCl	agitator, PH meter, vacuum filter, Beaker, volumetric flask,

Kinetics and Isotherm experiment	Arsenic trioxide, NaOH and HCl	Beaker, agitator, PH meter, vacuum filter,
Co-existing ion experiment	KH_2PO_4, Arsenic trioxide, NaOH and HCl, Na_2CO_3, H_2SO_4	Beaker, agitator, PH meter, vacuum filter,

3.2. Methods

3.2.1. Preparation of sugarcane bagasse (SCB)

Sugarcane bagasse (SCB) was used as the primary adsorbent in this study, the SCB samples were collected from Wonji sugar factory, Oromia, Ethiopia. The SCB was manually stripped, dried for three days in the hot sun, and then the bagasse was cut into smaller pieces and heated in a hot air oven for several hours at 105 °C until the constant weight of the adsorbents was not reached. Using an electrical grinder, the dried SCB was further ground to a 4 mm particle size. The powdered bagasse was soaked and rinsed with distilled water to eliminate any remaining particulates or foreign particles. It was then further dried at 80 ^{0}C in an oven for 24 hours (Divband Hafshejani et al., 2016).

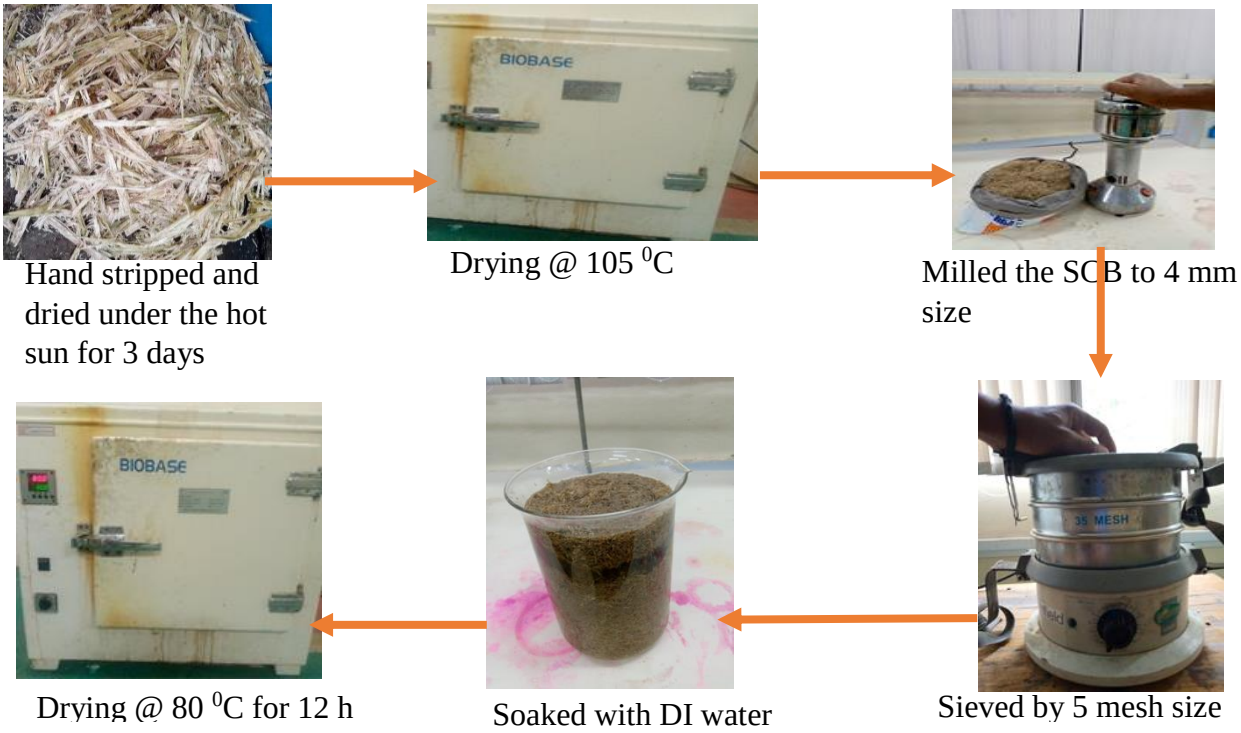

Figure 3.1: Preparation of Sugarcane bagasse

3.2.2. Pyrolysis of Sugarcane Bagasse (SCB)

The pyrolysis of SCB was conducted at 450 °C for 1 h in a muffle furnace. SCB Biochar produced from the pyrolysis was gently crushed and sieved into two size fractions: less than 0.5 and 0.5-1mm Only the latter was used in this experiments to minimize the presence of residual ash particles. The samples were also repeatedly washed with DI water to eliminate contaminants, and they were oven dried for 12 hours at 80 °C (Toscano Miranda et al., 2021).

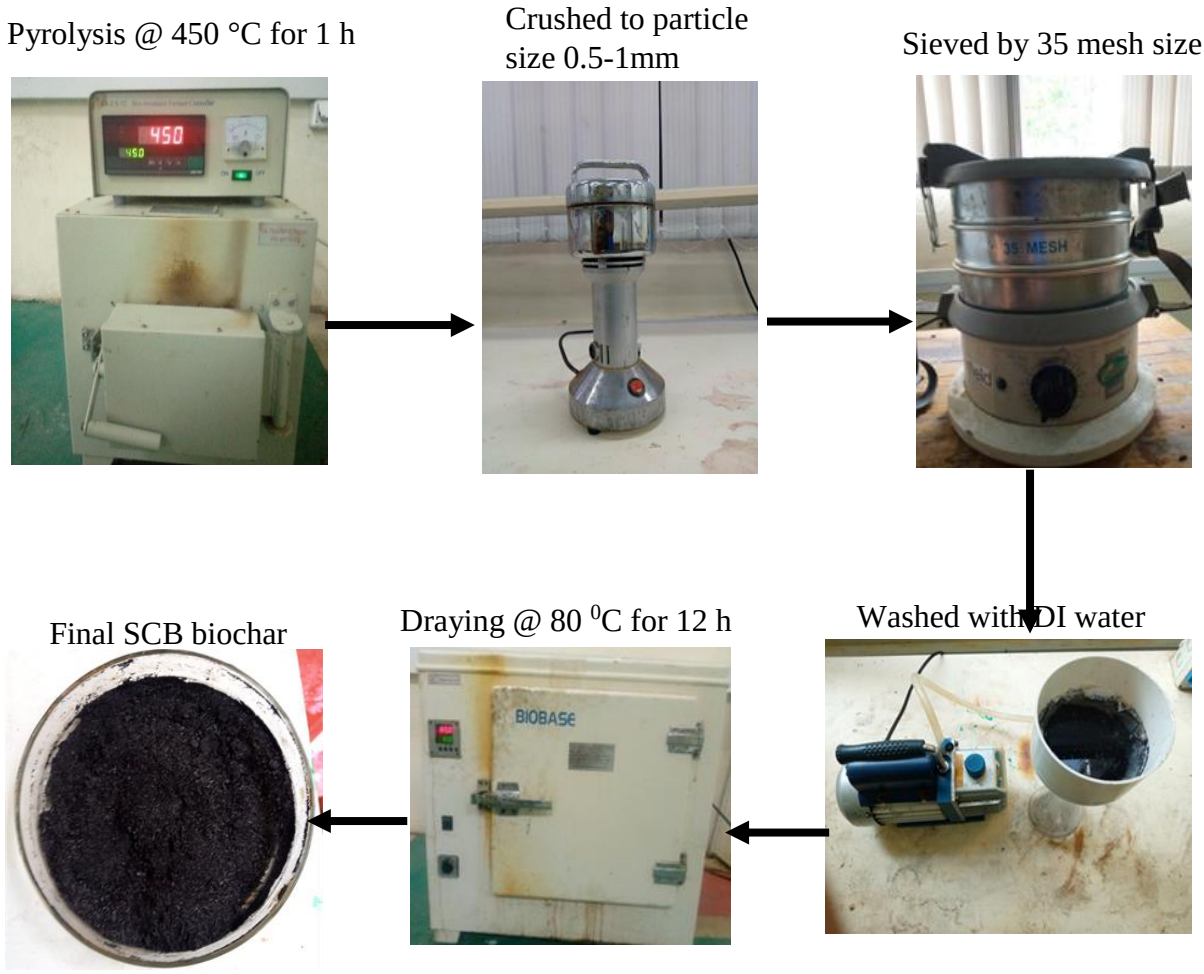

Figure 3.2: Pyrolysis of SCB at 450 ^{0}C for 1 h

3.2.3. Modification of sugarcane bagasse biochar by $FeCl_3 \cdot 6H_2O$

$FeCl_3 \cdot 6H_2O$ loaded SCB biochar were produced using impregnation method according to (Y. Chen et al., 2023) as shown in Figure 3.3. To introduce Fe particles onto SCB biochar 20 g of dried SCB biochar was immersed into 300 mL of 0.5 M $FeCl_3 \cdot 6H_2O$ solution and to achieve a homogeneous mixture, the system was stirred continuously using a hot plate magnetic stirrer for 24 h at room

temperature. The $FeCl_3 \cdot 6H_2O$ modified sugarcane bagasse biochar was separated from the mixer by filtration and washed with deionized water several times. Consequently, the $FeCl_3 \cdot 6H_2O$ modified SCB biochar was dried out in an oven at 80 °C for 12 h. The final products were sealed in a glass container before use.

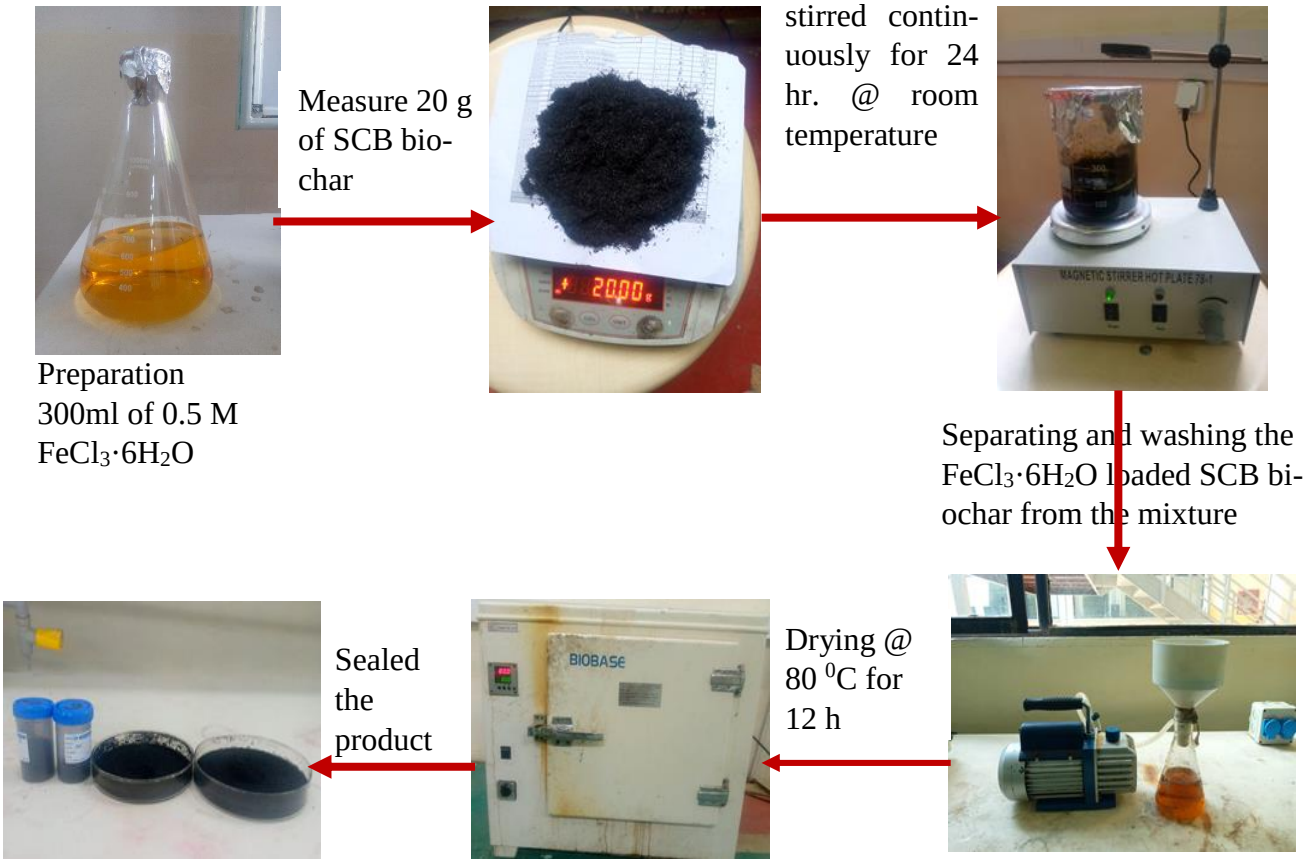

Figure 3.3: Modification of SCB by $FeCl_3 \cdot 6H_2O$

2.3.4. Determination of point Zero charge (PZC) of $FeCl_3 \cdot 6H_2O$ loaded SCB biochar

The point zero charge of $FeCl_3 \cdot 6H_2O$ loaded SCB biochar was determined using Salt addition method according to (Divband Hafshejani et al., 2016) method as shown in Figure 3.4: a series of 250 ml conical flask were filled with 50 ml of (0.1M) $NaNO_3$ solution to determine the pH value at the point of zero charge of $FeCl_3 \cdot 6H_2O$ loaded SCB biochar. The initial pH (pH_i) of solutions was adjusted by adding 0.1 M HCl or 0.1 M NaOH to a range of 3 to 12. After pH was adjusted, 2 g of $FeCl_3 \cdot 6H_2O$ modified SCB was added, and the suspension was shaken using water bath at a speed of 150 rpm at 30 ^{0}C for 24 h. The solutions were filtered using whatman filter paper after 24 hours and the filtrates final pH (pH_f) was measured. The difference between the initial and final

pH values (Δ pH = $pH_i - pH_f$) was plotted versus pH_i. The pH at which Δ pH = 0 is as pH value at the point of zero charge.

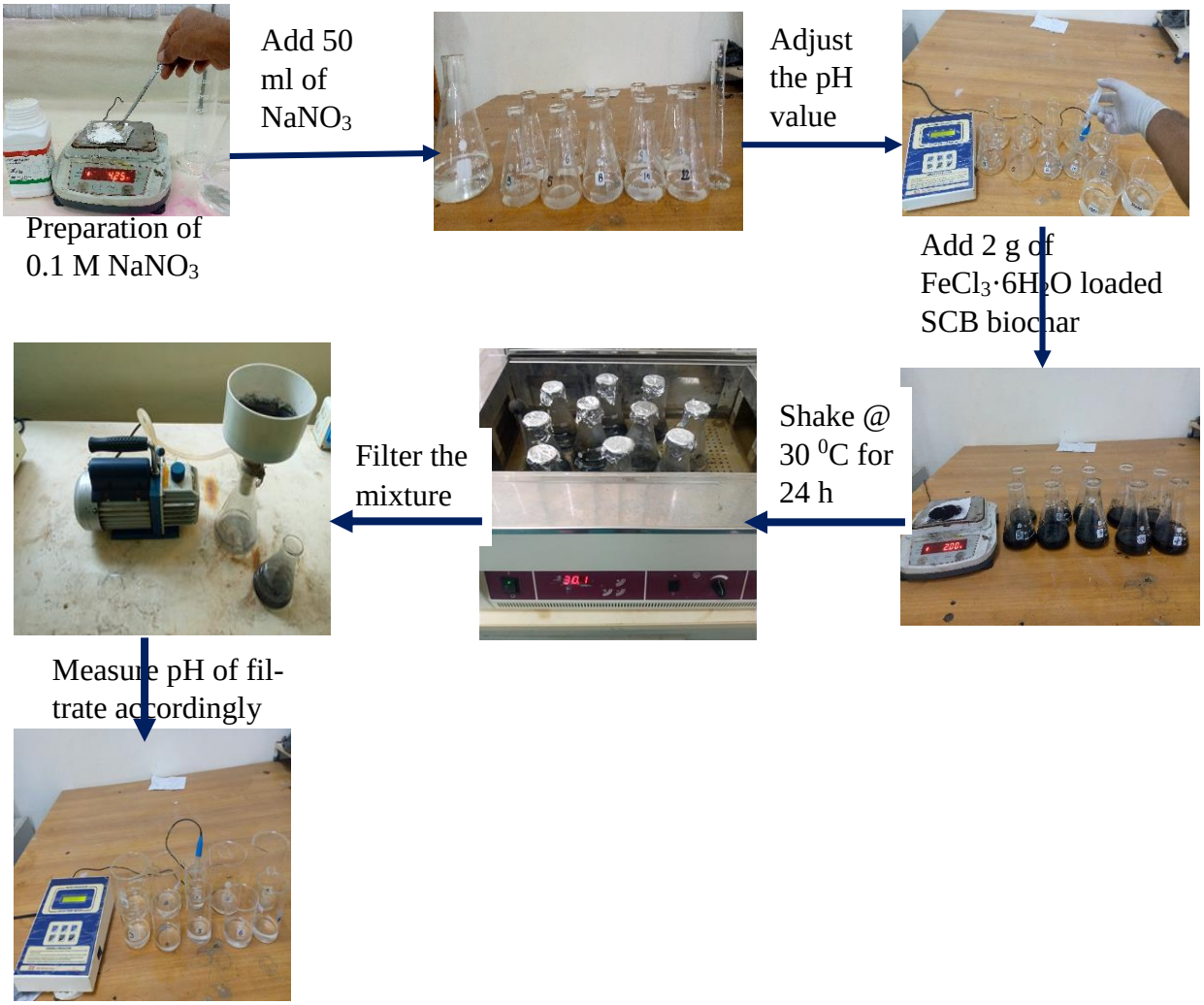

Figure3.4: Determination of PZC of $FeCl_3 \cdot 6H_2O$ Loaded SCB Biochar

3.3. Characterization of SCB biochar and $FeCl_3 \cdot 6H_2O$ modified SCB biochar

3.3.1. Functional Group Analysis (FT-IR)

Fourier transferred infrared radiation (FT-IR) with Model name FT-IR-6600 type A and Serial number A0186790 was used to monitor the prepared SCB biochar and $FeCl_3 6H_2O$ modified SCB biochar to identify the functional group. Moreover, this FT-IR was attenuated in total reflectance (ATR) mode with a resolution of 4 cm^{-1}, 64 scan rates, and a range of 4000 to 400 cm^{-1}.

3.3.2. Crystallographic structural analysis

The powder X-ray diffraction (XRD) patterns of the SCB bochar and $FeCl_3 \cdot 6H_2O$ modified SCB biochar material were recorded by a SHIZMADZU XRD-7000 at a scanning rate of 3°/min for 2Ɵ ranging from 10° to 70°. The relation between the distance between two planes (D-spacing) (d) and the angle of diffraction (2θ) was calculated by Bragg's equation Eq. 3.2.

Bragg's equation

$2d\sin\theta = n\lambda$…...……...Eq. 3.1

$d = \frac{n\lambda}{2\sin\theta}$……...……. Eq. 3.2

Where: d= Spacing, n= order of diffraction, = wave length of incident X-ray (0.15406 nm), n= order of diffraction (1) and = diffraction angle.

Scherrer equation

The average crystalline or grain size of nanoparticle were calculated using scherrer Eq. 3.3.

$D = \frac{K.\lambda}{\beta cos\theta}$……Eq. 3.3

Where, D= Crystallite size, K= shape factor (Scherrer constant) (0.9), = wave length of X-ray (0.15406 nm), = Full width half maxima (FWHM), = diffraction angle.

3.3.3. Thermo-Gravimetric analysis (TGA)

A thermogravimetric analyzer (TGA) instrument was used to evaluate the thermal stability of sugarcane bagasse biochar in order to understand the range of pyrolysis temperatures. Samples weighing between 8 and 10 mg were applied to an alumina support. With a heating rate of 10 °C/min and a temperature range of 30 °C to 600 °C (Varma & Mondal, 2016).

3.3.4. Brunauer-Emmett-Teller (BET)

The Brunauer-Emmett-Teller (BET) method is commonly applied to calculate the specific surface area based on nitrogen adsorption isotherm measurements at 77 K. In this study the specific surface area of the sugarcane bagasse biochar and $FeCl_3 \cdot 6H_2O$ loaded SCB biochar were carried out using Horriba surface area analyzer with model number SA9603 (USA) at 200 ^{O}C degassing temperature for 1 h in the presence of nitrogen gas.

3.4. Batch Adsorption Experiment

In order to conduct batch experiments, 250 mL of an aqueous arsenite solution was mixed with a certain amount of $FeCl_3.6H_2O$ modified sugarcane bagasse biochar in a 500 mL beaker. As(III) stock solution is prepared by dissolving Arsenic trioxide in DI water. As(III) solutions of various concentrations are prepared by diluting the Arsenic trioxide stock solution with DI water. The pH of the experimental solution was adjusted by adding 0.1 M NaOH or HCl solution. Batch experiments designed by one factor at a time was conduct at room temperature by a mechanical agitator at 250 rpm. After filtration, using whatman filter paper, remaining arsenite As(III) ion concentrations in the solution are analyzed by an UV visible spectrophotometry (Y. Chen et al., 2022). The removal percentage of As(III) and adsorption capacity of As(III) (q_e in mg/g) are calculated by Eq. 3.4 and Eq. 3.5.

$$\text{Removal efficiency}(\%) = \frac{(C_0 - C_e) \times 100}{C_0} \quad \text{..... Eq. 3.4}$$

$$q_e = \frac{(C_0 - C_e)V}{m} \quad \text{..... Eq. 3.5}$$

Where C_0 is the initial arsenite concentration (mg/L), and C_e is the residual or final concentration of arsenite (mg/L). V is the volume of solution (L) and m is mass of the modified biochar (g).

Figure 3.5: Batch adsorption experiment to test adsorption parameters

3.4.1. Effects of solution PH

For determination of the pH effect on the arsenite adsorption by $FeCl_3 \cdot 6H_2O$ modified SCB biochar adsorbent, initial pH of arsenite solutions with concentration of 15 mg/L were adjusted at different pH values of 2, 4, 6, 8, 10 and 12 by using 0.1 M HCl and 0.1 M NaOH. Then 1.5 g/L of $FeCl_3 \cdot 6H_2O$ modified SCB biochar adsorbent was added to 250 ml solution. The mixture was agitated at 250 rpm at room temperature. After 150 minutes, solid phase was separated by using whatman filter paper. Arsenite concentration in the filtered solution was analyzed immediately by UV spectrophotometer (Divband Hafshejani et al., 2016). The amount of arsenite adsorbed per unit weight of adsorbent (q_e in mg/g) and removal efficiency was calculated by Eq. 3.5 and Eq. 3.4.

3.4.2. Effects of contact Time

The effect of contact time on arsenite adsorption was studied by varying contact times at 30, 60, 90, 120, 150, 180, and 210 min with sample volume of 250 ml and adjusting the solution pH at 4 and 15 mg/L initial arsenite concentration and $FeCl_3 \cdot 6H_2O$ modified SCB biochar adsorbent dosage of 1.5 g/L. The mixtures were shaken with a speed of 250 rpm at room temperature for 180 minutes. Then solid phase was separated by using whatman filter paper Residual arsenite concentration in the filtered solution was determined by UV spectrophotometer (Rahdar et al., 2019). The amount of arsenite adsorbed per unit weight of adsorbent (q_e in mg/g) and removal efficiency was calculated by Eq. 3.5 and Eq. 3.4.

3.4.3. Effects of initial arsenite concentration

The effect of initial adsorbate concentration on arsenite adsorption was studied by varying initial arsenite concentration at 5, 10, 15, 20, 25 and 30 mg/L with sample volume of 250 ml, by adjusting the solution pH at 4 with $FeCl_3 \cdot 6H_2O$ modified SCB biochar adsorbent dosage of 1.5 g/L. The mixtures were shaken with a speed of 250 rpm at room temperature for 180 minutes. Then solid phase was separated by using whatman filter paper Residual arsenite concentration in the filtered solution was determined by UV spectrophotometer (Verma & Singh, 2019). The amount of arsenite adsorbed per unit weight of adsorbent (q_e in mg/g) and removal efficiency was calculated by Eq. 3.5 and Eq. 3.4

3.4.4. Effects of adsorbent dose

The effect of adsorbent dosage on arsenite adsorption was studied by adjusting the solution pH at 4 with an initial arsenite concentration of 10 mg/L, a sample volume of 250 mL and by adding the varying $FeCl_3 \cdot 6H_2O$ modified SCB biochar adsorbent dosage ranging 0.5, 1, 1.5, 2, 2.5 and 3 g/L. The mixtures were shaken with a speed of 250 rpm at room temperature for 180 minutes. Then solid phase was separated by using whatman filter paper Residual arsenite concentration in the filtered solution was determined by UV spectrophotometer (Divband Hafshejani et al., 2016). The amount of arsenite adsorbed per unit weight of adsorbent (q_e in mg/g) and removal efficiency was calculated by Eq. 3.5 and Eq. 3.4.

3.5. Adsorption isotherm

The adsorption experiment was conducted by varying the initial arsenite concentration to 10, 15, 20, 25, and 30 mg/L while using other adsorption parameters with their optimum values. The mixture was shaken at a speed of 250 rpm at room temperature by mechanical agitator and the mixture was filtered using vacuum filter. The filtrate was analyzed using UV visible spectrophotometry. Finally, the experiment data were simulated using Langmuir, Freundlich, and Temkin isotherm models. Eq. 3.6-3.16 provides the governing equations for these models (Berkessa et al., 2019).

3.5.1. Langmuir isotherm

The Langmuir isotherm model can be expressed by the following equation:

$$q_e = q_{max} \frac{K_L C_e}{1 + K_L C_e} \quad \text{..... Eq. 3.6}$$

$$\frac{C_e}{q_e} = \frac{1}{q_{max} K_L} + \frac{C_e}{q_{max}} \quad \text{.....Eq. 3.7}$$

$$\frac{1}{q_e} = \frac{1}{q_{max} K_L} . \frac{1}{C_e} + \frac{1}{q_{max}} \quad \text{..... Eq. 3.8}$$

Where, q_e is the amount adsorbed (mg/g), C_e is the equilibrium concentration of adsorbate (mg/L), while q_{max} and K_L are constants related to adsorption capacity and energy of adsorption, respectively. In addition, a dimensionless constant, commonly known as separation factor (R_L) defined by Webber and Chakkravorti, is presented in Eq. 3.9.

$$R_L = \frac{1}{K_L C_0} \quad \text{..... Eq. 3.9}$$

Where, K_L (L/mg) refers to the Langmuir constant and C_0 is the adsorbate initial concentration (mg/L). The computed R_L value suggests the adsorption nature to be either unfavorable ($R_L > 1$), linear ($R_L = 1$), favorable ($0 < R_L < 1$) or irreversible ($R_L = 0$) (Foo & Hameed, 2010).

3.5.2. Freundlich isotherm

The Freundlich isotherm models can be expressed using the following empirical equations:

$$q_e = k_f \ C_e^{1/n} \quad \text{.....Eq. 3.10}$$

$$lnq_e = lnk_{f+} \left(\frac{1}{n}\right) lnC_e \quad \text{.....Eq. 3.11}$$

Where C_e is the equilibrium concentration (mg/L), k_f, and n are Freundlich isotherm constants related to adsorption capacity and adsorption intensity, respectively. The magnitude of the exponent, 1/n, gives an indication of the favorability of adsorption. Values of n > 1 represent favorable adsorption condition. Values of K_f and n are calculated from the intercept and slope of the plot.

3.5.3 Temkin Isotherm

The following equations provide the Temkin isotherm model in linear form. Based on the linearized equation shown in Eq. 3.15, the adsorption parameters (AT and B) were calculated from the slope and intercept of the q_e versus ln C_e plot (Olalekan et al., 2012).

$$qe = \frac{RT}{b} \ln(A_T C_{e)} \quad \text{..... Eq. 3.12}$$

$$qe = \frac{RT}{b_T} \ln A_T + \frac{RT}{b_T} \ln C_e \quad \text{..... Eq. 3.13}$$

$$qe = \frac{RT}{b_T} \ln A_T + \frac{RT}{b_T} \ln C_e \quad \text{..... Eq. 3.14}$$

$$qe = B \ln A_T + B \ln C_e \quad \text{..... Eq. 3.15}$$

$$B = \frac{RT}{b_T} \quad \text{..... Eq. 3.16}$$

Where A_T = Temkin isotherm equilibrium binding constant (L/g), b_T = Temkin isotherm constant, R= Universal gas constant (8.314J/mol.k), T = Temperature 298 k, B = Constant related to heat of sorption (J/mol).

3.6. Adsorption Kinetics

The adsorption kinetics experiment was conducted by varying the contact time to 30, 60, 90, 120, 150, 180, and 210 minutes using the optimum values of other adsorption parameters obtained from batch experiment. The mixture was shaken at a speed of 250 rpm at room temperature, and then the mixture was filtered using vacuum filter. The filtrate was analyzed using UV visible spectrophotometry. Using the Pseudo first order kinetics, Pseudo second order kinetics, and Intraparticle diffusion models, the experiment data were tasted. The governing equations for these models are given in Eq. 3.17-3.21 (Berkessa et al., 2019).

3.6.1. Pseudo-first-order kinetics

The pseudo-first-order kinetics model can be expressed by the following equations:

$$\frac{dq_t}{dt} = k1(q_e - q_{t)} \quad \text{..... Eq. 3.17}$$

Where q_e (mg/g) and q_t (mg/g) are the amounts of arsenite adsorbed on the adsorbent at equilibrium and at any time t, respectively, and k_1 (min^{-1}) is the rate constant of the first-order adsorption. After integration and applying boundary conditions $q_t = 0$ at t=0 and $q_t = q_t$ at time=t, the integrated form:

$$\ln(q_e - q_t) = lnq_e - K_1 t \quad \text{..... Eq. 3.18}$$

The value of k_1 and q_e can be obtained from the slope and intercept of the linear plot of ln ($q_e - q_t$) versus t, respectively

3.6.2. Pseudo-second-order kinetics

The pseudo-second-order kinetic model can be expressed as the following equation

$$\frac{dq_t}{dt} = K_2(q_e - q_t)2 \quad \text{..... Eq. 3.19}$$

Where K_2 (g/mg min) is the rate constant of the second-order equation; q_e (mg/g) is the maximum adsorption capacity; and q_t (mg/g) is the amount of adsorbate adsorbed at time t (min). After integration:

$$\frac{t}{q_t} = \frac{1}{k_2\, qe2} + \frac{t}{q_e} \quad \text{..... Eq. 3.20}$$

The value of q_e and k_2 will be obtained from the slope and intercept of the linear plot of t/q_t versus t, respectively. The value of q_e and k_2 can be obtained from the slope and intercept of the linear plot of t/q_t versus t, respectively.

3.6.3 Intraparticle diffusion

The mathematical equation for intraparticle diffusion model is given in Eq. 3.21 (Pan et al., 2017):

$$q_t = K_p t^{0.5} + \mathrm{C} \quad \text{..... Eq. 3.21}$$

Where q_t is the amount of arsenite adsorbed (mg/g) at a given time t (min) and k_p (mg/g $min^{1/2}$) is the intraparticle diffusion rate constant and C is intercept. The k_p and C value were obtained from the slope and intercept plotting of q_t versus $t^{0.5}$.

3.7. Adsorption Thermodynamics

The adsorption thermodynamics experiment was carried out by varying temperature to 298, 303, and 308 K using the optimum adsorption parameters obtained from batch experiment. The mixture was stirred continuously for 180 minutes using magnetic stirrer, and then the mixture was filtered using vacuum filter. The filtrate was analyzed using UV visible spectrophotometry. The relationship between the adsorption factors can be established using the following equation (Tsamo et al., 2019).

$$\Delta \mathrm{G} = \Delta \mathrm{H} - \mathrm{T}\Delta \mathrm{S} \quad \text{..... Eq. 3.22}$$

T assigned to the absolute temperature in Kelvin. The difference in Gibbs free energy can be also determined by the Eq. 3.23:

$$\Delta \mathrm{G} = -\mathrm{RT}\ln K_d \quad \text{..... Eq. 3.23}$$

When; R assigned to the universal gas constant that equals 8.314 J/mol.K. K_d assigned to the thermodynamic equilibrium constant that equals (q_e/C_e) with a unit of mol or (L/g). The combination of the last two equations will give Eq. 3.24.

$$\ln K_d = \frac{\Delta \mathrm{S}}{\mathrm{R}} - \frac{\Delta \mathrm{H}}{\mathrm{RT}} \quad \text{..... Eq. 3.24}$$

The plot of $\ln K_d$ versus (1/T) will give a straight line with ($-\Delta H/R$) as a slope and ($\Delta S/R$) as an intercept. The resulting graph is known as Van't Hoff plot.

$$K_d = \frac{q_e}{C_e}$$ …….. Eq. 3.25

These parameters can be obtained from experiments at various temperatures using the equations prior to the ΔH^o and ΔS^o values are determined from the slope and intercept of a linear plot of (ln K_d) versus (1/T).

3.8. Effects of co-existing ions

Investigations were also conducted on the $FeCl_3.6H_2O$ loaded SCB biochar's ability to adsorb arsenite ion in the presence of competing anions such phosphate, sulphate, and carbonate, which are frequently found in real ground water. Experiments were carried out by adding concentrations of co-existing anions (5 mg/L) in arsenite solution (fixed arsenite concentration of 10 mg/L), optimum pH of 4, and an optimum adsorbent dosage of 1.5 g/L in different 500 ml beaker. The mixtures were shaken with a speed of 250 rpm at room temperature for 180 minutes. Then solid phase was separated from solution by whatman filter paper and residual arsenite concentration in the filtered solution was analyzed (Divband Hafshejani et al., 2016). The amount of arsenite adsorbed per unit weight of adsorbent (q_e in mg/g) and removal efficiency was calculated by Eq. 3.5 and Eq. 3.4.

3.9. Regeneration Experiments

According to (He et al., 2018), the regeneration experiment was carried out using the chemical desorption method. At a pH of 4, a contact time of 180 minutes, a dose of 1.5 g/L of $FeCl_3.6H_2O$-loaded SCB biochar as an adsorbent, and an initial As(III) concentration of 10 mg/L at 25 °C, batch adsorption tests were first conducted. The suspension was filtered and the exhausted adsorbent was collected then the adsorbent was washed using distilled water and oven-dried at 80 ^{0}C for 8 h. The dried $FeCl_3 \cdot 6H_2O$ loaded SCB biochar composite adsorbent was immersed with 50 ml of 1M NaOH for 24 h. The gently agitated solution washed by deionized water. The treated and separated adsorbent was subjected to oven dry for six hours at 70 ^{o}C. Then the adsorbent was ready for further adsorption and this process was repeated for four consecutive cycles to find the decrease in recycled adsorbent efficiency (Lee et al., 2015).

CHAPTER FOUR

RESULTS AND DISCUSSION

4.1. Characterization of Materials

4.1. 1. Crystallographic structural result analysis

XRD patterns of the dried powdered sugarcane bagasse biochar sample were shown in Figure 4.1. As shown from the Figure 4.1 SCB biochar shows the intense and sharper diffraction peak at 44.02° and 64.34° represents the degree of crystallinity of the graphitic Carbon present in the biochar. Graphitic Carbon is known to exhibit a well-defined and ordered crystal structure, which gives rise to sharp diffraction peaks in the XRD pattern of sugarcane bagasse biochar (Irawan et al., 2021). It has been observed that there only exists one broad peak with a range of 16°~ 28°, which represents amorphous carbon. The broadness of the peak suggest a lack of long-range ordering in the carbon atoms, which was characteristic of amorphous materials (Praipipat et al., 2023). There were clear diffraction peaks at 32.32° and 37.21° , which also confirmed within the result of that was done by (Irawan et al., 2021).

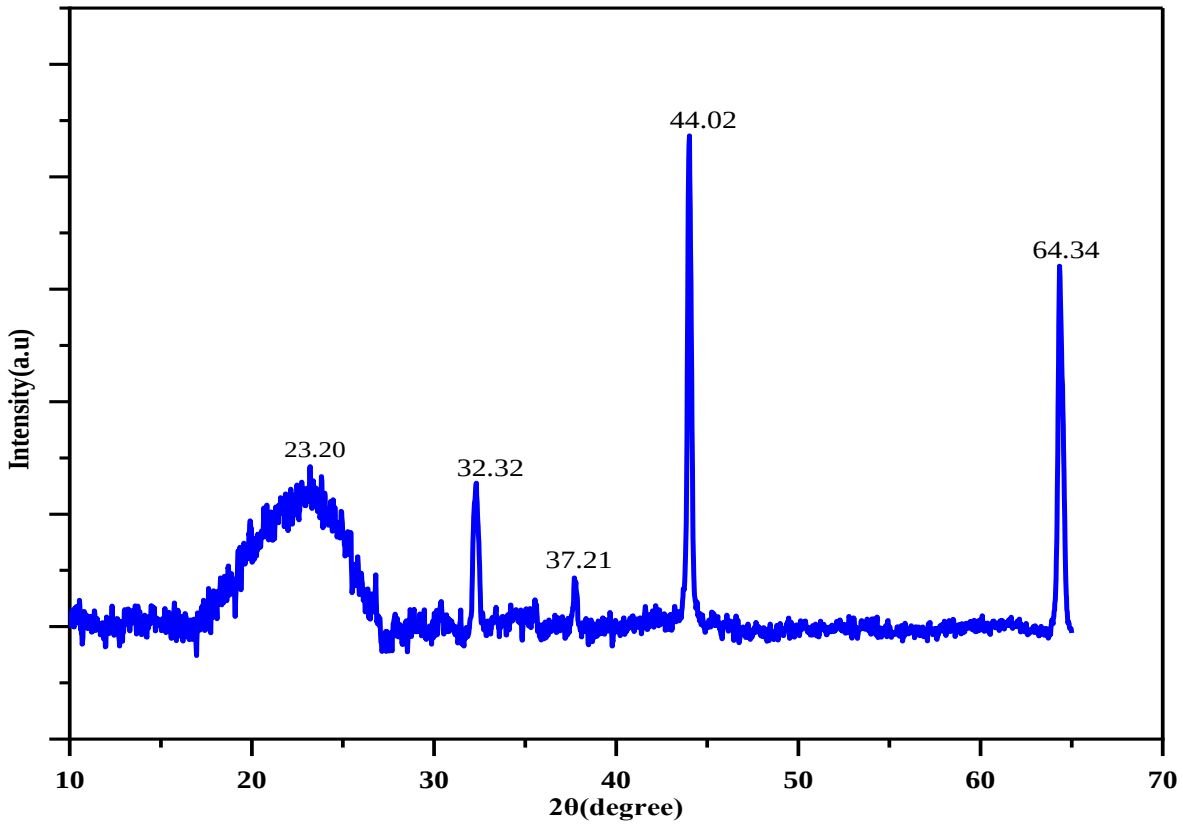

Figure 4.1: X-ray diffraction patterns of SCB biochar before adsorption

Table 4.1. Average Crystalline size and D-spacing for SCB and $FeCl_3.6H_2O$ loaded SCB biochar

Sample	Average crystal size (nm)	Average D-spacing (nm)
SCB biochar	15.91067	2.597022
$FeCl_3.6H_2O$ loaded SCB biochar	19.53957	1.997126

The XRD analysis was carried out to identify the crystal nature, phases, and average particle size of the dried powders of the $FeCl_3.6H_2O$ loaded SCB biochar. The $FeCl_3.6H_2O$ loaded SCB biochar shows the angles corresponding to the peaks at 2θ angles (°) of 29.16, 31.56, 34.58, 37.82, 47.44, 53.24 and 58.58, which were represents the crystalline phase of $FeCl_3.6H_2O$ loaded SCB biochar. The extreme broad peaks indicate the ultra-fine as well as small crystallite size of the particle. In $FeCl_3.6H_2O$ loaded SCB biochar XRD diffraction pattern the broadness of an amorphous carbon structure between 16°~ 28° became decreased relative to XRD diffraction pattern of SCB biochar. This imply that the $FeCl_3.6H_2O$ interact with the surface of biochar, promoting the formation of more ordered and crystalline regions within the amorphous carbon structure (Praipipat et al., 2023). The characteristics diffraction peaks of $FeCl_3.6H_2O$ loaded SCB biochar at 29.16°, 31.56°, 47.44°,53.24° and 58.58°, show the presence of iron particle which was aligned with previous literature (Zheng et al., 2017).

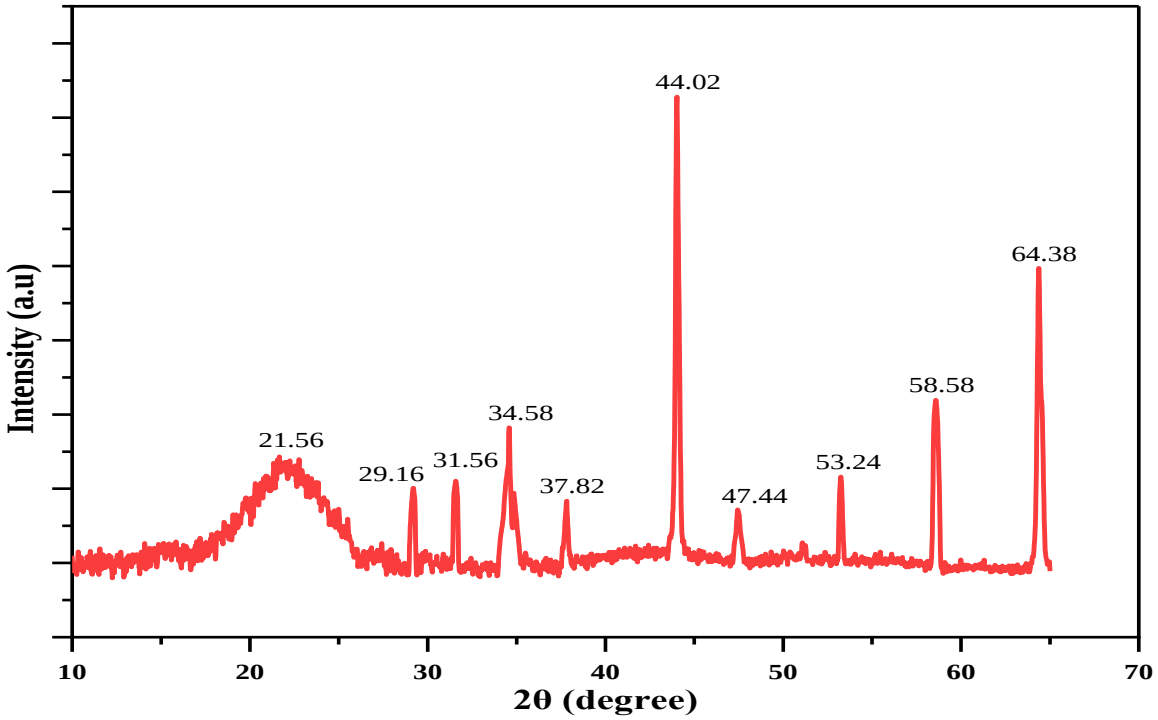

Figure 4.2: X-ray diffraction patterns of $FeCl_3.6H_2O$ loaded SCB biochar before adsorption

The average crystalline size of the $FeCl_3.6H_2O$ loaded SCB biochar was 19.53 nm which was greater than average crystalline size of SCB biochar 15.91 nm calculated from Scherrer equation. This suggests that that $FeCl_3.6H_2O$ acts as a crystallization agent or a nucleating agent. It could promote the formation and growth of larger crystals within the sugarcane bagasse biochar matrix and the presence of $FeCl_3.6H_2O$ may provide favorable conditions for the crystallization of certain compounds or minerals present in the biochar (Zheng et al., 2017). The detailed crystalline size values for each peaks were reported in Appendix B.

Table 4.2: Crystalline size and average D-spacing of $FeCl_3.6H_2O$ loaded SCB biochar

peak position(2 theta)	FWHM	Crystalline size D (nm)	Average crys-talline size (D)	Average D-spacing
22.01807	0.2903	27.87884	19.53957	1.997126
29.17162	0.3652	22.47768		
31.56973	0.3965	20.82121		
34.56602	0.4021	20.69123		
37.79635	0.5062	16.58815		
44.03369	0.4523	18.94585		
47.49658	0.5214	16.64598		
53.23955	0.5932	14.98016		
58.59261	0.4321	21.08162		
64.40985	0.61425	15.28494		

As shown from the XRD diffraction pattern of $FeCl_3.6H_2O$ loaded SCB biochar after adsorption in Figure 4.3. The diffraction peaks at 3 values of 16.86^o, 50.04^o, and 55.38^o that occurred after arsenite adsorption indicate that arsenite ion was successfully adsorbed on the positive layer of $FeCl_3.6H_2O$ loaded SCB biochar adsorbent (H. Lu et al., 2018).

The XRD diffraction pattern of sugarcane bagasse biochar after arsenite adsorption demonstrated in Figure 4.3 show alterations in peak positions, intensities, or the emergence of new peaks compared to the pattern before adsorption. These change would indicate modifications in the crystallographic structure of the biochar due to the adsorption of arsenite ion on the surface of SCB biochar adsorbent (Irawan et al., 2021).

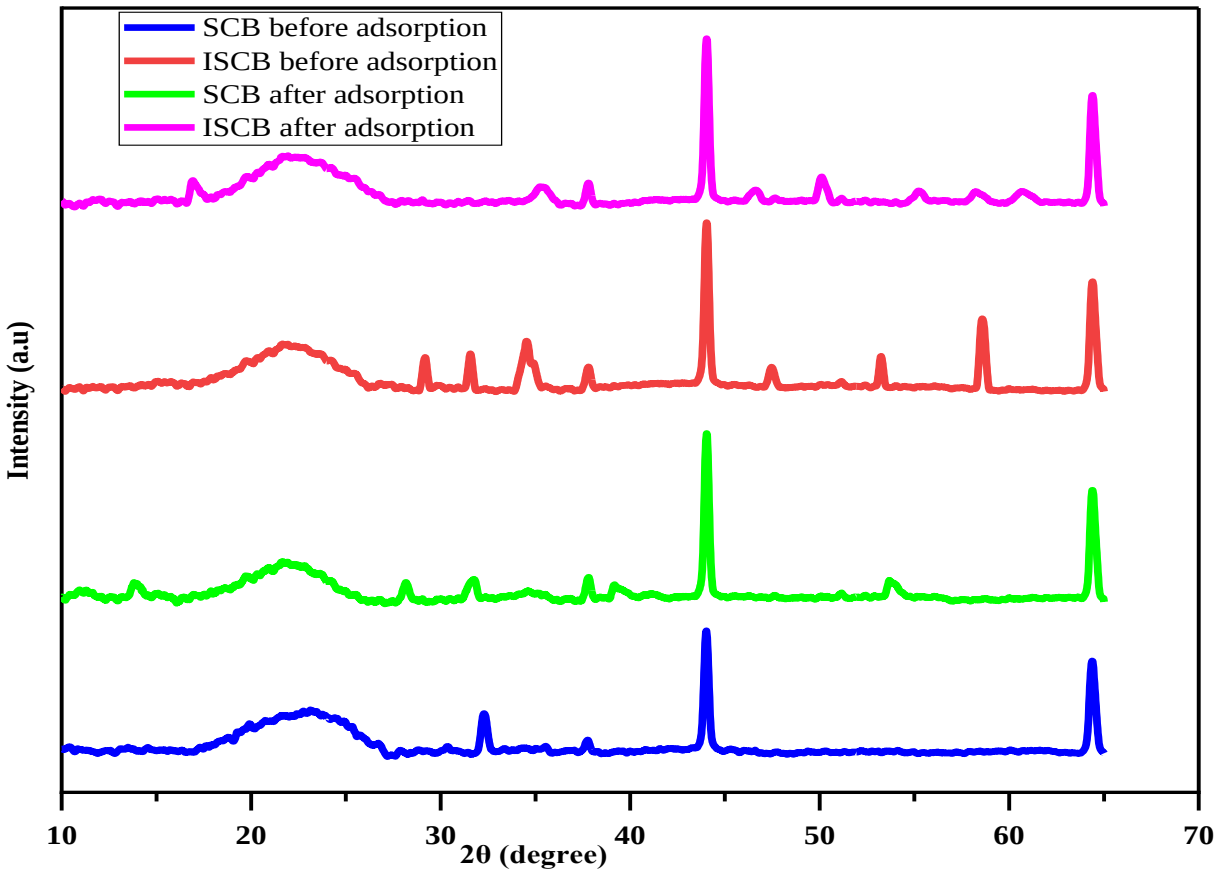

Figure 4.3: XRD diffraction pattern of SCB and $FeCl_3.6H_2O$ loaded SCB biochar before and after adsorption

4.1. 2. Functional groups result analysis

FT-IR spectroscopy was conducted to identify the surface functional groups of SCB biochar and $FeCl_3.6H_2O$ loaded SCB biochar before and after the adsorption of Arsenite ions from ground water. From the SCB biochar sample before adsorption the broad band observed at 3390 cm^{-1} represent the stretching vibration of hydroxyl functional groups O–H. The strong peaks at 1700 cm^{-1} were responsible to the presence of C=O stretching vibration of carbonyl groups. The sharp peaks obtained at 1590 cm^{-1} indicate the presence of symmetric stretching of aromatic C=C vibrations compounds. In the finger print region, the smaller peak around 1430 cm^{-1} corresponding to bending vibrations of C-H bonds in class of alkyl. Moreover, the broad band peaks at around 1120 cm^{-1} correspond to C-O stretching vibration of alcohols, carboxylic acid and ether groups. The peak at 756 cm^{-1} associated with vibrational modes of aromatic C-C bonds.

As observed from the FT-IR spectrum of SCB biochar after adsorption, the adsorption of arsenite ions onto sugarcane bagasse biochar lead to a decreased in the intensity of O-H stretching vibrations in the FT-IR spectrum. This was due to the arsenite ions interact and displace the hydrogen bonding in the stretching vibration of hydroxyl functional groups O–H, resulting in a weakened or altered O-H stretching vibration (Praipipat et al., 2023). The peak at 1700 cm^{-1} which represent the C=O stretching vibration of carbonyl groups on SCB biochar FT-IR spectrum slightly increased in the intensity after adsorption of arsenite ion due to the formation of specific complexes or hydrogen bonds between the adsorbed arsenite ions and the carbonyl groups, resulted in higher electron density around the C=O bond and enhanced vibrational intensity. The broad band of C-O stretching vibration of SCB biochar became broaden and slightly shifted from 1120 cm^{-1} to 1110 cm^{-1} after adsorption of arsenite ion due to changes in the adsorption mechanism or the formation of new chemical bonds between the biochar surface and the adsorbed arsenite ion.

From $FeCl_3.6H_2O$ loaded SCB biochar before adsorption FT-IR spectrum the strong and sharp peaks at 1711 represent carbonyl functional groups, such as ketones C=O or carboxylic acids C=O. Additionally, after iron chloride in anhydrous form was impregnated, the peak 1700 cm^{-1} on SCB biochar was slightly shifted to high frequencies 1711 cm^{-1} and sharpened because of iron chloride could change the surface properties of the biochar, including the arrangement and accessibility of functional groups and interactions between the C=O group and other molecules, causing changes in the observed spectroscopic characteristics. Spectrum shows the broad band at 3410 cm^{-1}, which correspond to the stretching vibration of the hydroxyl groups O–H. The O-H stretching bond in $FeCl_3.6H_2O$ loaded SCB biochar becomes more broad than un modified SCB biochar this was due to the activating catalyst $FeCl_3.6H_2O$ have a plenty of hydrogen and oxygen (6 mole of water molecules) injected to SCB biochar. Moreover, the peak at 3390 cm^{-1} was slightly shifted to high frequencies 3410 cm^{-1} after iron chloride in anhydrous form was impregnated. This imply that the modification with anhydrous iron chloride has resulted in enhanced interactions between the hydroxyl groups and the iron chloride, potentially lead to strong hydrogen bonding or changes in the chemical environment around the hydroxyl groups and potentially improve its properties or reactivity (Bai et al., 2021). A large number of O–H groups on the particle surface can contribute to the adsorption of arsenite ions.

The peaks obtained at 1590 cm^{-1} was associated with aromatic C=C stretching vibrations. The intensity of the aromatic C=C stretching vibrations peak was increased compared to un modified SCB biochar due to enhanced conjugation or delocalization of electrons within the aromatic system, resulted from interactions between iron chloride and the biochar surface. These interactions could strengthen the aromaticity and lead to a more pronounced peak. From the finger print region, the strong and small peaks obtained at 1440 cm^{-1} correspond to C-H stretching bond in class of alkanes. The peak at 1176 cm^{-1} was associated with the stretching vibration of C-O bonds. This peak might indicate the presence of functional groups such as alcohols, ethers, or esters. The position of the stretching vibration of C-O bonds slightly changed on $FeCl_3.6H_2O$ loaded SCB biochar FT-IR spectrum as shown in Figure 4.4. These change might be indicative of variations in the number or nature of C-O bonds, such as the presence of different oxygen-contain functional groups or alterations in the surface coverage of iron chloride on the biochar. The sharp peak obtained at 796 cm^{-1} attributed to Fe-O-H bending vibrations. The bending vibration of Fe-O-H bonds could arise from coordination complexes formed between iron chloride and hydroxyl groups on the biochar surface (Irawan et al., 2021). This peak represented the presence of iron-oxygen-hydrogen bonds formed during the modification process when iron chloride in anhydrous form interacted with sugarcane bagasse biochar (Noraini et al., 2016).

As illustrated in Figure 4.4. the stretching vibration of the hydroxyl groups O–H spectrum after adsorption of arsenite ion by $FeCl_3.6H_2O$ loaded SCB biochar became more broad and decreased in the intensity of the peaks. This broadening could raise from the formation of hydrogen bonds between the hydroxyl groups and the adsorbed arsenite ions, as well as changes in the local environment around the O–H groups (Bai et al., 2021). Additionally, the position of hydroxyl groups O–H shifted from 3410 cm^{-1} to 3285 cm^{-1} due to interactions between the hydroxyl groups on the biochar and the arsenite ions, lead to changes in the hydrogen bonding or electronic environment around the O–H groups (Noraini et al., 2016). From the FT-IR spectra the $FeCl_3.6H_2O$ loaded SCB biochar after adsorption the intensity of the carbonyl adsorption bands in the FT-IR spectrum was increased. This increased would suggests that the adsorbed arsenite ions were promoting the exposure or accessibility of the carbonyl groups, lead to enhanced adsorption of infrared radiation (Praipipat et al., 2023).

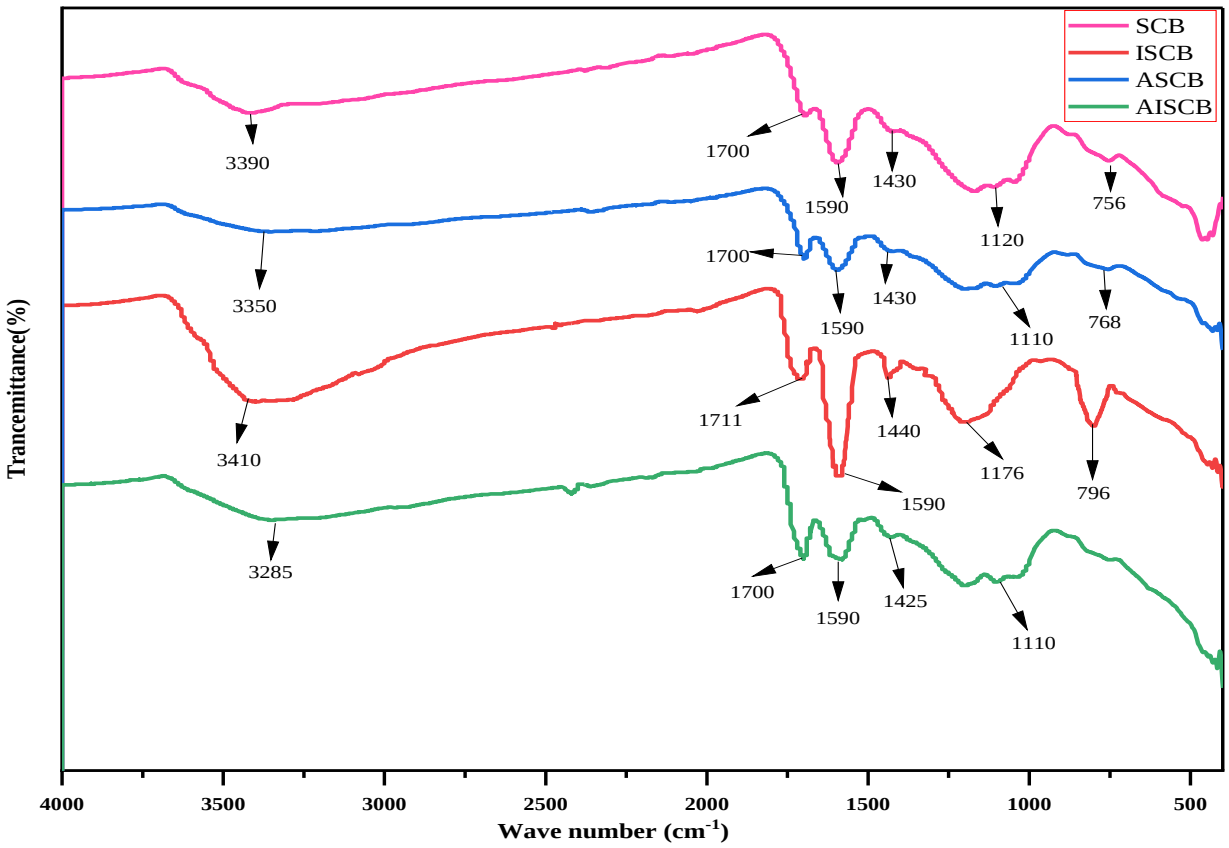

Figure 4.4: FT-IR spectra of SCB and $FeCl_3.6H_2O$ loaded SCB biochar before and after adsorption

3.1.3. BET surface area result analysis

The Brunauer-Emmett-Teller (BET) method was used to calculate the specific surface area of SCB biochar and $FeCl_3.6H_2O$ loaded SCB biochar. The specific surface area of $FeCl_3.6H_2O$ loaded SCB biochar was found to be 97.38 m^2/g, which was greater than specific surface area of SCB biochar, which has a surface area of 14.88 m^2/g, as shown in Table 4.3. Due to $FeCl_3 \cdot 6H_2O$ undergo chemical reaction with the organic compound present in the biochar. These reactions could resulted in the removal of impurities, volatiles, and low-molecular-weight compounds, thus create more porous structure and increased the surface area (Congsomjit & Areeprasert, 2020).

Table 4.3: BET surface area analysis for SCB biochar and $FeCl_3 \cdot 6H_2O$ loaded SCB biochar

Sample	**Surface area(m^2/g)**
Sugarcane bagasse biochar	14.886
$FeCl_3 \cdot 6H_2O$ modified SCB biochar	97.387

Furthermore, materials with a greater surface area offer excellent adsorption qualities such a lack of internal diffusion, a high surface binding energy, and adsorption activity (Noraini et al., 2016). The specific surface area result found by (Noraini et al., 2016) for magnetic sugarcane bagasse biochar was 111 m^2/g. The smaller amount of the surface area of $FeCl_3 \cdot 6H_2O$ loaded SCB biochar could be because of the agglomeration of the composite adsorbent to each other.

4.1.5. Thermogravimetric analysis of sugarcane bagasse

Thermogravimetric analysis (TGA-DTA) was performed on the sugarcane bagasse to determine the weight loss against temperature profile. Thermogravimetric Analysis of sugarcane bagasse was shown in Figure 4.5. The SCB displayed a three-step weight loss over the TG analysis's temperature range. The first endothermic mass loss from 30-200 ^oC was due to moisture loss and evaporation of surface adsorbed water. The second zone of mass loss from 200-370 ^oC mainly related to thermal degradation of hemicelluloses along with smaller amounts of cellulose and lignin, while the third zone from 370-550 ^oC was predominantly related to thermal degradation of cellulose along with smaller amounts of hemicelluloses and lignin. Lignin mass loss occurs at a huge temperature range, with higher mass loss at higher temperatures (Mesquita et al., 2018). The solid residue remaining at the end of the process consists of fix carbon and ashes (Machado et al., 2018). Derivative curve of the SCB showed that there were three major peaks indicating loss of mass and two major reaction temperatures (around 345°C and 433°C).

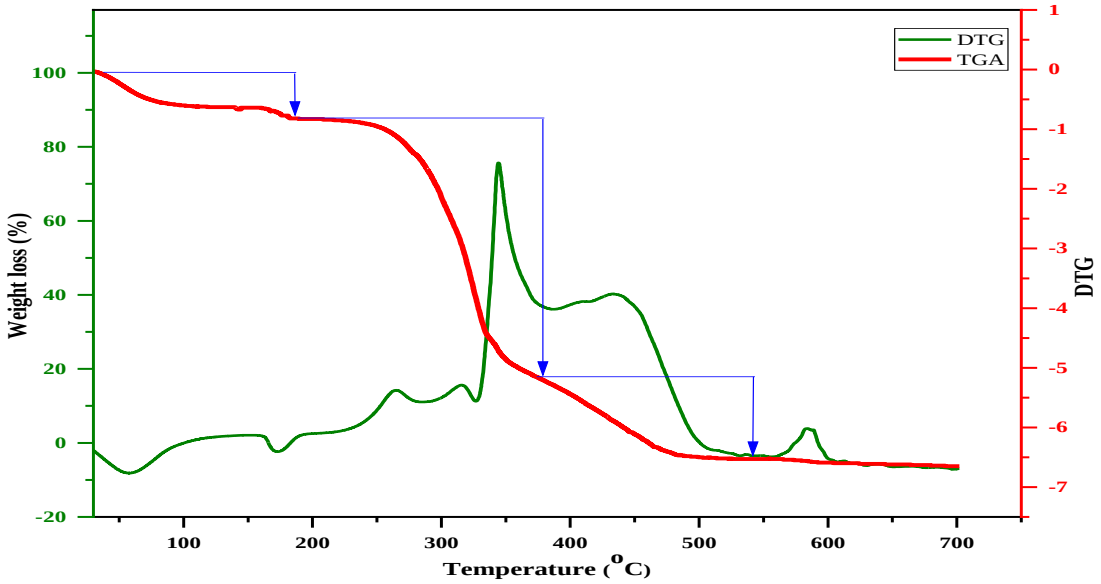

Figure 4.5: Thermogravimetric Analysis of sugarcane bagasse

4.2. Point zero charges of $FeCl_3 \cdot 6H_2O$ loaded SCB biochar adsorbent

The point of zero charges (PZC) of $FeCl_3 \cdot 6H_2O$ loaded sugarcane bagasse adsorbent materials were investigated to determine which pH value of each material is optimal for arsenite adsorption. Theoretically, the adsorbent's PZC is equal to a pH value that results in a net charge of zero (Praipipat et al., 2023). Figure 4.6. illustrated the plot of ΔpH vs pH_i for 0.1M of sodium nitrate and the curve intersect at a point 6.2, which represents the point of zero charge of the $FeCl_3.6H_2O$ loaded SCB biochar. When the pH of the solution is below the PZC, the solid surface carries a positive charge and attracts arsenite ions with a negative charge. Conversely, when the pH is above the PZC, the solid surface becomes negatively charged and favors the adsorption of arsenite ions with a positive charge (Al-Maliky et al., 2021). The high arsenite adsorption should happen at a pH of solution lower than the PZC ($pH_{solution} < pH_{pzc}$) due to the adsorbent's positively charged surface (Wang et al. 2019). Therefore, the high arsenite removal efficiencies of the $FeCl_3 \cdot 6H_2O$ loaded SCB biochar adsorbent materials should be obtained at pH less than 6.2.

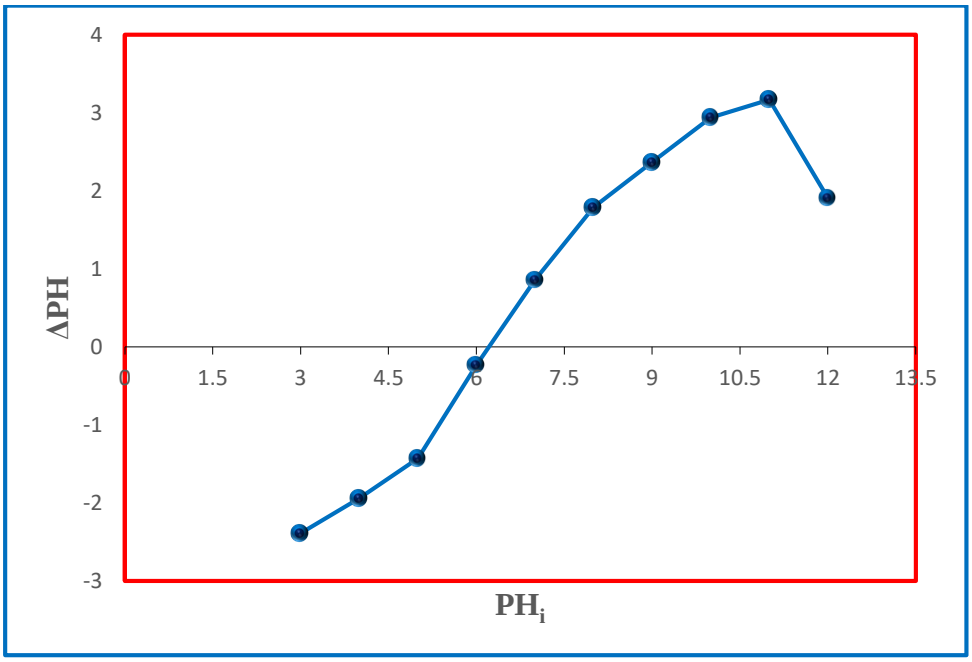

Figure 4.6: Determination of PZC of $FeCl_3 \cdot 6H_2O$ loaded SCB biochar

4.3. Bach adsorption Experiment

4.3.1. Effect of solution pH on the removal of arsenite

The adsorption of arsenite ions depends critically on the pH of an aqueous solution. It determines the surface characteristics of the adsorbent in terms of surface charges, ionization of the functional

groups, and the degree of functional group dissociation on adsorbents' active sites (Ezeonuegbu et al., 2021). By adjusting the initial solution pH to 2, 4, 6, 8,10 and 12 while maintaining the other adsorption parameters constant, the influence of solution pH on the adsorption of arsenite by $FeCl_3 \cdot 6H_2O$ modified SCB biochar adsorbent was investigated. As shown in Figures 4.7, at lower pH values that indicate an acidic medium condition ranging from pH 2.0 to 6.2, the hydration surface of $FeCl_3 \cdot 6H_2O$ modified SCB biochar underwent a protonation reaction. The dissolved arsenite ion was embedded in the adsorbent surface to obtain positive charge. At pH of 2 the adsorption of arsenite ion was low compared to pH of 4. Due to excess concentration of proton leads repulsive forces between the positively charged adsorbent and the negatively charged arsenite ions hinder their interaction and limit the adsorption process of arsenite ion (T. H. Nguyen et al., 2019). However, an increased in pH of solution lead to OH^- concentration in the solution increased and arsenite ion adsorption was decreased. Because OH^- ions at alkaline conditions could compete with arsenite anion for active sites under strong alkaline conditions, which resulted in the blocking of arsenite ion adsorption on the surface of the $FeCl_3 \cdot 6H_2O$ modified SCB biochar adsorbent, the removal of arsenite ions was relatively low in alkaline solution (pH > 6.2) as compared to that in lower pH values ranging from pH 2.0 to 6.2 (PZC). Therefore, the highest removal efficiency 85.21 % was obtained for $FeCl_3 \cdot 6H_2O$ modified SCB biochar at the condition of pH =4.

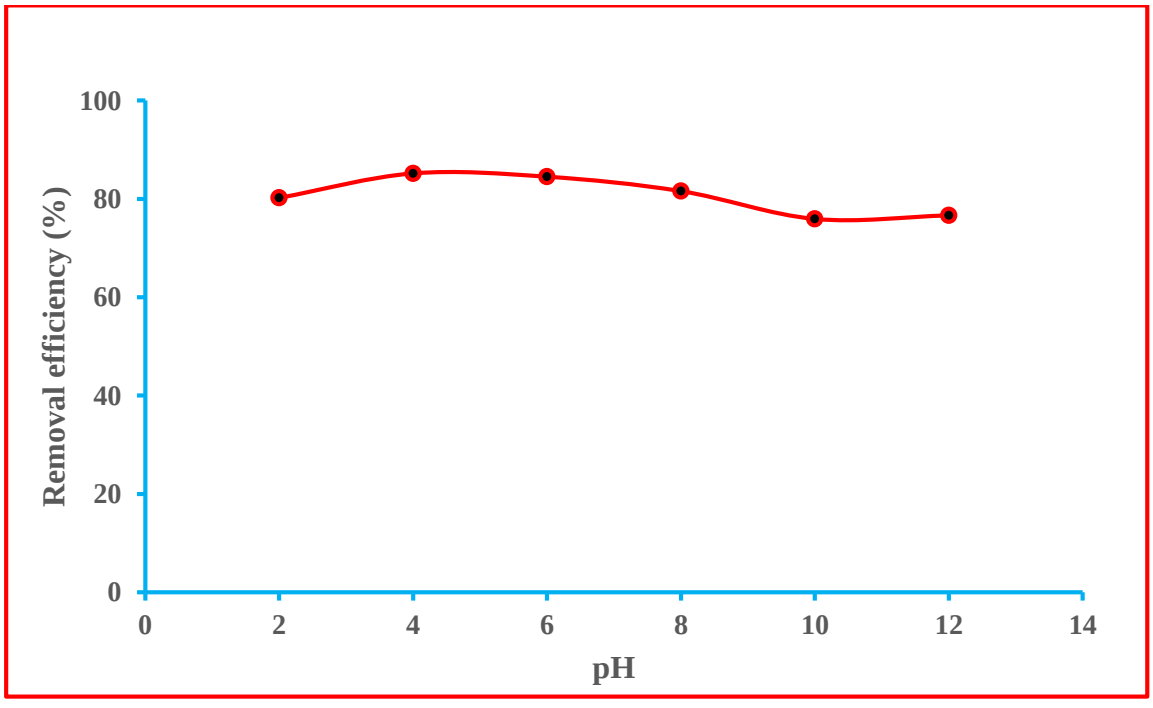

Figure 4.7: Effects of solution pH on arsenite adsorption

4.3.2. Effect of contact time on the removal of arsenite

For the practical removal of arsenite anions from aqueous solutions or ground water, it is desired and advantageous for the arsenite ions to interact quickly with the $FeCl_3 \cdot 6H_2O$ modified SCB biochar adsorbent (T. H. Nguyen et al., 2019). Figure 4.8, displayed the effect of contact time on the removal of arsenite using $FeCl_3 \cdot 6H_2O$ modified SCB biochar. It could be seen that the removal of arsenite ion was almost proportional to the increasing contact time from 30 to 180 min. The adsorption rate was relatively fast at the initial adsorption stage but then slowed down gradually after more sites were occupied by the adsorbed arsenite ions. The rise in arsenite removal could be assigned to an increased in the availability of active binding sites on biochars with time and there was high driving force for arsenate adsorption. However, the decreased in the removal efficiency and adsorption capacity could be a result of the enhanced filling of pores or active sites or repulsion between solute molecules (Kumar et al., 2021). The last step was an equilibrium stage after approximately 180 min adsorption. Therefore, optimum contact time for arsenite removal using $FeCl_3 \cdot 6H_2O$ modified SCB biochar was chosen at 180 min for further experiment.

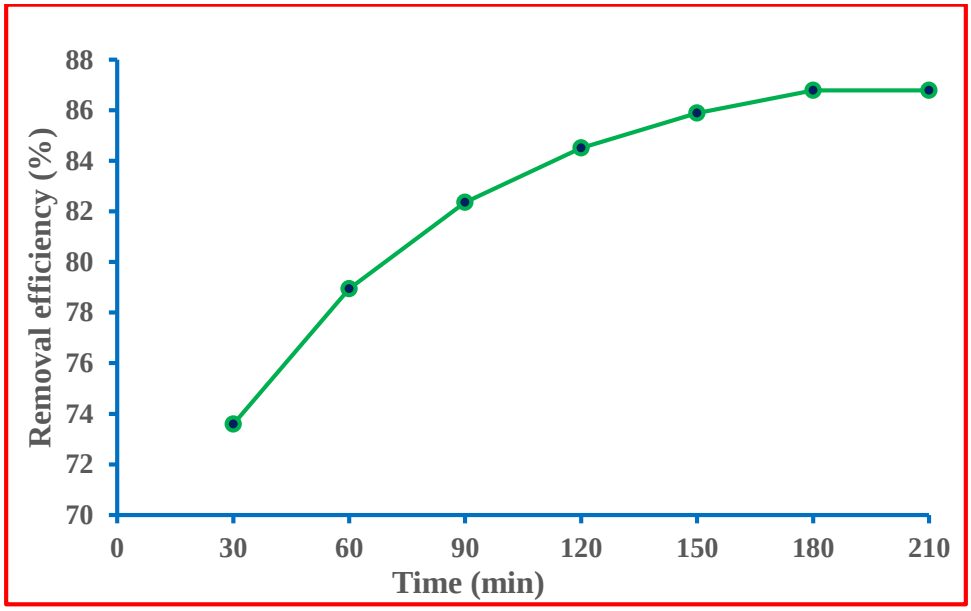

Figure 4.8: Effects of contact time on arsenite adsorption

4.3.3. Effect of Initial Concentration

Figure 4.9, demonstrated the removal efficiency of arsenite ion using $FeCl_3 \cdot 6H_2O$ loaded SCB biochar adsorbent as a function of initial arsenite ion concentration. The removal efficiencies of arsenite ion by $FeCl_3 \cdot 6H_2O$ loaded SCB biochar were 88.53 % at the low initial arsenite ion concentration (10 mg/L). $FeCl_3 \cdot 6H_2O$ loaded SCB biochar showed a high removal efficiency at low

initial arsenite ion concentration. Due to their high surface area and a large number of active sites available for the adsorption of arsenite. However, the removal efficiency of arsenite rapidly dropped at high initial arsenite concentrations. The results indicated that most of the adsorption sites available in the given amounts of adsorbents had been adsorbed by arsenite ions. Figure 4.9, shows the removal efficiency of $FeCl_3 \cdot 6H_2O$ loaded SCB biochar adsorbent decreased from 88.54 to 73.25% when the concentration increased from 5 to 30 mg/L.

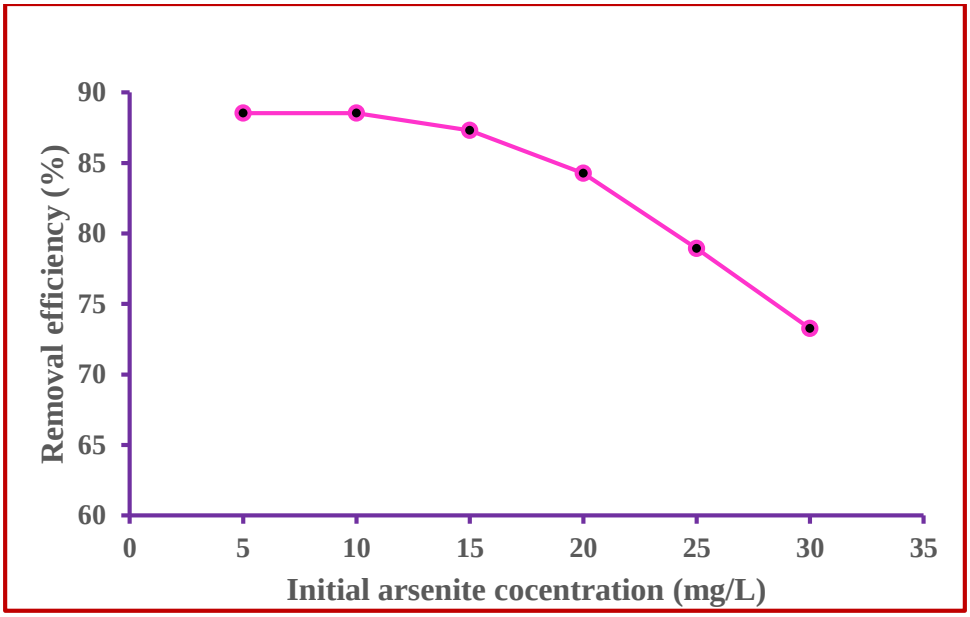

Figure 4.9: Effects of initial concentration on arsenite adsorption

4.3.4. Effect of Adsorbent dose on the removal of arsenite

Adsorbent dosage is a crucial component to take into account for efficient removal as it determined the system's adsorbent-adsorbate equilibrium (Kumar et al., 2021). Adsorbent dosage in the range of 0.5 to 3 g/L was used for the adsorption experiments by keeping other parameters constant, and the results were shown in Figure 4.10. This was done in order to examine the influence of the amount of $FeCl_3 \cdot 6H_2O$ loaded SCB biochar on arsenite adsorption. With an increased in $FeCl_3 \cdot 6H_2O$ loaded SCB biochar adsorbent doses, removal efficiency increased; however, above 1.5 g/L adsorbent dose, removal efficiency decreased due to the depleted availability of binding sites. As shown in Figure 4.10, a 1.5 g/L $FeCl_3 \cdot 6H_2O$ loaded SCB biochar adsorbent dosage resulted in a maximum removal efficiency of 89.88 %. The initial increased in the percentage of adsorption could be attributed to increased adsorbent surface area and the availability of more adsorption sites and the decreased in the adsorption amount may be attributed to overlapping or aggregation of adsorption sites resulted in formation of clusters in the adsorbents and diminished

surface area (Kiliç et al., 2017). Therefore, optimum $FeCl_3 \cdot 6H_2O$ loaded SCB biochar adsorbent for arsenite removal using $FeCl_3 \cdot 6H_2O$ modified SCB biochar was chosen at 1.5 g/L for further experiment.

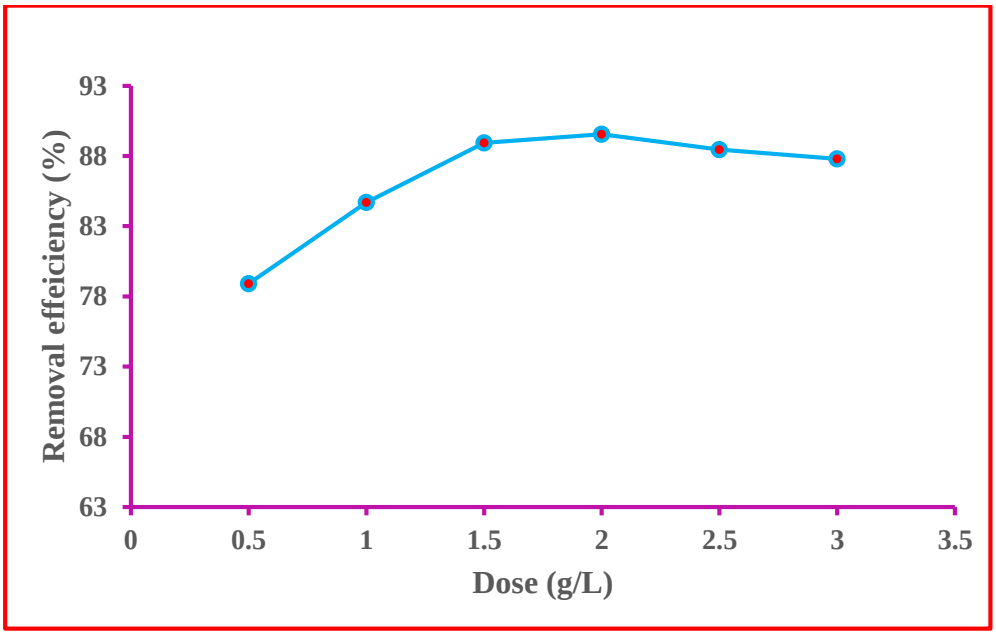

Figure 4.10: Effects of adsorbent dose on arsenite adsorption

4.4. Adsorption Isotherm

Studying isotherm can help to determine how adsorbate and adsorbent interact, which is essential for developing and optimizing the desired adsorption system (H. Zhang et al., 2015). The equilibrium concentration of arsenite ions was carried out at constant optimized conditions of, 1.5 g/L of $FeCl_3 \cdot 6H_2O$ loaded SCB biochar adsorbent, pH of 4, initial concentration of arsenite ion 10 mg/L and contact time of 180 minutes with agitation speed of 250 rpm at room temperature, by using three widely used isotherms, the Langmuir, Freundlich isotherms and Temkin isotherm, the adsorption isotherm data for the As(III) ion were analyzed. From the slope and intercept of the graph for each equation of the isotherms, their correlation coefficients and constant parameters of As(III) sorption by $FeCl_3 \cdot 6H_2O$ loaded SCB biochar were determined.

4.4.1. Langmuir Isotherm for arsenite adsorption by $FeCl_3 \cdot 6H_2O$ loaded SCB biochar

The difference between the amounts of adsorption and the solute concentration at equilibrium is determined by the adsorption isotherm. The adsorption isotherm of arsenite ion using $FeCl_3 \cdot 6H_2O$ loaded SCB biochar was investigated. The highest adsorption capacity of $FeCl_3 \cdot 6H_2O$ loaded SCB

biochar for arsenite ion removal was determined by studying the concentration of arsenite ions in their respective equilibrium phases at room temperature.

Table 4.4: Isotherm data for the removal of arsenite by $FeCl_3 \cdot 6H_2O$ loaded SCB biochar

C_o(mg/L)	C_e(mg/L)	ln (Ce)	$1/C_e$	q_e (mg/g)	$1/q_e$	Ln(q_e)	Ce/q_e
10	1.011	0.011	0.9891	5.9926	0.1668	1.791	0.1687
15	1.6605	0.507	0.602	8.893	0.1124	2.185	0.1867
20	2.474	0.906	0.404	11.684	0.0856	2.458	0.2117
25	3.805	1.336	0.263	14.130	0.0707	2.648	0.2692
30	5.709	1.742	0.175	16.194	0.0617	2.785	0.3525

According to the Langmuir model's results, all initial arsenite concentrations had separation factors (R_L) that were greater than 0 and lower than 1 this indicating that the Langmuir isotherm is favorable (H. Zhang et al., 2015). The intercept of the Langmuir plots of 1/Ce vs $1/q_e$ allows for the determination of the maximum adsorption capacity (q_{max}). The Langmuir isotherm model's maximum adsorption capacity (q_{max}) and energy of adsorption (K_L) were to be calculated as 27.70 mg/g and 0.2772 L/mg, respectively. For the Langmuir isotherm, the correlation factor (R^2) obtained values equal to 0.9966.

Table 4.5: R_L values at different initial arsenite concentration

C_o (mg/L)	R_L
10	0.360
15	0.240
20	0.180
25	0.144
30	0.120

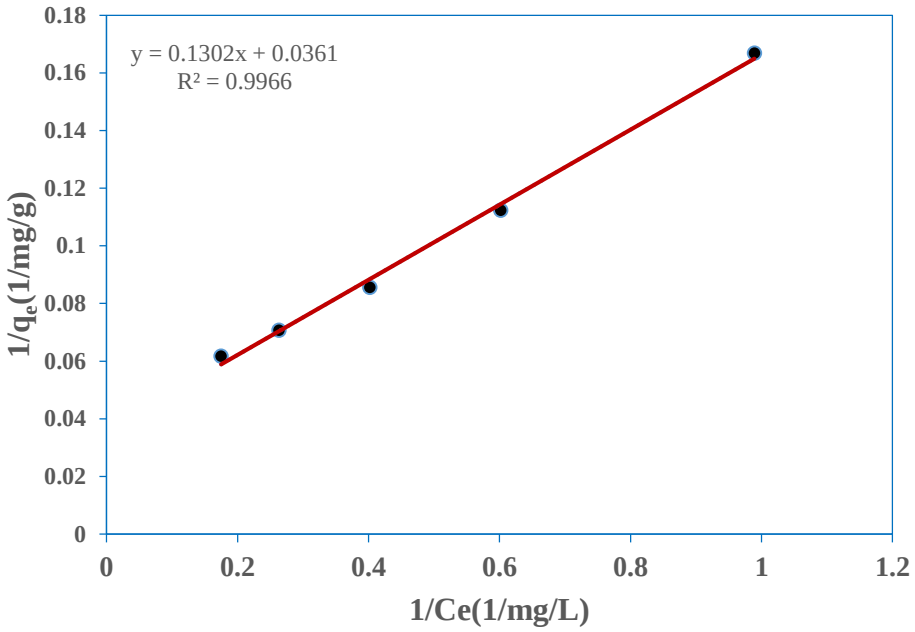

Figure 4.11: Langmuir isotherm for arsenite adsorption by $FeCl_3 \cdot 6H_2O$ loaded SCB biochar

4.4.2. Freundlich Isotherm for arsenite adsorption by $FeCl_3 \cdot 6H_2O$ loaded SCB biochar

An empirical equation that can be used to explain heterogeneous systems is the Freundlich isotherm. The multi-layer adsorption on of arsenite on the surface of the adsorbents was investigated using the linear form of the Freundlich isotherm model from Eq. 3.11. The magnitude of the exponent 1/n indicates the favorability of the adsorption. 1/n is a heterogeneous factor, which is related to adsorption intensity or surface heterogeneity. The value of $1/n < 1$ which equals to 0.5741 indicates normal adsorption (Keshav et al., 2019). The value of n should fall between 1 and 10 in order to achieve a favorable adsorption process. The value of n is shown in Table 4.6, to be 1.74, indicating favorable adsorption. The values of constant parameters from the Freundlich isotherm model, such as K_f and n, were determined through a linear regression plot of log (q_e) and log (C_e). The equilibrium isotherm data fit to the experimental data from the Freundlich isotherm model analysis indicated that adsorbed arsenite develops a monolayer surface coverage on the $FeCl_3 \cdot 6H_2O$ loaded SCB biochar and the chemisorption adsorption process occurs. For the Freundlich isotherm, the correlation factor (R^2) obtained is equal to 0.9694.

According to the research of (Ayawei et al., 2017), the slope and intercept of the linear plots were used to compute the relative parameters of the Langmuir and Freundlich adsorption isotherms. High correlation coefficients ($R^2 > 0.9205$) showed that the Langmuir and Freundlich models in

this study were both able to appropriately fit the experimental data. The result of the adsorption equilibrium isotherm indicated that the presence of both heterogeneous and homogeneous adsorption surfaces on the adsorbent involved in the adsorption of arsenite ions was suggested by the fitting of the equilibrium data to the Langmuir and Freundlich isotherm models. By comparing the correlation factor (R^2) values, it can be seen that the equilibrium adsorption provides a better fit for the Langmuir models, providing a greater R^2 of 0.9966 and a maximum adsorption capacity of 27.70 mg/g for the arsenite ion.

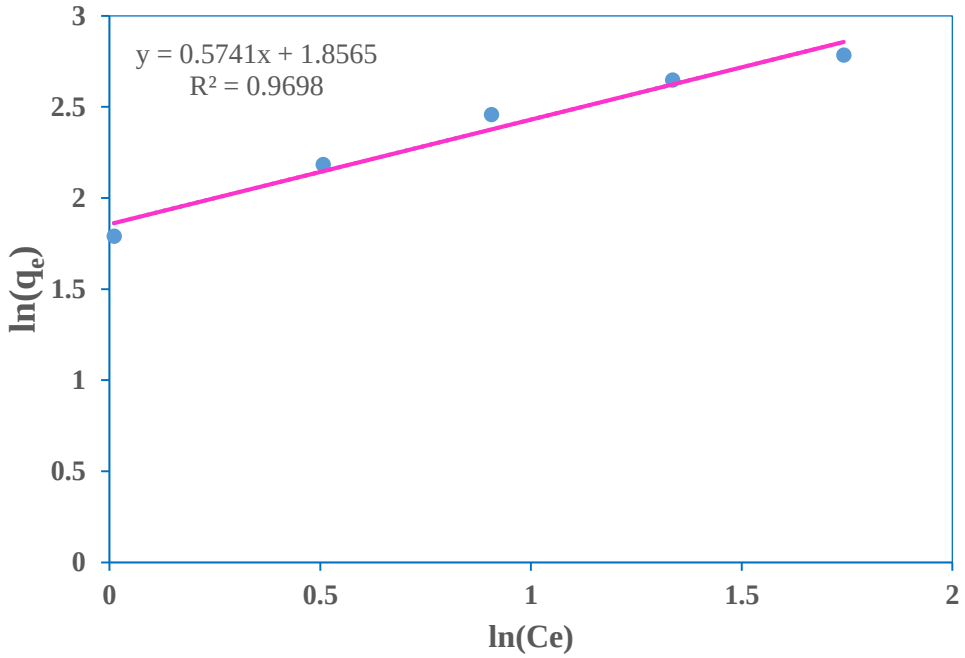

Figure 4.12: Freundlich Isotherm for arsenite adsorption by $FeCl_3 \cdot 6H_2O$ loaded SCB biochar

4.4.3. Temkin Isotherm

Equilibrium binding constant for a specific adsorption experiment, AT expresses the heat of adsorption and provides information on binding energy. From this model, a correlation coefficient (R^2) of 0.9511 was obtained. The result showed that the experimental data fitted to the model. However, the Temkin model's results was the one with the smallest correlation coefficient when compared to Langmuir and Freundlich. The positive value of B (6.1621 J/mol) indicates the adsorption process was exothermic. According to previous study by (Keshav et al., 2019) for Temkin isotherm the following is predicted: a positive B (heat) value would indicate that arsenite ion binds to iron loaded biochar in an exothermic process, whereas a negative value would indicate an endothermic process.

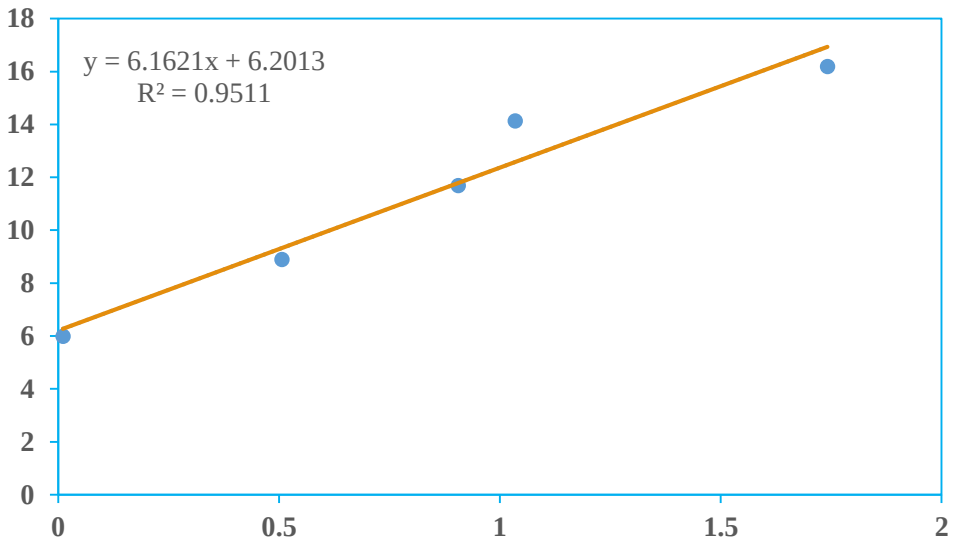

Figure 4. 13: Temkin isotherm model for arsenite adsorption

Table 4.6: Isotherm parameters for the removal of arsenite by $FeCl_3 \cdot 6H_2O$ loaded SCB biochar

Isotherm	**parameters**	**Value**
Langmuir	q_{max} (mg/g)	27.70
	K_L (L/mg)	0.2772
	R^2	0.9966
Freundlich	n	1.74
	1/n	0.5741
	k_f (mg/g)(1/mg)$^{1/n}$	5.046
	R^2	0.9698
Temkin	B (J/mole)	6.1621
	b_T	402.066
	A_T (L/mg)	2.735
	R^2	0.9511

4.5. Adsorption Kinetics

A kinetic experiment was conducted to examine the rate of arsenite adsorption and the time needed to attain equilibrium on $FeCl_3 \cdot 6H_2O$ loaded SCB biochar adsorbent. The goal of studying equilibrium kinetics is to determine the adsorbent retention time, provide details regarding the time required to reach the maximum adsorption capacity, and discover the governing mechanism in processes involving mass transfer or chemical reactions (Tohfegar et al., 2019). The most suitable kinetic models for the elimination of arsenite were determined in this study by analyzing pseudo-first-order, pseudo-second-order and intraparticle diffusion kinetic models. At constant room temperature, 10 mg/L initial arsenite concentration, pH = 4, and 1.5 g/L of adsorbent dosage, the time dependency of arsenite's kinetics was studied for 30 to 210 min.

Table 4.7: Pseudo first and second order kinetics and constant values

Time (min)	C_o (mg/L)	Ce(mg/L)	q_t (mg/g)	q_e (mg/g)	$\ln(q_e-q_t)$	t/q_t (g.min/mg)	$t^{0.5}$
0	0	0	0	0	0	0	0
30	10	1.57	5.620	5.991	-0.991	5.338	5.477
60	10	1.463	5.691	5.991	-1.204	10.542	7.745
90	10	1.356	5.762	5.991	-1.474	15.619	9.486
120	10	1.251	5.832	5.991	-1.838	20.576	10.954
150	10	1.147	5.902	5.991	-2.419	25.415	12.247
180	10	1.013	5.991	5.991	-	30.045	13.416
210	10	1.013	5.991	5.991	-	30.045	14.491

The pseudo-second-order model clearly fit the adsorption kinetic of arsenite onto $FeCl_3 \cdot 6H_2O$ loaded SCB biochar and the adsorption processes were chemisorption when the correlation coefficients of the two kinetic models were compared.

As demonstrated in Figure 4.15, the pseudo-second-order rate model exhibits the best agreement with the results from experiments, indicating that chemical adsorption served as the process' rate limiting step throughout. According to the pseudo-second-order kinetic model, the arsenite ions and the $FeCl_3 \cdot 6H_2O$ loaded SCB biochar was share electrons, which was result in valance forces in the adsorption behavior. Additionally, the estimated and experimental adsorption capacities confirmed, demonstrating the validity of the model used. In Table 4.7, the kinetic parameter values were given.

4.5.1. Pseudo first order kinetics

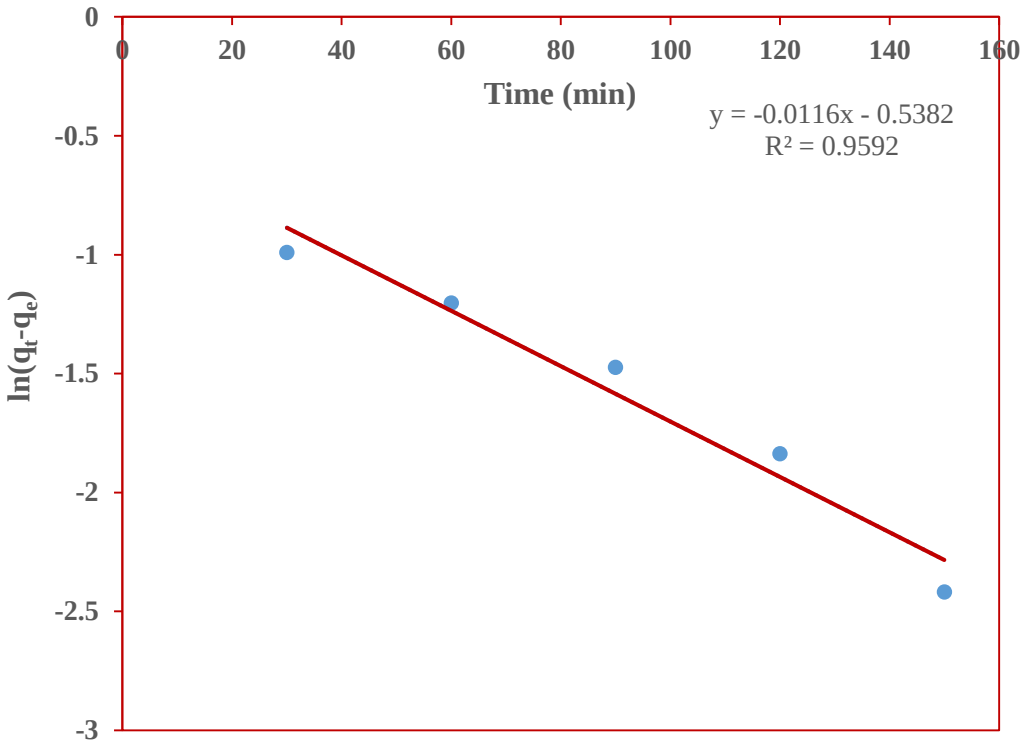

Figure 4.14: Pseudo first order for adsorption of arsenite ions

Table 4.8: Kinetics parameters for the removal of arsenite by FeCl3·6H2O loaded SCB biochar

Kinetics	Intercept	slope	q_e (mg/g)	R^2
Pseudo first order	-0.5382	-0.0116	2.18	0.95
Pseudo second order	2.0939	0.1463	6.835	0.9737
Intraparticle diffusion model	5.3865	0.0424		0.96

4.5.2. Pseudo second order kinetics

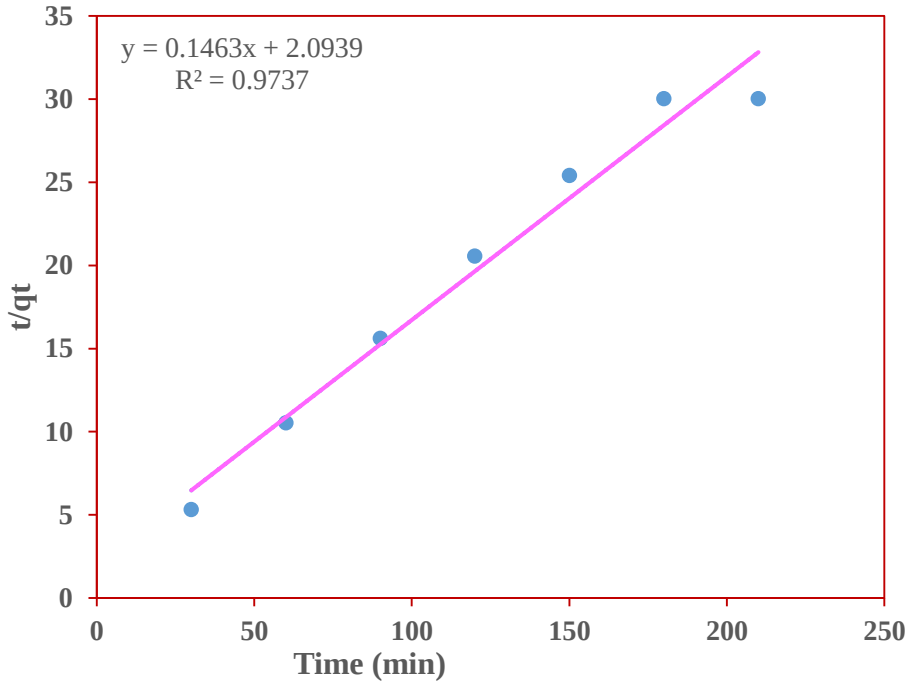

Figure 4.15: Pseudo second order for adsorption of arsenite ions

4.5.3. Intraparticle diffusion model

According to the intraparticle diffusion model, the rate of adsorption is dependent on how quickly adsorbate diffuses towards adsorbent. The result analyzed from the adsorption equilibrium data of intraparticle diffusion model the graph $t^{0.5}$ versus q_t was linear which demonstrates that the intra-particle diffusion was involved inside the adsorption process. The graph of $t^{0.5}$ vs q_t did not pass through the origin, as can be seen in Figure 4.16, indicating that intraparticle diffusion is not the only rate-determining step. This shows that intraparticle diffusion became not the only rate-limiting step within the adsorption of arsenite ion. As a result, alternative mass transfer processes, such as film diffusion and bulk diffusion, may be involved in figuring out how arsenite ions are transferred from the bulk solution to the $FeCl_3 \cdot 6H_2O$ loaded SCB biochar adsorbent surface. The diffusion process may affect the arsenite ion adsorption process on $FeCl_3 \cdot 6H_2O$ loaded SCB biochar as result of the porous structure of the adsorbent and the attractive effect of arsenite ions.

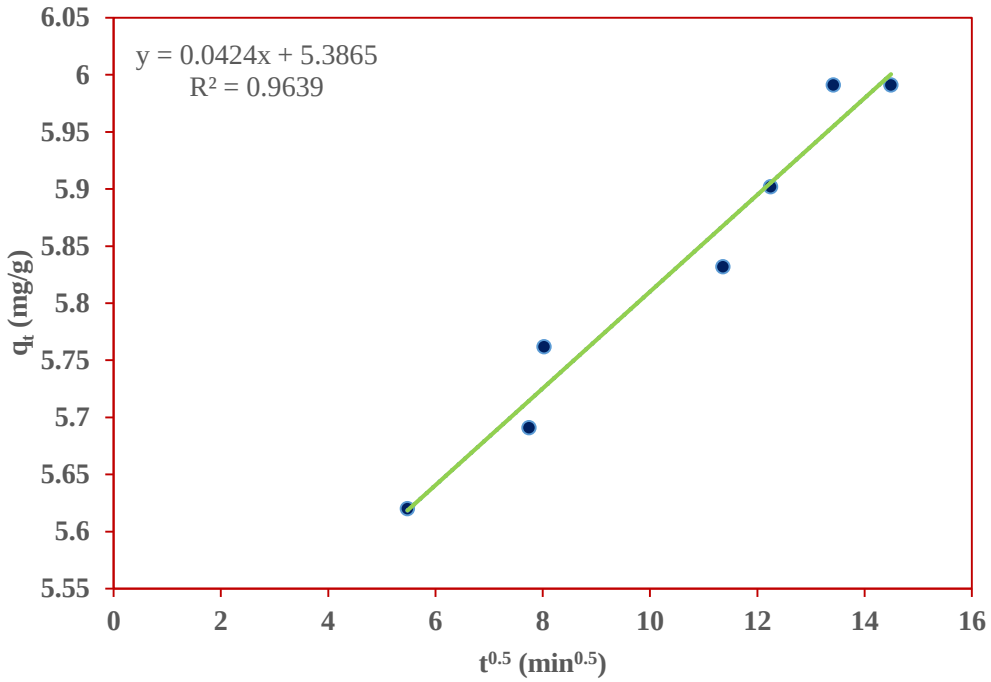

Figure 4.16: Intraparticle diffusion model for adsorption of arsenite ions

4.6. Thermodynamics study

The thermodynamic characteristics for arsenite adsorption on $FeCl_3 \cdot 6H_2O$ loaded SCB biochar adsorbent were measured at three different temperatures: 298 K, 303 K, and 308 K, respectively. As it summarized in Table 4.8, the values of Gibbs free change energy (ΔG^o) was found to be negative for adsorption of arsenite ion on $FeCl_3 \cdot 6H_2O$ loaded SCB biochar adsorbent. The specific values G^o to be found include -4.55, -5.04, and -5.45 KJ/mol which confirms that the spontaneity and viability of adsorption process as a result of negative values of Gibbs free energy changes at all temperatures. The magnitude of G^o also becomes more negative as temperature rises for arsenite adsorption, implying that adsorption occurs more spontaneously at higher temperatures (Maneechakr & Mongkollertlop, 2020). Higher temperature makes the adsorption easier due to higher driving force of adsorption. The endothermic nature of the adsorption process is confirmed by the positive value of change in enthalpy ΔH^o (22.149 KJ/mol), which also suggests that arsenite adsorption is more favorable at higher temperatures. In the other case the positive values of ΔS^o (89.616 J/mol K) demonstrates that the process is entropy driven and the randomness between solid-solution interface increases throughout adsorption process (Maneechakr & Mongkollertlop, 2020).

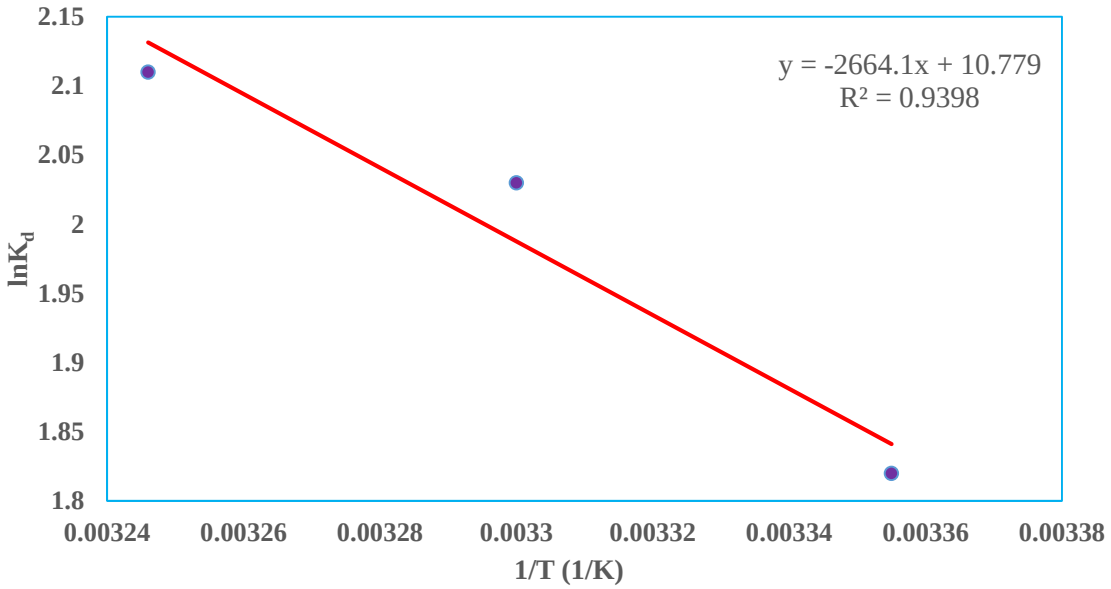

Figure 4.17: Adsorption thermodynamics of arsenite ion on $FeCl_3 \cdot 6H_2O$ loaded SCB biochar

Table 4.9: Thermodynamic parameters of arsenite adsorption on $FeCl_3 \cdot 6H_2O$ loaded SCB biochar

Adsorbent	qe (mg/g)	Temperature (K)	K_d	lnk_d	ΔG^o (KJ mol^{-1})	ΔH^o (KJ mol^{-1})	ΔS^o (J mol^{-1} K^{-1})	R^2
Fe_3O_4 loaded CSH	6.02	298	6.21	1.82	-4.55	22.149	89.616	0.939
	8.13	303	7.61	2.03	-5.04			
	8.17	308	8.28	2.11	-5.45			

4.7. Effects of Co-Existing Ions

Normally, the common inorganic anions which include PO_4^{3-}, SO_4^{2-} and CO_3^{-} frequently coexist with As^{3-} in ground water sources, that can act as competing ions and strongly interfere with the adsorption process of As^{3-}, resulting in inefficiency. Due to this reason, it is necessary to evaluate the effect of the competing anions. Increasing the coexisting anion would cause an obvious decrease in arsenite adsorption capacity, which would result from the competitive effect of anions for available adsorption sites of adsorbent. Therefore, the effects of these competitive anions were investigated in this study. As Figure 4.18, demonstrates the effect of three co-existing ions such

as Phosphates, sulphates and Carbonates of 5 mg/L of each on arsenite removal at optimum parameters were investigated. The results indicated that the anions have substantial effect on arsenite removal. The effect of sulphates was not prominent as compared to phosphates and carbonate. The presence of phosphate ion within arsenite reduce the percentages of arsenite removal from 89.89% to 72.67%. In addition, carbonate was another influential ion, which reduce the arsenite removal efficiency to 78.67%. Therefore, Phosphate was the greatest competitor for arsenite followed by carbonate and sulphate. This is because high concentration of phosphates leads to lack of available surface area on $FeCl_3 \cdot 6H_2O$ loaded SCB biochar adsorbent sites. The basic characteristics of anions to be considered for the selective adsorptions includes the solubility, ionic radius, hydration energy and bulk coefficient (Rafiee, 2014). The competing anions reduce the removal efficiency of arsenite in the order of sulphate > carbonate > phosphate.

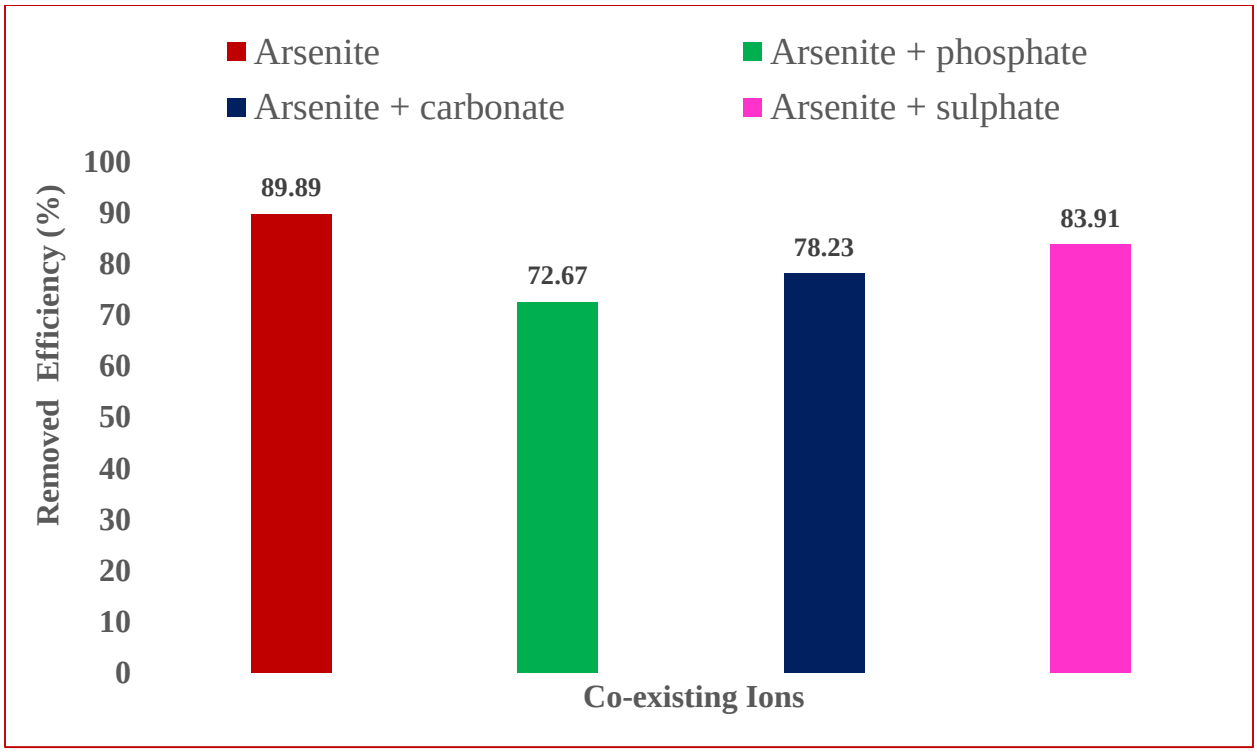

Figure 4.18: Effects of Co-existing ions on arsenite adsorption by $FeCl_3 \cdot 6H_2O$ loaded SCB biochar

4.8. Regeneration Study

Regeneration and reuse studies were conducted for the adsorption of arsenite during four successive adsorption-desorption cycles in order to evaluate the durability of this adsorbent (Lee et al., 2015). A solution of 1M of NaOH was chosen as the eluent in the desorption process. High reus-

ability of adsorbent is very indispensable for any adsorbent, which significantly increase the economic value of the adsorption process. To study regeneration of $FeCl_3 \cdot 6H_2O$ loaded SCB biochar adsorbent 1.5 g/L of adsorbent dose, pH of 4, 10 mg/L of initial arsenite concentration at 180 min with 250 rpm agitation speed at room temperature. As shown in bar graph on Figure 4.19, the removal efficiency of the first cycle was 85.21% while the second cycle resulted 80.06%. At the third and fourth cycle, the removal efficiency of arsenite ion was 74.27 and 69.16% respectively. This value ensures that the prepared adsorbent could be reused different times with smallest loss of adsorption ability. Therefore, $FeCl_3 \cdot 6H_2O$ loaded SCB biochar is a promising adsorbent for removal of arsenite ion from ground water.

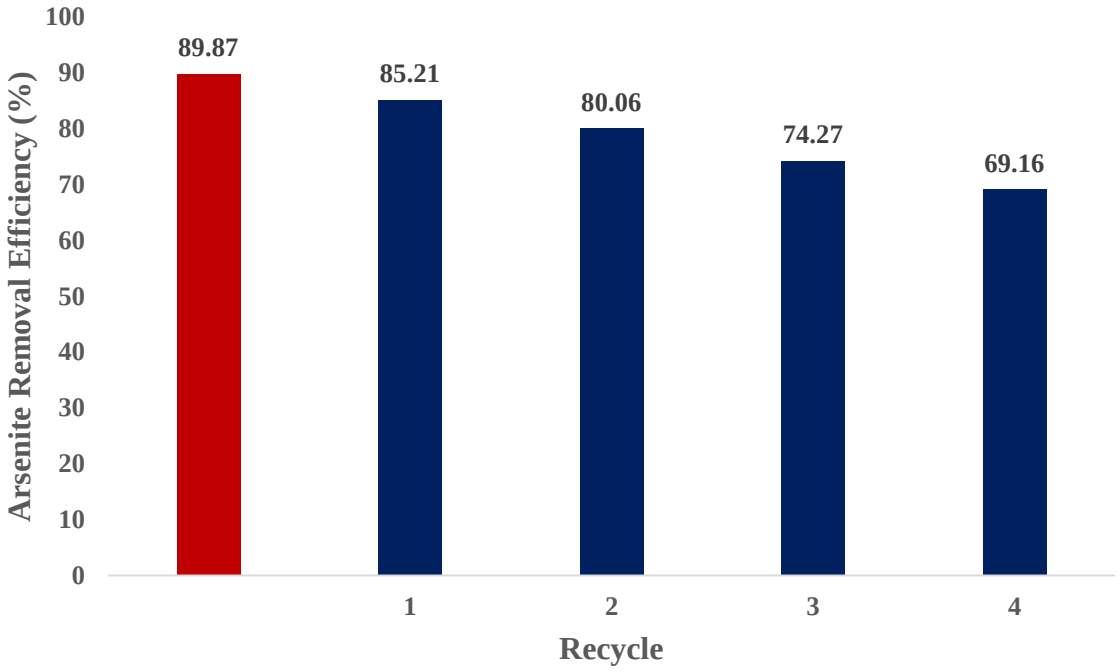

Figure 4.19: Reusability performance of $FeCl_3 \cdot 6H_2O$ loaded SCB biochar.

4.9. Removal of Arsenite from Real ground water

In order to apply the laboratory experimental result in to the practical real world application, the investigation carried out by taking the real ground water, which have highest amount of arsenic from Awasa-Abaya-Chamo lakes. The concentration of the water sample was analyzed using UV spectrophotometry and found to be 0.032 mg/L of arsenite. For the adsorption of real ground water contains arsenic the optimum parameter from batch adsorption of synthetic wastewater were used. The optimum parameter includes, pH = 4, contact time =180 min, $FeCl_3 \cdot 6H_2O$ loaded SCB biochar

= 1.5 g/L. The initial arsenic concentration obtained from UV spectrophotometry, which was 0.032 mg/L.

Table 4.10: Adsorption results of real ground water sample

Initial concentration (mg/L)	Final Concentration (mg/L)	Removal Efficiency R_e (%)
0.032	0.01161	63.71

The removal efficiency of arsenite on the $FeCl_3 \cdot 6H_2O$ loaded SCB biochar adsorbent was found 63.7 %. This result was significantly slower than the removal performance of arsenite containing synthetic ground water. The reason behind this result could be the presence of fluoride, Nitrite, sulphate and chloride. Those ions compete in the adsorption process, which leads decrement in the removal efficiency of arsenite. It would be possible to separate those ions from the real ground water sample to get the highest adsorption capacity and a greater arsenite removal efficiency.

4.10. Comparison study of Arsenite by different adsorbents

The synthetic $FeCl_3 \cdot 6H_2O$ loaded SCB biochar adsorbent's performance for removing Arsenite from water was contrasted with other adsorbents presented in related papers. Table 4.10 showed comparisons between the ideal pH, isotherm model, kinetics models, and q_{max} for arsenite removal.

Table 4.11: Adsorption capacities and other parameters for removal of arsenite by different adsorbent

Adsorbent	**Optimum pH**	**Isotherm**	**kinetics**	**q_{max} (mg/g)**	**Reference**
magnetite precipitated onto Douglas fir biochar	7	Langmuir	Pseudo-first order	5.49	(Navarathna et al., 2019)
peanut shell biochar	6.2	Langmuir	Pseudo-second order	14.75	(Sattar et al., 2019)
iron-modified sorghum straw biochar	4.3	Langmuir	Pseudo-second order	23.0	(Zang et al., 2021)

Iron-Modified Biochar Derived from Rice Straw	4.3	Langmuir	Pseudo-first order	28.49	(T. H. Nguyen et al., 2019)
$FeCl_3 \cdot 6H_2O$ loaded SCB biochar	4	Langmuir	Pseudo- second order	27.70	This study
rice straw biochar	5	Langmuir	Pseudo- second order	26.9	(Nham et al., 2019)

CHAPTER FIVE

CONCLUSIONS AND RECOMMENDATIONS

5.1. Conclusions

This research work focus on the Preparation and characterization of $FeCl_3 \cdot 6H_2O$ loaded sugar cane bagasse biochar adsorbent from Wonji sugar factory by-product to remove the arsenite ions from groundwater. Analysis of the XRD, FT-IR, and SEM results showed that the $FeCl_3 \cdot 6H_2O$ loaded SCB biochar adsorbent was successful in adsorbing the arsenite ion. The effective attachment of $FeCl_3.6H_2O$ to the SCB biochar was well validated by the adsorption peak between 200 and 450 cm^{-1}, which denotes the stretching vibration of Fe-O. According to BET analysis, the $FeCl_3 \cdot 6H_2O$ loaded SCB biochar has a specific surface area of 97.38 m^2/g. The effect of variation in pH, initial arsenite concentration, contact time, and adsorbent dose was investigated for arsenite removal from ground water. At pH = 4, C_o = 10 mg/L, t = 180 min, and dosage = 1.5 g/L, an optimal removal efficiency of 89.89 percent was achieved. The outcome demonstrates that those parameters' interactions had a considerable impact on the adsorption process.

With a maximum adsorption capacity and correlation coefficient (R^2) of 27.7 mg/g and 0.9966, respectively, the Langmuir isotherm model demonstrated a better agreement with the experimental data. This implies that the adsorption process was carried out in a monolayer on the surface of a limited number of identical adsorption sites. The pseudo-second-order kinetics model provided a precise justification of the kinetics of arsenite adsorption (R^2 = 0.9737), implying that chemical adsorption became the controlling mechanism of the adsorption process. In addition, the thermodynamics parameters suggested that the arsenite removal was endothermic and spontaneous.

It was determined that the competing ions showed an effect on arsenite adsorption by $FeCl_3 \cdot 6H_2O$ loaded SCB biochar in the following order: sulphate < carbonate <phosphate. The most notable desorption agent, 1M NaOH, was used as the eluent to explore the adsorption regeneration study of $FeCl_3 \cdot 6H_2O$ loaded SCB biochar adsorbent. Four cycles of adsorption and desorption were completed successfully. The results of this investigation show that the adsorbent is the most effective and promising for removing arsenite ions from ground water and wastewater.

The batch experimental studies for real ground water from Awasa-Abaya-Chamo lakes as arsenite source. The result investigated showed that 63.71% of arsenite was removed from ground water.

The reduction in removal efficiency from that of synthetic wastewater was due to the presence of other capitating ions like phosphates, nitrite, fluoride, and chloride, which competes within arsenite ions during the adsorption process.

5.2. Recommendation

For the future work, the following recommendations suggested based on the result obtained from this study.

- It is recommended that study the effects of adsorption parameters such as particle size, temperature and agitation speed.
- For better understanding Analysis morphology of raw Sugarcane bagasse biochar, and $FeCl_3 \cdot 6H_2O$ loaded SCB biochar sample before and after adsorption should be done using a scanning electron microscope (SEM).
- In this work batch equilibrium isotherm, kinetics and thermodynamics were conducted. In order to get accurate adsorption result for industrial scale a continuous column adsorption study should be considered.
- The regeneration of the adsorbent was investigated by using NaOH as eluent agent. The determination of the most preferable regenerating solution is a very essential. Therefore, further studies on effectiveness of other regenerating solutions such as H_2SO_4, HCl, $NaNO_3$, NH_4Cl, and $CaCl_2$ should be investigated.

Research Fund Acknowledgement

This research project is funded by Adama Science and Technology University under the grant number ASTU/SM-R/900/23 Adama, Ethiopia.

REFERENCE

Abdalla, M. M., Lung, C. Y. K., Neelakantan, P., & Matinlinna, J. P. (2020). A novel, doped calcium silicate bioceramic synthesized by sol–gel method: Investigation of setting time and biological properties. *Journal of Biomedical Materials Research - Part B Applied Biomaterials*, *108*(1), 56–66. https://doi.org/10.1002/jbm.b.34365

Agrafioti, E., Kalderis, D., & Diamadopoulos, E. (2014). Arsenic and chromium removal from water using biochars derived from rice husk, organic solid wastes and sewage sludge. *Journal of Environmental Management*, *133*, 309–314. https://doi.org/10.1016/j.jenvman.2013.12.007

Al-anber, M. A. (2011). *Thermodynamics Approach in the Adsorption of Heavy Metals*.

Al-Maliky, E. A., Gzar, H. A., & Al-Azawy, M. G. (2021). Determination of Point of Zero Charge (PZC) of Concrete Particles Adsorbents. *IOP Conference Series: Materials Science and Engineering*, *1184*(1), 012004. https://doi.org/10.1088/1757-899x/1184/1/012004

Al Arni, S. (2018). Comparison of slow and fast pyrolysis for converting biomass into fuel. *Renewable Energy*, *124*, 197–201. https://doi.org/10.1016/j.renene.2017.04.060

Alam, M. A., Shaikh, W. A., Alam, M. O., Bhattacharya, T., Chakraborty, S., Show, B., & Saha, I. (2018). Adsorption of As (III) and As (V) from aqueous solution by modified Cassia fistula (golden shower) biochar. *Applied Water Science*, *8*(7), 1–14. https://doi.org/10.1007/s13201-018-0839-y

Ali, S., Rizwan, M., Shakoor, M. B., Jilani, A., & Anjum, R. (2020). High sorption efficiency for As(III) and As(V) from aqueous solutions using novel almond shell biochar. *Chemosphere*, *243*(Iii), 125330. https://doi.org/10.1016/j.chemosphere.2019.125330

Alka, S., Shahir, S., Ibrahim, N., Ndejiko, M. J., Vo, D. V. N., & Manan, F. A. (2021). Arsenic removal technologies and future trends: A mini review. *Journal of Cleaner Production*, *278*. https://doi.org/10.1016/j.jclepro.2020.123805

Alothman, Z. A., Yilmaz, E., Habila, M., & Soylak, M. (2015). Solid phase extraction of metal ions in environmental samples on 1-(2-pyridylazo)-2-naphthol impregnated activated carbon cloth. *Ecotoxicology and Environmental Safety*, *112*, 74–79. https://doi.org/10.1016/j.ecoenv.2014.10.032

Amen, R., Bashir, H., Bibi, I., Shaheen, S. M., Niazi, N. K., Shahid, M., Hussain, M. M., Antoniadis, V., Shakoor, M. B., Al-Solaimani, S. G., Wang, H., Bundschuh, J., & Rinklebe, J. (2020). A critical review on arsenic removal from water using biochar-based sorbents: The significance of modification and redox reactions. *Chemical Engineering Journal*, *396*, 125195. https://doi.org/10.1016/j.cej.2020.125195

Ayawei, N., Ebelegi, A. N., & Wankasi, D. (2017). Modelling and Interpretation of Adsorption Isotherms. *Journal of Chemistry*, *2017*. https://doi.org/10.1155/2017/3039817

Bai, L., Su, X., Feng, J., & Ma, S. (2021). Preparation of sugarcane bagasse biochar/nano-iron oxide composite and mechanism of its Cr (VI) adsorption in water. *Journal of Cleaner Production*, *320*(July), 128723. https://doi.org/10.1016/j.jclepro.2021.128723

Baig, S. A., Sheng, T., Hu, Y., Lv, X., & Xu, X. (2013). Adsorptive removal of arsenic in saturated sand filter containing amended adsorbents. *Ecological Engineering*, *60*, 345–353. https://doi.org/10.1016/j.ecoleng.2013.09.001

Baig, S. A., Zhu, J., Muhammad, N., Sheng, T., & Xu, X. (2014). Effect of synthesis methods on magnetic Kans grass biochar for enhanced As(III, V) adsorption from aqueous solutions. *Biomass and Bioenergy*, *71*(V), 299–310. https://doi.org/10.1016/j.biombioe.2014.09.027

Bakhshi, S., Shamma, D. A., & Gilbert, E. (2014). Faces engage us: Photos with faces attract more likes and comments on instagram. *Conference on Human Factors in Computing Systems - Proceedings*, 965–974. https://doi.org/10.1145/2556288.2557403

Bakraoui, M., Karouach, F., Ouhammou, B., Aggour, M., Essamri, A., & El Bari, H. (2020). Biogas production from recycled paper mill wastewater by UASB digester: Optimal and mesophilic conditions. *Biotechnology Reports*, *25*, e00402. https://doi.org/10.1016/j.btre.2019.e00402

Bakshi, S., Banik, C., Rathke, S. J., & Laird, D. A. (2018). Arsenic sorption on zero-valent iron-biochar complexes. *Water Research*, *137*, 153–163. https://doi.org/10.1016/j.watres.2018.03.021

Battas, A., El Gaidoumi, A., Ksakas, A., & Kherbeche, A. (2019). Adsorption study for the removal of nitrate from water using local clay. *Scientific World Journal*, *2019*. https://doi.org/10.1155/2019/9529618

Beesley, L., & Marmiroli, M. (2011). The immobilisation and retention of soluble arsenic, cadmium and zinc by biochar. *Environmental Pollution*, *159*(2), 474–480. https://doi.org/10.1016/j.envpol.2010.10.016

Berkessa, Y. W., Mereta, S. T., & Feyisa, F. F. (2019). Simultaneous removal of nitrate and phosphate from wastewater using solid waste from factory. *Applied Water Science*, *9*(2), 1–10. https://doi.org/10.1007/s13201-019-0906-z

Bissen, M., & Frimmel, F. (2003). Arsenic – A Review. Part I: Occurrence, Toxicity, Speciation, Mobility. *Acta Hydrochimica et Hydrobiologica*, *31*, 9–18.

Bordoloi, S., Nath, S. K., Gogoi, S., & Dutta, R. K. (2013). Arsenic and iron removal from groundwater by oxidation-coagulation at optimized pH: Laboratory and field studies. *Journal of Hazardous Materials*, *260*, 618–626. https://doi.org/10.1016/j.jhazmat.2013.06.017

Bostick, B. C., & Fendorf, S. (2003). Arsenite sorption on troilite (FeS) and pyrite (FeS2). *Geochimica et Cosmochimica Acta*, *67*(5), 909–921. https://doi.org/10.1016/S0016-7037(02)01170-5

Braghiroli, F. L., Bouafif, H., Neculita, C. M., & Koubaa, A. (2018). Activated Biochar as an Effective Sorbent for Organic and Inorganic Contaminants in Water. *Water, Air, and Soil Pollution*, *229*(7). https://doi.org/10.1007/s11270-018-3889-8

Chen, I. C., Hill, J. K., Ohlemüller, R., Roy, D. B., & Thomas, C. D. (2011). Rapid range shifts of species associated with high levels of climate warming. *Science*, *333*(6045), 1024–1026. https://doi.org/10.1126/science.1206432

Chen, X., Chen, G., Chen, L., Chen, Y., Lehmann, J., McBride, M. B., & Hay, A. G. (2011). Adsorption of copper and zinc by biochars produced from pyrolysis of hardwood and corn straw in aqueous solution. *Bioresource Technology*, *102*(19), 8877–8884. https://doi.org/10.1016/j.biortech.2011.06.078

Chen, Y., Hassan, M., Nuruzzaman, M., Zhang, H., Naidu, R., Liu, Y., & Wang, L. (2022). Iron-modified biochar derived from sugarcane bagasse for adequate removal of aqueous imidacloprid: sorption mechanism study. *Environmental Science and Pollution Research*, *0123456789*. https://doi.org/10.1007/s11356-022-22357-6

Chen, Y., Hassan, M., Nuruzzaman, M., Zhang, H., Naidu, R., Liu, Y., & Wang, L. (2023). Iron-modified biochar derived from sugarcane bagasse for adequate removal of aqueous imidacloprid: sorption mechanism study. *Environmental Science and Pollution Research*, *30*(2), 4754–4768. https://doi.org/10.1007/s11356-022-22357-6

Chwirka, J. D., Thomson, B. M., & Stomp, J. M. (2000). Removing arsenic from groundwater. *Journal / American Water Works Association*, *92*(3), 79–88. https://doi.org/10.1002/j.1551-8833.2000.tb08911.x

Congsomjit, D., & Areeprasert, C. (2020). *Hydrochar-derived activated carbon from sugar cane bagasse employing hydrothermal carbonization and steam activation for syrup decolorization*. *Ii*.

Dai, Y., Zhang, N., Xing, C., Cui, Q., & Sun, Q. (2019). The adsorption, regeneration and engineering applications of biochar for removal organic pollutants: A review. *Chemosphere*, *223*, 12–27. https://doi.org/10.1016/j.chemosphere.2019.01.161

Das, N. (2010). Recovery of precious metals through biosorption - A review. *Hydrometallurgy*, *103*(1–4), 180–189. https://doi.org/10.1016/j.hydromet.2010.03.016

Dhakal, D. (2018). *ARSENIC ADSORPTION FROM GROUND WATER USING NON-TOXIC WASTE AS ADSORBENTS ARSENIC ADSORPTION FROM GROUND WATER USING NON-TOXIC WASTE AS*.

Dhyani, V., & Bhaskar, T. (2018). A comprehensive review on the pyrolysis of lignocellulosic biomass. *Renewable Energy*, *129*, 695–716. https://doi.org/10.1016/j.renene.2017.04.035

Divband Hafshejani, L., Hooshmand, A., Naseri, A. A., Mohammadi, A. S., Abbasi, F., & Bhatnagar, A. (2016). Removal of nitrate from aqueous solution by modified sugarcane bagasse biochar. *Ecological Engineering*, *95*, 101–111. https://doi.org/10.1016/j.ecoleng.2016.06.035

Ezeonuegbu, B. A., Machido, D. A., Whong, C. M. Z., Japhet, W. S., Alexiou, A., Elazab, S. T., Qusty, N., Yaro, C. A., & Batiha, G. E. S. (2021). Agricultural waste of sugarcane bagasse as efficient adsorbent for lead and nickel removal from untreated wastewater: Biosorption, equilibrium isotherms, kinetics and desorption studies. *Biotechnology Reports*, *30*, e00614. https://doi.org/10.1016/j.btre.2021.e00614

Fang, J., Zhan, L., Ok, Y. S., & Gao, B. (2018). Minireview of potential applications of hydrochar derived from hydrothermal carbonization of biomass. *Journal of Industrial and Engineering Chemistry*, *57*, 15–21. https://doi.org/10.1016/j.jiec.2017.08.026

Feng, Z., Yuan, R., Wang, F., Chen, Z., Zhou, B., & Chen, H. (2021). Preparation of magnetic biochar and its application in catalytic degradation of organic pollutants: A review. *Science of the Total Environment*, *765*, 142673. https://doi.org/10.1016/j.scitotenv.2020.142673

Foo, K. Y., & Hameed, B. H. (2010). *Insights into the modeling of adsorption isotherm systems*. *156*, 2–10. https://doi.org/10.1016/j.cej.2009.09.013

Fu, M. M., Mo, C. H., Li, H., Zhang, Y. N., Huang, W. X., & Wong, M. H. (2019). Comparison of physicochemical properties of biochars and hydrochars produced from food wastes. *Journal of Cleaner Production*, *236*, 117637. https://doi.org/10.1016/j.jclepro.2019.117637

Ghadiri, S. K., Nasseri, S., Nabizadeh, R., Khoobi, M., Nazmara, S., & Mahvi, A. H. (2017). Adsorption of nitrate onto anionic bio-graphene nanosheet from aqueous solutions: Isotherm and kinetic study. *Journal of Molecular Liquids*, *242*, 1111–1117. https://doi.org/10.1016/j.molliq.2017.06.122

Godwin, P. M., Pan, Y., Xiao, H., & Afzal, M. T. (2019). Progress in Preparation and Application of Modified Biochar for Improving Heavy Metal Ion Removal From Wastewater. *Journal of Bioresources and Bioproducts*, *4*(1), 31–42. https://doi.org/10.21967/jbb.v4i1.180

Hadjittofi, L., Prodromou, M., & Pashalidis, I. (2014). Activated biochar derived from cactus fibres - Preparation, characterization and application on Cu(II) removal from aqueous solutions. *Bioresource Technology*, *159*, 460–464. https://doi.org/10.1016/j.biortech.2014.03.073

Hao, L., Liu, M., Wang, N., & Li, G. (2018). A critical review on arsenic removal from water using iron-based adsorbents. *RSC Advances*, *8*(69), 39545–39560. https://doi.org/10.1039/c8ra08512a

Hashimi, S. Q., Hong, S. H., Lee, C. G., & Park, S. J. (2022). Adsorption of Arsenic from Water Using Aluminum-Modified Food Waste Biochar: Optimization Using Response Surface Methodology. *Water (Switzerland)*, *14*(17). https://doi.org/10.3390/w14172712

He, R., Peng, Z., Lyu, H., Huang, H., Nan, Q., & Tang, J. (2018). Synthesis and characterization of an iron-impregnated biochar for aqueous arsenic removal. *Science of the Total Environment*, *612*, 1177–1186. https://doi.org/10.1016/j.scitotenv.2017.09.016

Ho, Y. S., Porter, J. F., & Mckay, G. (2002). *DIVALENT METAL IONS ONTO PEAT : COPPER , NICKEL AND LEAD SINGLE COMPONENT SYSTEMS*. 1–33.

Huang, J., Liu, C., Tong, H., Li, W., & Wu, D. (2012). Theoretical studies on pyrolysis mechanism of xylopyranose. *Computational and Theoretical Chemistry*, *1001*, 44–50. https://doi.org/10.1016/j.comptc.2012.10.015

Huang, Y., Lee, X., Grattieri, M., Yuan, M., Cai, R., Macazo, F. C., & Minteer, S. D. (2020). Modified biochar for phosphate adsorption in environmentally relevant conditions. *Chemical Engineering Journal*, *380*, 122375. https://doi.org/10.1016/j.cej.2019.122375

Inyang, M., Gao, B., Pullammanappallil, P., Ding, W., & Zimmerman, A. R. (2010). Biochar from anaerobically digested sugarcane bagasse. *Bioresource Technology*, *101*(22), 8868–8872. https://doi.org/10.1016/j.biortech.2010.06.088

Irawan, C., Putra, M. D., Wijayanti, H., Juwita, R., Meliana, Y., & Nata, I. F. (2021). The amine functionalized sugarcane bagasse biocomposites as magnetically adsorbent for contaminants removal in aqueous solution. *Molecules*, *26*(19). https://doi.org/10.3390/molecules26195867

Jabasingh, S. A., & Ki, Z. (2016). *Expanding sustenance in Ethiopia based on renewable energy resources – A comprehensive review*. *July*. https://doi.org/10.1016/j.rser.2016.11.082

Jafri, N., Wong, W. Y., Doshi, V., Yoon, L. W., & Cheah, K. H. (2018). A review on production and characterization of biochars for application in direct carbon fuel cells. *Process Safety and Environmental Protection*, *118*, 152–166. https://doi.org/10.1016/j.psep.2018.06.036

Jeffery, S., Verheijen, F. G. A., Velde, M. Van Der, & Bastos, A. C. (2011). Agriculture , Ecosystems and Environment A quantitative review of the effects of biochar application to soils on crop productivity using meta-analysis. *"Agriculture, Ecosystems and Environment," 144*(1), 175–187. https://doi.org/10.1016/j.agee.2011.08.015

Keshav, V., Franklyn, P., & Kondiah, K. (2019). *Recombinant Fusion Protein PbrD Cross-Linked to Calcium Alginate Nanoparticles for Pb Remediation*.

https://doi.org/10.1021/acsomega.9b01624

Khairul, I., Wang, Q. Q., Jiang, Y. H., Wang, C., & Naranmandura, H. (2017). Metabolism, toxicity and anticancer activities of arsenic compounds. *Oncotarget*, *8*(14), 23905–23926. https://doi.org/10.18632/oncotarget.14733

Kiliç, M., Kirbiyik, Ç., Çepelioğullar, Ö., & Pütün, A. E. (2013). Adsorption of heavy metal ions from aqueous solutions by bio-char, a by-product of pyrolysis. *Applied Surface Science*, *283*, 856–862. https://doi.org/10.1016/j.apsusc.2013.07.033

Kuila, T., Bose, S., Mishra, A. K., Khanra, P., Kim, N. H., & Lee, J. H. (2012). Chemical functionalization of graphene and its applications. *Progress in Materials Science*, *57*(7), 1061–1105. https://doi.org/10.1016/j.pmatsci.2012.03.002

Kulikov, A. Y., & Novikov, I. V. (2017). Фармакоэкономические Аспекты Применения Препаратов Группы Агонистов Глюкагоноподобного Пептида-1 (Гпп-1) В Комбинации С Метформином При Сахарном Диабете 2 Типа. *Pharmacoeconomics: Theory and Practice*, *5*(1), 84–84. https://doi.org/10.30809/phe.1.2017.21

Kumar, A., Bhattacharya, T., Shaikh, W. A., Roy, A., Mukherjee, S., & Kumar, M. (2021). Performance evaluation of crop residue and kitchen waste-derived biochar for eco-efficient removal of arsenic from soils of the Indo-Gangetic plain: A step towards sustainable pollution management. *Environmental Research*, *200*(July), 111758. https://doi.org/10.1016/j.envres.2021.111758

Lee, S., Lee, J., Song, M. K., Ryu, J. C., An, B., Lee, C. G., Park, C., Lee, S. H., & Choi, J. W. (2015). Effective regeneration of an adsorbent for the removal of organic contaminants developed based on UV radiation and toxicity evaluation. *Reactive and Functional Polymers*, *95*, 62–70. https://doi.org/10.1016/j.reactfunctpolym.2015.08.008

Lehmann, J. (2007). Bio-energy in the black. *Frontiers in Ecology and the Environment*, *preprint*(2007), 1. https://doi.org/10.1890/060133

Li, B., Yang, L., Wang, C. quan, Zhang, Q. pei, Liu, Q. cheng, Li, Y. ding, & Xiao, R. (2017). Adsorption of Cd(II) from aqueous solutions by rape straw biochar derived from different modification processes. *Chemosphere*, *175*(Ii), 332–340. https://doi.org/10.1016/j.chemosphere.2017.02.061

Li, L., Wei, Z., Liu, X., Yang, Y., Deng, C., Yu, Z., Guo, Z., Shi, J., Zhu, C., Guo, W., & Sun, Z. (2020). Biomaterials cross-linked graphene oxide composite aerogel with a macro–nanoporous network structure for efficient Cr (VI) removal. *International Journal of Biological Macromolecules*, *156*(Vi), 1337–1346. https://doi.org/10.1016/j.ijbiomac.2019.11.174

Liu, Y., Kumar, M., Katul, G. G., & Porporato, A. (2019). Reduced resilience as an early warning signal of forest mortality. *Nature Climate Change*, *9*(11), 880–885. https://doi.org/10.1038/s41558-019-0583-9

Lu, H., Liu, S., Zhang, H., Qiu, Y., Zhao, J., & Zhu, Z. (2018). Decontamination of arsenic in actual water samples by calcium containing layered double hydroxides from a convenient synthesis method. *Water (Switzerland)*, *10*(9). https://doi.org/10.3390/w10091150

Lu, P. J., Lin, H. C., Yu, W. Te, & Chern, J. M. (2011). Chemical regeneration of activated carbon used for dye adsorption. *Journal of the Taiwan Institute of Chemical Engineers*, *42*(2), 305–311. https://doi.org/10.1016/j.jtice.2010.06.001

Machado, G., Santos, F., Faria, D., de Queiroz, T. N., Zinani, F., de Queiroz, J. H., & Gomes, F. (2018). Characterization and Potential Evaluation of Residues from the Sugarcane Industry of Rio Grande do Sul in Biorefinery Processes. *Natural Resources*, *09*(05), 175–187. https://doi.org/10.4236/nr.2018.95011

Mamtimin, X., & Wang, Y. (2022). *Arsenic adsorption by functionalized polystyrene microplastics : kinetics and mechanisms*. 1–25.

Maneechakr, P., & Mongkollertlop, S. (2020). Investigation on adsorption behaviors of heavy metal ions (Cd2+, Cr3+, Hg2+and Pb2+) through low-cost/active manganese dioxide-modified magnetic biochar derived from palm kernel cake residue. *Journal of Environmental Chemical Engineering*, *8*(6), 104467. https://doi.org/10.1016/j.jece.2020.104467

Mesquita, R. G. de A., Mendes, L. M., Sanadi, A. R., de Sena Neto, A. R., Claro, P. I. C., Corrêa, A. C., & Marconcini, J. M. (2018). Urea Formaldehyde and Cellulose Nanocrystals Adhesive: Studies Applied to Sugarcane Bagasse Particleboards. *Journal of Polymers and the Environment*, *26*(7), 3040–3050. https://doi.org/10.1007/s10924-018-1189-4

Mohan, D., & Pittman, C. U. (2007). Arsenic removal from water/wastewater using adsorbents-A critical review. *Journal of Hazardous Materials*, *142*(1–2), 1–53. https://doi.org/10.1016/j.jhazmat.2007.01.006

Mondal, P., Bhowmick, S., Chatterjee, D., Figoli, A., & Van der Bruggen, B. (2013). Remediation of inorganic arsenic in groundwater for safe water supply: A critical assessment of technological solutions. *Chemosphere*, *92*(2), 157–170. https://doi.org/10.1016/j.chemosphere.2013.01.097

Mor, S., Chhoden, K., & Ravindra, K. (2016). Application of agro-waste rice husk ash for the removal of phosphate from the wastewater. *Journal of Cleaner Production*, *129*, 673–680. https://doi.org/10.1016/j.jclepro.2016.03.088

Mpatani, F. M., Aryee, A. A., Kani, A. N., Han, R., Li, Z., Dovi, E., & Qu, L. (2021). A review of treatment techniques applied for selective removal of emerging pollutant-trimethoprim from aqueous systems. *Journal of Cleaner Production*, *308*(April), 127359. https://doi.org/10.1016/j.jclepro.2021.127359

Nabhan, A. (2019). *Nitrate removal from water using activated carbon prepared from olive stone by microwave heating*.

Navarathna, C. M., Karunanayake, A. G., Gunatilake, S. R., Pittman, C. U., Perez, F., Mohan, D., & Mlsna, T. (2019). Removal of Arsenic(III) from water using magnetite precipitated onto Douglas fir biochar. *Journal of Environmental Management*, *250*(August), 109429. https://doi.org/10.1016/j.jenvman.2019.109429

Nguyen, H. T. (2022). *ARSENIC REMOVAL FROM WATER BY NOVEL IRON-BASED ADSORBENTS*.

Nguyen, T. H., Pham, T. H., Nguyen Thi, H. T., Nguyen, T. N., Nguyen, M. V., Tran Dinh, T., Nguyen, M. P., Do, T. Q., Phuong, T., Hoang, T. T., Mai Hung, T. T., & Thi, V. H. T. (2019). Synthesis of Iron-Modified Biochar Derived from Rice Straw and Its Application to Arsenic Removal. *Journal of Chemistry*, *2019*. https://doi.org/10.1155/2019/5295610

Nham, N. T., Tahtamouni, T. M. A., Nguyen, T. D., Huong, P. T., Jitae, K., Viet, N. M., Noi, N. Van, Phuong, N. M., & Anh, N. T. H. (2019). Synthesis of iron modified rice straw biochar toward arsenic from groundwater. *Materials Research Express*, *6*(11).

https://doi.org/10.1088/2053-1591/ab4b98

Nhuchhen, D. R., & Afzal, M. T. (2018). *Characteristics of biochar and bio-oil produced from wood pellets pyrolysis using a bench scale fixed bed , microwave reactor Abstract Microwave pyrolysis of wood pellets was investigated in a pilot scale fixed bed microwave reactor at various biomass loa*.

Niazi, A., Rahimi, V. B., Soheili-far, S., Askari, N., Devin, R., Far, Z. S., Sahebkar, A., Rakhshan-, H., & Askari, V. R. (2018). *A Systematic Review on Prevention and Treatment of Nipple Pain and Fissure : Are They Curable ?* 139–150.

Nie, C., Yang, X., Niazi, N. K., Xu, X., Wen, Y., Rinklebe, J., Ok, Y. S., Xu, S., & Wang, H. (2018). Impact of sugarcane bagasse-derived biochar on heavy metal availability and microbial activity: A field study. *Chemosphere*, *200*, 274–282. https://doi.org/10.1016/j.chemosphere.2018.02.134

Noraini, M. N., Abdullah, E. C., Othman, R., & Mubarak, N. M. (2016). Single-route synthesis of magnetic biochar from sugarcane bagasse by microwave-assisted pyrolysis. *Materials Letters*, *184*, 315–319. https://doi.org/10.1016/j.matlet.2016.08.064

Nsami, J. N., & Mbadcam, J. K. (2013). *The Adsorption Efficiency of Chemically Prepared Activated Carbon from Cola Nut Shells by ZnCl 2 on Methylene Blue*. *2013*.

Oladipo, A. A., Ifebajo, A. O., Nisar, N., & Ajayi, O. A. (2017). High-performance magnetic chicken bone-based biochar for efficient removal of rhodamine-B dye and tetracycline: Competitive sorption analysis. *Water Science and Technology*, *76*(2), 373–385. https://doi.org/10.2166/wst.2017.209

P., A., K., V., M., S., T., G., K., R., P.N., S., & Sukumaran, A. (2017). Removal of toxic heavy metal lead (II) using chitosan oligosaccharide-graft-maleic anhydride/polyvinyl alcohol/silk fibroin composite. *International Journal of Biological Macromolecules*, *104*(Ii), 1469–1482. https://doi.org/10.1016/j.ijbiomac.2017.05.111

Patel, M., Kumar, R., Pittman, C. U., & Mohan, D. (2021). Ciprofloxacin and acetaminophen sorption onto banana peel biochars: Environmental and process parameter influences. *Environmental Research*, *201*, 111218. https://doi.org/10.1016/j.envres.2021.111218

Praipipat, P., Ngamsurach, P., & Sanghuayprai, A. (2023). Modification of sugarcane bagasse

with iron(III) oxide-hydroxide to improve its adsorption property for removing lead(II) ions. *Scientific Reports*, *13*(1), 1–23. https://doi.org/10.1038/s41598-023-28654-5

Qian, L., Zhang, W., Yan, J., Han, L., Gao, W., Liu, R., & Chen, M. (2016). Effective removal of heavy metal by biochar colloids under different pyrolysis temperatures. *Bioresource Technology*, *206*, 217–224. https://doi.org/10.1016/j.biortech.2016.01.065

Rafiee, R. N. J. and M. (2014). *Counterion Effects on Nitrate Adsorption from Aqueous Solution onto Functionalized Polyacrylonitrile Coated with Iron Oxide Nanoparticles - 287-293.pdf*.

Rahdar, S., Taghavi, M., Khaksefidi, R., & Ahmadi, S. (2019). Adsorption of arsenic (V) from aqueous solution using modified saxaul ash: isotherm and thermodynamic study. *Applied Water Science*, *9*(4), 1–9. https://doi.org/10.1007/s13201-019-0974-0

Rajapaksha, A. U., Chen, S. S., Tsang, D. C. W., Zhang, M., Vithanage, M., Mandal, S., Gao, B., Bolan, N. S., & Ok, Y. S. (2016). Engineered/designer biochar for contaminant removal/immobilization from soil and water: Potential and implication of biochar modification. *Chemosphere*, *148*, 276–291. https://doi.org/10.1016/j.chemosphere.2016.01.043

Rathi, B. S., & Kumar, P. S. (2021). A review on sources, identification and treatment strategies for the removal of toxic Arsenic from water system. *Journal of Hazardous Materials*, *418*(June), 126299. https://doi.org/10.1016/j.jhazmat.2021.126299

Sankar, M. S., Vega, M. A., Defoe, P. P., Kibria, M. G., Ford, S., Telfeyan, K., Neal, A., Mohajerin, T. J., Hettiarachchi, G. M., Barua, S., Hobson, C., Johannesson, K., & Datta, S. (2014). Elevated arsenic and manganese in groundwaters of Murshidabad, West Bengal, India. *Science of the Total Environment*, *488–489*(1), 570–579. https://doi.org/10.1016/j.scitotenv.2014.02.077

Sarker, T. C., Azam, S. M. G. G., El-Gawad, A. M. A., Gaglione, S. A., & Bonanomi, G. (2017). Sugarcane bagasse: a potential low-cost biosorbent for the removal of hazardous materials. *Clean Technologies and Environmental Policy*, *19*(10), 2343–2362. https://doi.org/10.1007/s10098-017-1429-7

Sattar, M. S., Shakoor, M. B., Ali, S., Rizwan, M., Niazi, N. K., & Jilani, A. (2019). Comparative efficiency of peanut shell and peanut shell biochar for removal of arsenic from

water. *Environmental Science and Pollution Research*, *26*(18), 18624–18635. https://doi.org/10.1007/s11356-019-05185-z

Shaheen, N. A., Alqahtani, A. A., Assiri, H., Alkhodair, R., & Hussein, M. A. (2018). Public knowledge of dehydration and fluid intake practices: Variation by participants' characteristics. *BMC Public Health*, *18*(1), 1–8. https://doi.org/10.1186/s12889-018-6252-5

Shaheen, S. M., Mosa, A., Natasha, Abdelrahman, H., Niazi, N. K., Antoniadis, V., Shahid, M., Song, H., Kwon, E. E., & Rinklebe, J. (2022). Removal of toxic elements from aqueous environments using nano zero-valent iron- and iron oxide-modified biochar: a review. *Biochar*, *4*(1), 1–21. https://doi.org/10.1007/s42773-022-00149-y

Shang, J., He, W., & Fan, C. (2015). Adsorption of dimethyl trisulfide from aqueous solution on a low-cost adsorbent: thermally activated pinecone. *Chinese Journal of Oceanology and Limnology*, *33*(1), 169–175. https://doi.org/10.1007/s00343-015-4085-y

Shankar, S., Shanker, U., & Shikha. (2014). Arsenic contamination of groundwater: A review of sources, prevalence, health risks, and strategies for mitigation. *Scientific World Journal*, *2014*. https://doi.org/10.1155/2014/304524

Shen, D. K., & Gu, S. (2009). The mechanism for thermal decomposition of cellulose and its main products. *Bioresource Technology*, *100*(24), 6496–6504. https://doi.org/10.1016/j.biortech.2009.06.095

Siddiq, O. M., Tawabini, B. S., Soupios, P., & Ntarlagiannis, D. (2022). Removal of arsenic from contaminated groundwater using biochar: a technical review. *International Journal of Environmental Science and Technology*, *19*(1), 651–664. https://doi.org/10.1007/s13762-020-03116-x

Singh, P., Sarswat, A., Pittman, C. U., Mlsna, T., & Mohan, D. (2020). Sustainable Low-Concentration Arsenite [As(III)] Removal in Single and Multicomponent Systems Using Hybrid Iron Oxide-Biochar Nanocomposite Adsorbents - A Mechanistic Study. *ACS Omega*, *5*(6), 2575–2593. https://doi.org/10.1021/acsomega.9b02842

Smedley, P. L., & Kinniburgh, D. G. (2002). A review of the source, behaviour and distribution of arsenic in natural waters. *Applied Geochemistry*, *17*(5), 517–568. https://doi.org/10.1016/S0883-2927(02)00018-5

Sorlini, S., & Gialdini, F. (2010). Conventional oxidation treatments for the removal of arsenic with chlorine dioxide, hypochlorite, potassium permanganate and monochloramine. *Water Research*, *44*(19), 5653–5659. https://doi.org/10.1016/j.watres.2010.06.032

Sun, C., Chen, T., Huang, Q., Wang, J., Lu, S., & Yan, J. (2019). Enhanced adsorption for Pb(II) and Cd(II) of magnetic rice husk biochar by KMnO4 modification. *Environmental Science and Pollution Research*, *26*(9), 8902–8913. https://doi.org/10.1007/s11356-019-04321-z

Tan, X., Liu, Y., Zeng, G., Wang, X., Hu, X., Gu, Y., & Yang, Z. (2015). Application of biochar for the removal of pollutants from aqueous solutions. *Chemosphere*, *125*, 70–85. https://doi.org/10.1016/j.chemosphere.2014.12.058

Tchounwou, P. B., Yedjou, C. G., Patlolla, A. K., & Sutton, D. J. (2012). Molecular, clinical and environmental toxicicology Volume 3: Environmental Toxicology. In *Molecular, Clinical and Environmental Toxicology* (Vol. 101). https://doi.org/10.1007/978-3-7643-8340-4

Tena Gashaw, E., Mekbib, F., & Ayana, A. (2018). Sugarcane Landraces of Ethiopia: Germplasm Collection and Analysis of Regional Diversity and Distribution. *Advances in Agriculture*, *2018*. https://doi.org/10.1155/2018/7920724

Tohfegar, E., Moghaddas, J. S., Sharifzadeh, E., & Esmaeilzadeh–Dilmaghani, S. (2019). Synthesis and Characterization of Waterglass-Based Silica Aerogel Under Heat Treatment for Adsorption of Nitrate from Water : Batch and Column Studies. *Iranian Journal of Chemical Engineering*, *16*(4), 53–72.

Tomczyk, A., Sokołowska, Z., & Boguta, P. (2020). Biochar physicochemical properties: pyrolysis temperature and feedstock kind effects. *Reviews in Environmental Science and Biotechnology*, *19*(1), 191–215. https://doi.org/10.1007/s11157-020-09523-3

Toscano Miranda, N., Lopes Motta, I., Maciel Filho, R., & Wolf Maciel, M. R. (2021). Sugarcane bagasse pyrolysis: A review of operating conditions and products properties. *Renewable and Sustainable Energy Reviews*, *149*(July), 111394. https://doi.org/10.1016/j.rser.2021.111394

Tripathi, M., Sahu, J. N., & Ganesan, P. (2016). Effect of process parameters on production of biochar from biomass waste through pyrolysis: A review. *Renewable and Sustainable Energy Reviews*, *55*, 467–481. https://doi.org/10.1016/j.rser.2015.10.122

Tsamo, C., Paltahe, A., Fotio, D., Vincent, T. A., & Sales, W. F. (2019). *Thermodynamic Evaluation of Co (II) Removal from Aqueous Solution Using Dead Neem Leaves*. *2019*.

Varma, A. K., & Mondal, P. (2016). Physicochemical Characterization and Pyrolysis Kinetic Study of Sugarcane Bagasse Using Thermogravimetric Analysis. *Journal of Energy Resources Technology, Transactions of the ASME*, *138*(5), 1–11. https://doi.org/10.1115/1.4032729

Verma, L., & Singh, J. (2019). Synthesis of novel biochar from waste plant litter biomass for the removal of Arsenic (III and V) from aqueous solution: A mechanism characterization, kinetics and thermodynamics. *Journal of Environmental Management*, *248*(April), 109235. https://doi.org/10.1016/j.jenvman.2019.07.006

Wang, C., Riyu, P., Xiaoyang, W., Yilin, T., Linkang, X., Cyrus, S. H., & C.H., R. (2020). Immediate Psychological Responses and Associated Factors during the Initial Stage of the 2019 Coronavirus Disease (COVID-19) Epidemic among the General Population in China. *International Journal of Environmental Research and Public Health*, *17*(5), 1–25. https://www.ncbi.nlm.nih.gov/pmc/articles/PMC7084952/

Wang, J., & Guo, X. (2020). Adsorption isotherm models: Classification, physical meaning, application and solving method. *Chemosphere*, *258*, 127279. https://doi.org/10.1016/j.chemosphere.2020.127279

Wang, S. ye, Tang, Y. kui, Chen, C., Wu, J. tao, Huang, Z., Mo, Y. yuan, Zhang, K. xuan, & Chen, J. bo. (2015). Regeneration of magnetic biochar derived from eucalyptus leaf residue for lead(II) removal. *Bioresource Technology*, *186*, 360–364. https://doi.org/10.1016/j.biortech.2015.03.139

WHO, & World Health Organization. (2019). Preventing Disease through Healthy Environment. Exposure to Arsenic: A Major Public Health Concern. *Preventing Disease through Healthy Environment*, 1–5. http://www.who.int/ipcs/features/arsenic.pdf?ua=1

Wu, H., Wen, Q., Hu, L., & Gong, M. (2018). Effect of Adsorbate Concentration to Adsorbent Dosage Ratio on the Sorption of Heavy Metals on Soils. *Journal of Environmental Engineering*, *144*(2). https://doi.org/10.1061/(asce)ee.1943-7870.0001306

Xiao, Y., Luo, R., Ji, Y., Li, S., Hu, H., & Zhang, X. (2022). Removal of Copper(II) from

Aqueous Environment Using Silk Sericin-Derived Carbon. *International Journal of Molecular Sciences*, *23*(19). https://doi.org/10.3390/ijms231911202

Yaashikaa, P. R., Kumar, P. S., Varjani, S., & Saravanan, A. (2020). A critical review on the biochar production techniques, characterization, stability and applications for circular bioeconomy. *Biotechnology Reports*, *28*, e00570. https://doi.org/10.1016/j.btre.2020.e00570

Yang, H., Waugh, D. W., Orbe, C., Patra, P. K., Jöckel, P., Lamarque, J. F., Tilmes, S., Kinnison, D., Elkins, J. W., & Dlugokencky, E. J. (2019). Evaluating Simulations of Interhemispheric Transport: Interhemispheric Exchange Time Versus SF 6 Age. *Geophysical Research Letters*, *46*(2), 1113–1120. https://doi.org/10.1029/2018GL080960

Yang, X., Blagodatsky, S., Lippe, M., Liu, F., Hammond, J., Xu, J., & Cadisch, G. (2016). Forest Ecology and Management Land-use change impact on time-averaged carbon balances : Rubber expansion and reforestation in a biosphere reserve , South-West China. *FOREST ECOLOGY AND MANAGEMENT*, *372*, 149–163. https://doi.org/10.1016/j.foreco.2016.04.009

Yi, Y., Huang, Z., Lu, B., Xian, J., Tsang, E. P., Cheng, W., Fang, J., & Fang, Z. (2020). Magnetic biochar for environmental remediation: A review. *Bioresource Technology*, *298*, 122468. https://doi.org/10.1016/j.biortech.2019.122468

Yu, K. L., Lau, B. F., Show, P. L., Ong, H. C., Ling, T. C., Chen, W. H., Ng, E. P., & Chang, J. S. (2017). Recent developments on algal biochar production and characterization. *Bioresource Technology*, *246*, 2–11. https://doi.org/10.1016/j.biortech.2017.08.009

Zang, S., Zuo, Y., Wang, J., Liu, X., Gomez, M. A., & Wei, L. (2021). Adsorption removal of roxarsone, arsenite(III), and arsenate(V) using iron-modified sorghum straw biochar and its kinetics. *Acta Geochimica*, *40*(3), 409–418. https://doi.org/10.1007/s11631-021-00466-2

Zhang, H., Liu, Q., Wang, J., Liu, J., Yan, H., Jing, X., & Zhang, B. (2015). Preparation of magnetic calcium silicate hydrate for the efficient removal of uranium from aqueous systems. *RSC Advances*, *5*(8), 5904–5912. https://doi.org/10.1039/c4ra08678c

Zhang, Q., Li, Q., Zhang, L., Yu, Z., Jing, X., Wang, Z., Fang, Y., & Huang, W. (2017). Experimental study on co-pyrolysis and gasification of biomass with deoiled asphalt. *Energy*, *134*, 301–310. https://doi.org/10.1016/j.energy.2017.05.157

Zheng, K., Di, M., Zhang, J., Bao, W., Liang, D., Pang, G., Fang, Z., & Li, C. (2017). Solvothermal synthesis of magnetic Fe3O4 nanospheres and their efficiency in photo-Fenton degradation of xylenol orange. *Chemical Research in Chinese Universities*, *33*(4), 648–654. https://doi.org/10.1007/s40242-017-6493-3

Zhou, L., Bao, Q., Liu, Y., Wu, G., Wang, W.-C., Wang, X., He, B., Yu, H., & Li, J. (2015). Journal of Advances in Modeling Earth Systems. *Journal of Advances in Modeling Earth Systems*, *6*, 513–526. https://doi.org/10.1002/2015MS000470.Received

Zhou, Y., Qin, S., Verma, S., Sar, T., Sarsaiya, S., Ravindran, B., Liu, T., Sindhu, R., Kumar, A., & Kumar, M. (2021). Bioresource Technology Production and beneficial impact of biochar for environmental application : A comprehensive review. *Bioresource Technology*, *337*(May), 125451. https://doi.org/10.1016/j.biortech.2021.125451

Zhu, C. S., Wang, L. P., & Chen, W. bin. (2009). Removal of Cu(II) from aqueous solution by agricultural by-product: Peanut hull. *Journal of Hazardous Materials*, *168*(2–3), 739–746. https://doi.org/10.1016/j.jhazmat.2009.02.085

Appendix A: BET surface area analysis of SCB and $FeCl_3.6H_2O$ loaded SCB biochar

Horiba Instruments, Inc.
SA-9600 Series Surface Area Analyzer

Analysis Report
Sep/06/2023

Customer	: Mulugeta	Operator ID	: SARA
Description	: Different Experiment	Analysis Date	: Sep/06/2023
Filename	: mulugeta 3.sa2	Analysis Time	: 10:18:06

Condition Settings

Room Temp	: 27.0 (°C)	Atm. Pres	: 700.0 (mm)
Gas Used	: Nitrogen	Gas Conc	: 0.300, 0.000, 0.000 %

	Channel: 1	Channel: 2	Channel: 3
Sample Name	SCB	ISCB	
Tube Number	1	2	0
Tare Weight	10.1320 (gm)	10.1180 (gm)	0.0000 (gm)
Sample Weight	10.2100 (gm)	10.1970 (gm)	1.0000 (gm)
Degas Temp.	200 (°C)	200 (°C)	0 (°C)
Degas Time	60 (min)	60 (min)	0 (min)
Surface Area (M^2/gm)	97.387	14.886	-1.#IO
Slope	454.891	2884.187	-1.#IO
Intercept	3.234	75.083	-1.#IO
Vm	0.002	0.000	-1.#IO
BET Const	141.644	39.413	-1.#IO
Pearson Coef	0.999	1.000	0.000
X[1] - 0.269	126.491	849.212	1.#IO
X[2] - 0.179	83.309	597.523	1.#IO
X[3] - 0.090	44.844	331.538	1.#IO

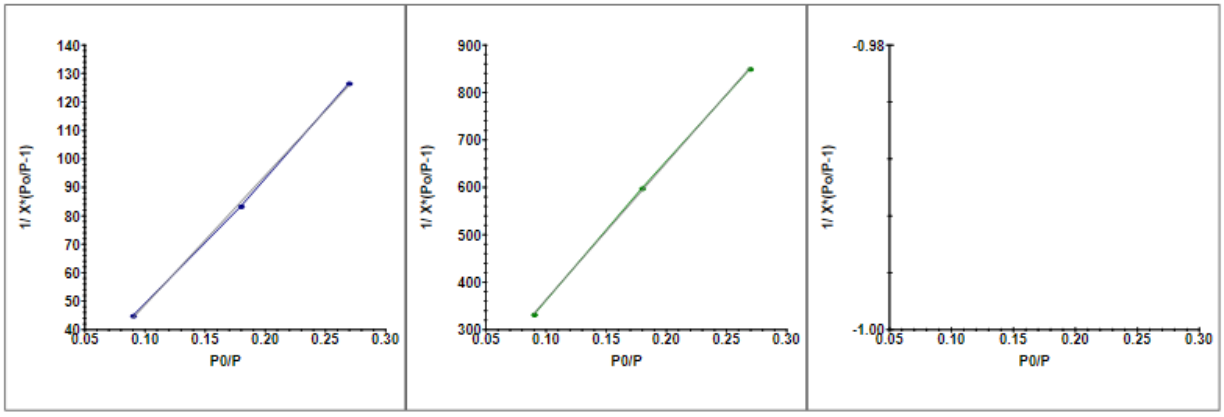

Appendix B: Crystalline size of SCB and $FeCl_3.6H_2O$ loaded SCB biochar

Crystalline size SCB			
peak position(2 theta)	FWHM	**Crystallite Size**	**Average crystalline size (nm)**
22.54963	0.29627	27.34203754	15.91067
32.26808	0.5968	13.85725489	
32.26808	0.6879	12.02211037	
44.01729	0.6968	12.29723617	
64.39141	0.6689	14.03472238	

$FeCl_3.6H_2O$ loaded SCB biochar			
peak position(2 theta)	FWHM	**Crystallite Size (nm)**	**Average crystalline size (nm)**
22.01807	0.2903	27.87884	19.53957
29.17162	0.3652	22.47768	
31.56973	0.3965	20.82121	
34.56602	0.4021	20.69123	
37.79635	0.5062	16.58815	
44.03369	0.4523	18.94585	
47.49658	0.5214	16.64598	
53.23955	0.5932	14.98016	
58.59261	0.4321	21.08162	
64.40985	0.61425	15.28494	

Appendix C: Adsorption Parameters data

a. Effects of solution PH

run	PH	dose(g/l)	time(min)	Co(mg/l)	absorb-ance	Ce(mg/l)	R(%)
1	2	1.5	150	15	0.2256	2.965	80.23
2	4	1.5	150	15	0.1688	2.2185	85.21
3	6	1.5	150	15	0.1764	2.319	84.54
4	8	1.5	150	15	0.2098	2.758	81.61
5	10	1.5	150	15	0.2744	3.607	75.95
6	12	1.5	150	15	0.2661	3.498	76.68

a. Effects of contact time

run	PH	C0(mg/L)	dose(g/L)	time(min)	absorb-ance	Ce(mg/L)	R(%)
1	4	15	1.5	30	0.3014	3.961	73.59
2	4	15	1.5	60	0.2404	3.159	78.94
3	4	15	1.5	90	0.2013	2.646	82.36
4	4	15	1.5	120	0.1767	2.323	84.51
5	4	15	1.5	150	0.161	2.116	85.89
6	4	15	1.5	180	0.1507	1.981	86.79
7	4	15	1.5	210	0.1509	1.983	86.78

a. Effects of initial arsenite concentration

run	PH	dose(g/L)	time(min)	conc(mg/l)	absorb-ance	Ce(mg/l)	R(%)
1	4	1.5	150	5	0.044	0.573	88.54
2	4	1.5	150	10	0.087	1.147	88.53
3	4	1.5	150	15	0.145	1.903	87.31
4	4	1.5	150	20	0.239	3.144	84.28
5	4	1.5	150	25	0.401	5.2675	78.93
6	4	1.5	150	30	0.61	8.025	73.25

b. Effects of adsorbent dose

run	C0(mg/L)	PH	TIME(min)	Dose(g/L)	absorb-ance	Ce(mg/L)	R(%)
1	10	4	180	0.5	0.2408	2.11	78.9
2	10	4	180	1	0.1746	1.53	84.7
3	10	4	180	1.5	0.1372	1.106	88.94
4	10	4	180	2	0.1237	1.046	89.54
5	10	4	180	2.5	0.1155	1.154	88.46
6	10	4	180	3	0.1187	1.22	87.8

Appendix D: Thermal Analysis Result

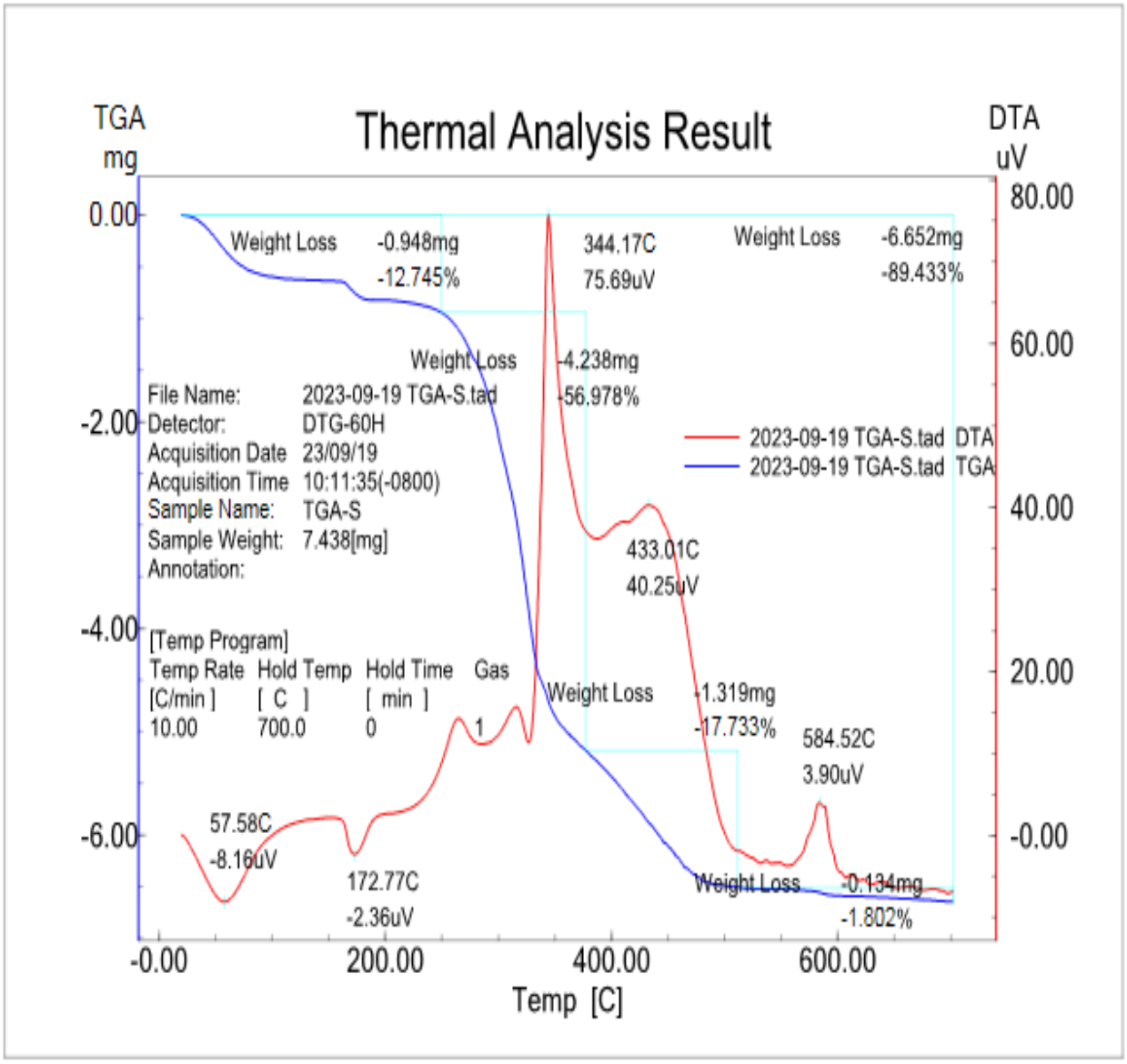

Appendix E: Arsenite Calibration Curve